DISSECTION OF THE GENETICS AND MECHANISMS CONFERRING RESISTANCE TO *FUSARIUM VERTICILLIOIDES* IN MAIZE

A Dissertation

Presented to the Faculty of the Graduate School

of Cornell University

In Partial Fulfillment of the Requirements for the Degree of

Doctor of Philosophy

by

Laura Morales

December 2017

DISSECTION OF THE GENETICS AND MECHANISMS CONFERRING RESISTANCE TO *FUSARIUM VERTICILLIOIDES* IN MAIZE

Laura Morales, Ph. D.

Cornell University 2017

Maize, an important food and commodity crop worldwide, can be infected by the fungal pathogen *Fusarium verticillioides*. *F. verticillioides* causes the disease Fusarium ear rot (FER) and produces the toxic fungal secondary metabolite (mycotoxin) fumonisin, which can reduce yields and marketability of maize grain. More importantly, fumonisin exposure is associated with health risks for humans and animals. This dissertation aimed to dissect the genetics and mechanisms conferring resistance to FER and fumonisin contamination in maize. Employing point and inundative *F. verticillioides* inoculation methods with a panel of 50 maize inbred lines, the symptomatology of *F. verticillioides* infection (FVI) was dissected, showing that kernel bulk density is an accurate predictor of fumonisin contamination in maize kernels. Quantitative trait locus mapping and correlation analyses further demonstrated the link between kernel bulk density and resistance to FVI and revealed the diverse modes of pathogenesis and resistance loci present in four tropical-by-temperate recombinant inbred line maize families. Inter-trait correlation analyses, genome-wide association mapping, and genomic prediction of 29 publicly available disease resistance (including FER) and morphophysiological traits on the maize core diversity panel revealed that height and inflorescence traits were associated and shared loci disease resistance.

BIOGRAPHICAL SKETCH

Laura Morales was born in Miami, Florida, USA on September 8, 1988 to Colombian immigrant parents Alvaro and Marcela Morales. After Hurricane Andrew destroyed her family's home in 1992, Laura spent her childhood with her parents and younger brother Nicolas in Delray Beach. She attended high school and worked at Walt Disney World's Magic Kingdom during the summers in Orlando.

In 2007, Laura began her undergraduate studies as a pre-medical major at the University of Florida in Gainesville, Florida. An ethnobotany course during her first semester inspired Laura to change her major and seek out research opportunities in the plant sciences. From 2008-2011, she gained experience in maize molecular biology in Dr. Karen E. Koch's laboratory. In 2009, Laura spent the summer as a field assistant in the Costa Rican rain forest with Dr. Silvia Alvarez-Clare. Laura graduated with a Bachelor of Science in biology with a concentration in biotechnology in May of 2011.

Laura moved to Ithaca, New York in July of 2011 to begin her PhD work in plant breeding and genetics at Cornell University with Dr. Rebecca J. Nelson. She spent her first two years gaining experience in Kenyan food systems through the Food Systems and Poverty Reduction IGERT program, which led her to focus her graduate research on elucidating the genetics and mechanisms of resistance to mycotoxin contamination in maize. From 2012-2016, Laura spent her summers conducting field experiments near Raleigh, North Carolina in collaboration with Dr. James B. Holland from North Carolina State University and the USDA-ARS.

For my grandparents, whose leap of faith opened so many doors

ACKNOWLEDGMENTS

First and foremost, I would like to thank my parents for instilling the joy of learning in me and for encouraging me to live honestly and *con energía*. Thank you to my advisor Rebecca for always inspiring me to think about the bigger picture. Many thanks to Judy for ensuring that I had the materials, support, and candy necessary for completing my dissertation. To my collaborators at NCSU – Jim, Jason, Charlie, Peter, David, and Thiago – thank you for making my field experiments possible. Thank you to my undergraduate assistants Cara, Jade, and Melissa for all of your help dealing with my toxic corn. Thanks to Tiffany, Santiago, Samuel, Jaci, Jenny, Tyr, Anthony, Henry, Anne, Danilo, and my favorite brother Nick for the great lab comradery. Thank you to Karen for being my first role model of women in science. Thanks to my committee members Ed and Gary for providing advice throughout the development of my dissertation. For much logistic, administrative, and technical support over the past six years, I thank Molly, Sara, Mary Ellen, Kim, Alicia, Jackie, Tracy, Heather, and Chad. Kelly, thank you for making me want to be a better person in life and in science.

TABLE OF CONTENTS

LIST OF FIGURES

LIST OF TABLES

LIST OF ABBREVIATIONS

AGP: accessioned golden path

ANOVA: analysis of variance

ASI: anthesis-silking interval

BIK: bikaverin

BLUP: best linear unbiased predictor

bp: base pair

CI: confidence interval

cM: centimorgan

CV: cross validation

$BDEN_{inoc}$: kernel bulk density under *Fusarium verticillioides* inoculation

$BDEN_{uninoc}$: kernel bulk density under uninoculated conditions

DEN: kernel bulk density under *Fusarium verticillioides* inoculation

DTA: days to anthesis

DTS: days to silk

EHT: ear height

ELISA: enzyme-linked immunosorbent assay

ERN: ear row number

FAO: Food and Agriculture Organization of the United Nations

FDR: false discovery rate

FER: Fusarium ear rot

FUM: fumonisin

FUM:FER: ratio of fumonisin to Fusarium ear rot

FVI: *Fusarium verticillioides* infection

GBS: genotyping-by-sequencing

GLM: general linear model

GLS: gray leaf spot

GO: gene ontology

GWAS: genome wide association study

GxE: genotype-by-environment interaction

H: broad-sense heritability

h^2: narrow-sense heritability

kbp: kilo base pair

LD: linkage disequilibrium

LDA: linear discriminant analysis

L-R: likelihood-ratio

LS: least-square

MAF: minor allele frequency

Mbp: mega base pair

MDS: multidimensional scaling

MLA: middle leaf angle

MLM: mixed linear model

NAM: nested association mapping

NLB: northern leaf blight

NPH: node count

P: p-value

PC: principal component

PCA: principal component analysis

PHT: plant height

PLS: partial least squares

ppm: parts per million ($\mu g\ g^{-1}$)

QTL: quantitative trait locus

RIL: recombinant inbred line

RPR: rind penetrometer resistance

SLB: southern leaf blight

SNP: single nucleotide polymorphism

ULA: upper leaf angle

PREFACE

This dissertation presents work aimed at elucidating the genetics and mechanisms underlying resistance to fumonisin contamination and *Fusarium verticillioides* infection (FVI) in maize. The first chapter introduces the relevance of and existing knowledge on this topic as well as the three broad motivating questions addressed by the three research chapters (2-4). The first question inquires about how the mode of inoculation influences FVI symptomatology and inference on genetic variation in resistance. The second motivating question asks what morphophysiological traits are associated with fumonisin contamination and FVI severity, and the third questions what loci are unique to resistance to FER and shared among resistance to FER and morphophysiological traits.

I compare two *F. verticillioides* inoculation methods representing distinct infection pathways (point vs. widespread) in chapter 1. I compare FVI severity (based on FER, fumonisin, bikaverin, and bulk density) and genetic variation in FVI severity under the two inoculation methods. I also leverage the diverse FVI symptomatology resulting from the two inoculation methods to investigate the use of kernel bulk density and bikaverin as proxies for fumonisin contamination.

In chapter 2, I combine personal data on five indicators of FVI – Fusarium ear rot (FER), fumonisin, kernel bulk density under *F. verticillioides* inoculation ($BDEN_{inoc}$), and symptom type – with publicly available data on kernel bulk density under uninoculated conditions ($BDEN_{uninoc}$) from four recombinant inbred line (RIL) families from the maize nested association mapping (NAM) population. The NAM is composed of 25 RIL families derived from 25 diverse inbred lines crossed to one recurrent parent (B73), and the four families that I screened for FVI resistance were derived from tropical-by-temperate (B73) crosses. I investigate how indicators of FVI are correlated and share loci with each other and with $BDEN_{uninoc}$.

Chapter 4 employs publicly available data on 29 morphophysiological and disease resistance traits (including FER) from the maize core diversity panel, composed of 282 diverse inbred lines. I explore inter-trait relationships with correlation analyses and use genome wide association studies (GWAS) to characterize loci specific to disease resistance and loci shared among disease resistance and morphophysiological traits. I also attempt to predict disease severity phenotypes using top GWAS loci associated with morphophysiological traits.

CHAPTER 1

INTRODUCTION

Global importance of maize and its diseases

Wide adaptation, high yields, and versatility as a food source make maize (*Zea mays* L) a staple crop in many parts of the world. In 2013, the FAO estimated that more than one billion metric tons of maize were produced globally, with 125 million produced for human consumption (1). The three major maize-producing countries (in descending order: USA, China, and Brazil) accounted for more than two-thirds of the total production but only produced 15% of the maize intended for human consumption in 2013; in contrast, the least developed nations in the world collectively produced one third of the maize food supply (1). Although maize productivity per hectare is lowest in the developing world, such as sub-Saharan Africa, maize accounts for 10-60% of daily caloric intake per capita (based on a diet of 2000 kcal per day) (1).

Despite the steady increase in maize yields over the past century, yield losses due to diseases and pests have remained virtually constant (2). In the US maize-producing states and in Ontario, Canada, diseases have accounted for 8-16% of total annual yield losses over the past four years, with approximately half of the disease losses caused by toxic fungal secondary metabolite (mycotoxin) contamination (2). Mycotoxin contamination and the severity of ear rots (kernel diseases caused by mycotoxigenic fungi) are positively correlated (3,4); however, in the case of the US and Ontario, mycotoxin-related yield losses were most likely due to the reduced crop value of mycotoxin-contaminated grain (5) rather than ear rots (kernel diseases caused by mycotoxigenic fungi), as annual losses due to ear rots were low (<1%) (2). An estimated 25% of the world's crops are contaminated with mycotoxins (6), and the health risks associated with human and animal mycotoxin exposure surpass the impacts of reduced yields (5). Mycotoxin exposure is especially concerning in the

tropics and sub-tropics, where environmental conditions are conducive to infection by mycotoxigenic fungi but where monitoring of mycotoxin contamination in the food system are limited or nonexistent (7–12).

Health implications of fumonisin contamination

The filamentous ascomycete fungus *Fusarium verticillioides* can infect maize throughout plant development and is the most prevalent fungal species found in maize kernels (13). *F. verticillioides* causes Fusarium ear rot (FER) and produces the mycotoxin fumonisin, reducing yields and compromising human and animal health (2,7). Fumonisin exposure and contamination in maize foodstuffs has been associated with increased incidence of esophageal cancer (14,15), neural tube defects (12,16,17), and growth retardation (8) around the globe. Fumonisin also induces equine leukoencephalomalacia (18), characterized by rapid deterioration of the brain, and porcine pulmonary edema and hydrothorax (19).

Genetic, morphological, and biochemical components of resistance to F. verticillioides infection and fumonisin contamination in maize

Resistance to can be defined as the host's ability to limit the proliferation and growth of the pathogen within its tissues. Substantial work has been done to elucidate the genetics behind resistance to FER and fumonisin accumulation in maize. Resistances to FER and fumonisin contamination are quantitatively controlled, moderately to highly heritable, and genetically correlated (20–23). The quantitative nature of these traits makes them more durable over time when compared to qualitative forms of disease resistance that are easily overcome by pathogens (24). Trade-offs between FER resistance and favorable agronomic traits have not been established (22,25,26).

Ear and kernel morphology have been associated with fumonisin contamination and FVI, as *F. verticillioides* can enter the kernel via the stylar canal, direct penetration of the pericarp, or the pedicel (27–36). The stylar canal is the mode of entry for *F. verticillioides* when mechanical injury is absent, and the architecture (relative openness) of the stylar canal opening has been implicated in differential resistance of maize hybrids (27,37). Kernel pericarp characteristics (e.g. thickness, surface wax content, and texture) have likewise been associated with resistance, presumably because *F. verticillioides* can directly penetrate the pericarp (27–29,38). Components of kernel hardness, including kernel type (soft endosperm vs. hard endosperm), kernel bulk density and size, and starch granule compaction and branching, also differentially facilitate *F. verticillioides* infection and subsequent fumonisin accumulation (27,32,36,39–41). With respect to the ear, husk tightness and layering as well as delayed silk senescence have been observed in lines with higher levels of resistance (28,37,42,43). Genotype-specific differences in the extent of colonization of the cob tissues and kernel pedicel by *F. verticillioides* have also been reported (44).

No major resistance genes have been implicated in defense against *F. verticillioides* in maize. However, biochemical signatures have been associated with resistance to FER, FVI, and fumonisin accumulation. Phenylpropanoids, such as diferulates (DFAs), mediate cross-linking between polysaccharides and between polysaccharides and lignin, which strengthen the kernel pericarp (45). Pericarp DFAs have been implicated in resistance to *F. verticillioides* and fumonisin contamination, although it is unknown whether DFAs play a passive role in resistance via pericarp hardening or whether DFAs have an active inhibitory effect on *F. verticillioides* (33). Phenylpropanoid pathway genes involved in lignin biosynthesis have also been shown to upregulate in maize kernels upon infection by *F. verticillioides* (46). Maize lipids

and oxylipins have been shown to modulate fumonisin production and conidiation by *F. verticillioides* (34). Lipid profiles have also been associated with fumonisin contamination in maize kernels, with oxylipins and sphingolipids being the most important for differentiating high-fumonisin (≥ 2 ppm) from low-fumonisin (< 2 ppm) samples (47). In response to infection by *F. verticillioides*, the upregulation of genes involved in the biosynthesis of plant hormones, such as ethylene, abscisic acid, salicylic acid, and jasmonic acid, has been reported in maize kernels (46,48).

Pre- and post-harvest interventions for the reduction of fumonisin levels in maize

Once in the food system, fumonisin cannot be completely removed. However, pre- and post-harvest interventions can reduce its accumulation and exposure. Good agronomic practices, such as crop rotation, tillage, and irrigation, have been associated with decreased FVI severity and fumonisin levels (49,50). The role of nitrogen fertilization in FVI and fumonisin accumulation is more complex. At one end of the spectrum, nitrogen deficiency induces plant stress and subsequent fumonisin production (51,52). Conversely, high nitrogen application can lead to a denser canopy structure and increased FVI and fumonisin accumulation (30). However, many of these agronomic practices are not entirely relevant in the context of developing countries. For example, in Kenya low income groups produce more than 70% of the maize, and smallholder farmers often do not use nitrogen fertilizer or use less than the minimum recommended amount because of resource constraints (53).

Post-harvest techniques have been shown to influence fumonisin levels in maize grain. Basic visual sorting, mechanical decortication (pericarp removal), and prevention of kernel damage caused by mechanical shelling have been shown to reduce fumonisin levels and the incidence of *F. verticillioides infection* (54,55). At the industrial level, high temperature treatment combined with extrusion processing can

remove up to 95% of fumonisin (56). Nixtamalization, the traditional Central American lime cooking process used to make maize tortillas, reduces fumonisin content in maize products by 50-82% and hydrolyzes a large portion of the fumonisin, rendering it non-carcinogenic (56–58).

The cost of fumonisin quantification per sample via antibody-based or chromatographic methods is high, making the identification of proxies for fumonisin essential. Sorting based on spectral properties has proven to be effective at reducing the majority of fumonisin in bulk maize samples by removing the small portion of highly contaminated kernels with high sensitivity and specificity (59–61). Although there is substantial evidence in the literature that kernel hardness and density are negatively associated with fumonisin contamination, little has been reported about using these types of kernel traits as proxies for fumonisin contamination. Sorting based on buoyancy in saline solution has been shown to reduce fumonisin content in maize grain (62). Other FVI-related traits have the potential to serves as proxies for fumonisin. Horne et al. (22) demonstrated the indirect reduction of fumonisin contamination via selection for FER resistance, a trait that only involves visual assessment. In addition, bikaverin, a red fungal pigment produced by *F. verticillioides*, has also been used as an indicator of FER (63). The biosynthesis of bikaverin is co-regulated with that of fumonisin (64,65), suggesting that bikaverin could also be an indicator of fumonisin levels.

Bridging the gap between fumonisin resistance and morphophysiology

Although (1) the genetic architectures of maize kernel morphology and composition and resistance to FER and fumonisin contamination have been dissected via quantitative trait locus (QTL) mapping and genome wide association studies (GWAS) (21,23,26,66–69) and (2) kernel composition and morphology have been

implicated in resistance to FER, FVI, and fumonisin accumulation (29,32,37,70), little has been done to connect these two realms of knowledge. The literature has demonstrated that yield components (e.g. kernel and cob traits) and biochemical pathways involved in general plant processes (e.g. lignification and hormones) are associated with fumonisin and FVI, suggesting that the genetics underlying resistance may also influence morphological and physiological traits and vice versa. Thus, understanding the role of maize morphophysiology – the intersection between form and function – on the maize-*F. verticillioides* pathosystem is necessary for assessing the trade-offs between resistance and agronomics and has the potential to inform breeding decisions and grain sorting efforts.

REFERENCES

1. Food and Agriculture Organization of the United Nations. FAOSTAT Database. Rome, Italy; 2017. Available from: http://www.fao.org/faostat
2. Mueller DS, Wise KA, Sisson AJ, Allen TW, Bergstrom GC, Bosley DB, et al. Corn yield loss estimates due to diseases in the United States and Ontario, Canada from 2012 to 2015. Plant Health Prog. 2016;17:211–22.
3. Robertson-Hoyt LA, Betrán J, Payne GA, White DG, Isakeit T, Maragos CM, et al. Relationships among resistances to Fusarium and Aspergillus ear rots and contamination by fumonisin and aflatoxin in maize. Phytopathology. 2007;97:311–7.
4. Mesterházy Á, Lemmens M, Reid LM. Breeding for resistance to ear rots caused by *Fusarium* spp. in maize - a review. Plant Breed. 2012;131:1–19.
5. Schmale DG, Munkvold GP. Mycotoxins in crops: a threat to human and domestic animal health. Plant Heal Instr. 2014;DOI: 10.1094/PHI-I-2009-0715-01.
6. Bhat R, Rai R, Karim A. Mycotoxins in food and feed: present status and future concerns. Compr Rev Food Sci Food Saf. 2010;9:57–81.
7. Wild CP, Gong YY. Mycotoxins and human disease: A largely ignored global health issue. Carcinogenesis. 2009;31:71–82.
8. Kimanya ME, De Meulenaer B, Roberfroid D, Lachat C. Fumonisin exposure through maize in complementary foods is inversely associated with linear growth of infants in Tanzania. Mol Nutr Food Res. 2010;54:1659–67.
9. Mutiga SK, Were V, Hoffmann V, Harvey JW, Milgroom MG, Nelson RJ. Extent and drivers of mycotoxin contamination: inferences from a survey of Kenyan maize mills. Phytopathology. 2014;104:1221–31.
10. Fandohan P, Gnonlonfin B, Hell K, Marasas WFO, Wingfield MJ. Natural occurrence of *Fusarium* and subsequent fumonisin contamination in preharvest and stored maize in Benin, West Africa. Int J Food Microbiol. 2005;99:173–83.
11. Marasas WFO, Riley RT, Hendricks KA, Stevens VL, Sadler TW, Gelineau-van Waes J, et al. Fumonisins disrupt sphingolipid metabolism, folate transport, and neural tube development in embryo culture and in vivo: a potential risk factor for human neural tube defects among populations consuming fumonisin-contaminated maize. J Nutr. 2004;134:711–6.
12. Missmer SA, Suarez L, Felkner M, Wang E, Alfred H, Rothman KJ, et al. Exposure to fumonisins and the occurrence of neural tube defects along the Texas-Mexico border. Environ Health Perspect. 2006;114:237–41.
13. Munkvold GP, Desjardins AE. Fumonisins in maize: Can we reduce their occurrence? Plant Dis. 1997;81:556–65.
14. Yoshizawa T, Yamashita A, Luo Y. Fumonisin occurrence in corn from high- and low-risk areas for human esophageal cancer in China. Appl Environ Microbiol. 1994;60:1626–9.
15. Sydenham EW, Thiel PG, Marasas WF, Shephard GS, Schalkwyk DJ Van, Koch KR. Natural occurrence of some *Fusarium* mycotoxins in corn from low and

high esophageal cancer prevalence areas of Transkei, southern Africa. J Agric Food Chem. 1990;38:1900–3.
16. Marasas WFO, Riley RT, Hendricks KA, Stevens VL, Sadler TW, Waes JG, et al. Fumonisins disrupt sphingolipid metabolism, folate transport, and neural tube development in embryo culture and in vivo: a potential risk factor for human neural tube defects among populations consuming. J Nutr. 2004;134:711–6.
17. Blom HJ, Shaw GM, den Heijer M, Finnell RH. Neural tube defects and folate: case far from closed. Nat Rev Neurosci. 2006;7:724–31.
18. Kellerman T, Marasas W, Thiel P, Gelderblom WCA, Cawood M, Coetzer J. Leukoencephalomalacia in two horses induced by oral dosing of fumonisin B1. Onderstepoort J Vet Res. 1990;57:269–75.
19. Colvin BM, Harrison LR. Fumonisin-induced pulmonary edema and hydrothorax in swine. Mycopathologia. 1992;117:79–82.
20. Robertson LA, Kleinschmidt CE, White DG, Payne GA, Maragos CM, Holland JB. Heritabilities and correlations of Fusarium ear rot resistance and fumonisin contamination resistance in two maize populations. Crop Sci. 2006;46:353–61.
21. Robertson-Hoyt LA, Jines MP, Balint-Kurti PJ, Kleinschmidt CE, White DG, Payne GA, et al. QTL mapping for Fusarium ear rot and fumonisin contamination resistance in two maize populations. Crop Sci. 2006;46:1734–43.
22. Horne DW, Eller MS, Holland JB. Responses to recurrent index selection for reduced Fusarium ear rot and lodging and for increased yield in maize. Crop Sci. 2016;56:85–94.
23. Zila CT, Ogut F, Romay MC, Gardner CA, Buckler ES, Holland JB. Genome-wide association study of Fusarium ear rot disease in the U.S.A. maize inbred line collection. BMC Plant Biol. 2014;14:372.
24. Poland JA, Balint-Kurti PJ, Wisser RJ, Pratt RC, Nelson RJ. Shades of gray: the world of quantitative disease resistance. Trends Plant Sci. 2009;14:21–9.
25. Eller MS, Holland JB, Payne GA. Breeding for improved resistance to fumonisin contamination in maize. Toxin Rev. 2008;27:371–89.
26. Chen J, Shrestha R, Ding J, Zheng H, Mu C, Wu J, et al. Genome-wide association study and QTL mapping reveal genomic loci associated with Fusarium ear rot resistance in tropical maize germplasm. G3. 2016;6:3803–15.
27. Costa RS, Môro FV, Môro JR, da Silva HP, Panizzi RDC. Relação entre características morfológicas da cariopse e fusariose em milho. Pesqui Agropecu Bras. 2003;38:27–33.
28. Hoenisch RW, Davis RM. Relationship between kernel pericarp thickness and susceptibility to Fusarium ear rot in field corn. Plant Dis. 1994;78:517–9.
29. Sampietro DA, Vattuone MA, Presello DA, Fauguel CM. The pericarp and its surface wax layer in maize kernels as resistance factors to fumonisin accumulation by *Fusarium verticillioides*. Crop Prot. 2009;28:196–200.
30. Blandino M, Reyneri A, Colombari G, Pietri A. Comparison of integrated field programmes for the reduction of fumonisin contamination in maize kernels. Field Crop Res. 2009;111:284–9.

31. Presello DA, Iglesias J, Botta G, Eyherabide GH. Severity of Fusarium ear rot and concentration of fumonisin in grain of Argentinian maize hybrids. Crop Prot. 2007;26:852–5.
32. Bluhm BH, Woloshuk CP. Amylopectin induces fumonisin B1 production by *Fusarium verticillioides* during colonization of maize kernels. MPMI. 2005;18:1333–9.
33. Sampietro DA, Fauguel CM, Vattuone MA, Presello DA, Catalán CAN. Phenylpropanoids from maize pericarp: Resistance factors to kernel infection and fumonisin accumulation by *Fusarium verticillioides*. Eur J Plant Pathol. 2013;135:105–13.
34. Gao X, Kolomiets M V. Host-derived lipids and oxylipins are crucial signals in modulating mycotoxin production by fungi. Toxin Rev. 2009;28:79–88.
35. Martins VF, Vaughan MM, Huffaker A, Schmelz EA., Christensen S, Sims J, et al. Seed treatment with live or dead *Fusarium verticillioides* equivalently reduces the severity of subsequent stalk rot. J Phytopathol. 2014;162:201–4.
36. Mutiga SK, Morales L, Angwenyi S, Wainaina J, Harvey J, Das B, et al. Association between agronomic traits and aflatoxin accumulation in diverse maize lines grown under two soil nitrogen levels in Eastern Kenya. F Crop Res. 2017;205:124–34.
37. Duncan KE, Howard RJ. Biology of maize kernel infection by *Fusarium verticillioides*. Mol Plant-Microbe Interact. 2010;23:6–16.
38. Murillo I, Cavallarin L, San Segundo B. Cytology of infection of maize seedlings by *Fusarium moniliforme* and immunolocalization of the pathogenesis-related PRms protein. Phytopathology. 1999;89:737–47.
39. Blandino M, Reyneri A. Comparison between normal and waxy maize hybrids for *Fusarium*-toxin contamination in NW Italy. Maydica. 2007;52:127–34.
40. Fox G, Manley M. Hardness methods for testing maize kernels. J Agric Food Chem. 2009;57:5647–57.
41. Czembor E, Ochodzki P. Resistance of flint and dent maize forms for colonization by *Fusarium* spp. and mycotoxins contamination. Maydica. 2009;54:263–7.
42. Butron A, Santiago R, Mansilla P, Pintos-Varela C, Ordas A, Malvar RA. Maize (*Zea mays* L.) genetic factors for preventing fumonisin contamination. J Agric Food Chem. 2006;54:6113–7.
43. Headrick JM, Pataky JK, Juvik JA. Relationships among carbohydrate content of kernels, condition of silks after pollination, and the response of sweet corn inbred lines to infection of kernels by *Fusarium moniliforme*. Phytopathology. 1990;80:487–94.
44. Zummo N, Scott GE. Cob and kernel infection by *Aspergillus flavus* and *Fusarium* moniliforme in inoculated, field-grown maize ears. Plant Dis. 1990;74:627–31.
45. Burr S, Fry S. Feruloylated arabinoxylans are oxidatively cross-linked by extracellular maize peroxidase but not by horseradish peroxidase. Mol Plant. 2009;2:883–92.
46. Lanubile A, Ferrarini A, Maschietto V, Delledonne M, Marocco A, Bellin D. Functional genomic analysis of constitutive and inducible defense responses to

Fusarium verticillioides infection in maize genotypes with contrasting ear rot resistance. BMC Genomics. 2014;15:710.
47. Dall'Asta C, Giorni P, Cirlini M, Reverberi M, Gregori R, Ludovici M, et al. Maize lipids play a pivotal role in the fumonisin accumulation. World Mycotoxin J. 2015;8:87–97.
48. Wang Y, Zhou Z, Gao J, Wu Y, Xia Z, Zhang H, et al. The mechanisms of maize resistance to *Fusarium verticillioides* by comprehensive analysis of RNA-seq data. Front Plant Sci. 2016;7:1654.
49. Munkvold GP. Cultural and genetic approaches to managing mycotoxins in maize. Annu Rev Phytopathol. 2003;41:99–116.
50. Arino A, Herrera M, Juan T, Estopanan G, Carraminana JJ, Rota C, et al. Influence of agricultural practices on the contamination of maize by fumonisin mycotoxins. J Food Prot. 2009;72:898–902.
51. Jimenez M, Mateo JJ, Hinojo MJ, Mateo R. Sugars and amino acids as factors affecting the synthesis of fumonisins in liquid cultures by isolates of the *Gibberella fujikuroi* complex. Int J Food Microbiol. 2003;89:185–93.
52. Kohut G, Ádám AL, Fazekas B, Hornok L. N-starvation stress induced FUM gene expression and fumonisin production is mediated via the HOG-type MAPK pathway in *Fusarium proliferatum*. Int J Food Microbiol. 2009;130:65–9.
53. Freeman H, Omiti J. Fertilizer use in semi-arid areas of Kenya: analysis of smallholder farmers' adoption behavior under liberalized markets. Nutr Cycl Agroecosystems. 2003;66:22–31.
54. Afolabi CG, Bandyopadhyay R, Leslie JF, Ekpo EJA. Effect of sorting on incidence and occurrence of fumonisins and *Fusarium verticillioides* on maize from Nigeria. J Food Prot. 2006;69:2019–23.
55. Fandohan P, Ahouansou R, Houssou P, Hell K, Marasas WFO, Wingfield MJ. Impact of mechanical shelling and dehulling on *Fusarium* infection and fumonisin contamination in maize. Food Addit Contam. 2006;23:415–21.
56. Humpf H-U, Voss KA. Effects of thermal food processing on the chemical structure and toxicity of fumonisin mycotoxins. Mol Nutr Food Res. 2004;48:255–69.
57. Dombrink-Kurtzman MA, Dvorak TJ, Barron ME, Rooney LW. Effect of nixtamalization (alkaline cooking) on fumonisin-contaminated corn for production of masa and tortillas. J Agric Food Chem. 2000;48:5781–6.
58. Palencia E, Torres O, Hagler W, Meredith FI, Williams LD, Riley RT. Total fumonisins are reduced in tortillas using the traditional nixtamalization method of Mayan communities. J Nutr. 2003;133:3200–3.
59. Stasiewicz MJ, Falade TDO, Mutuma M, Mutiga SK, Harvey JJW, Fox G, et al. Multi-spectral kernel sorting to reduce aflatoxins and fumonisins in Kenyan maize. Food Control. 2017;78:203–14.
60. Pearson TC, Wicklow DT, Pasikatan MC. Reduction of aflatoxin and fumonisin contamination in yellow corn by high-speed dual-wavelength sorting. Cereal Chem. 2004;81:490–8.
61. Pearson TC, Wicklow DT, Brabec DL. Characteristics and sorting of white food corn contaminated with mycotoxins. Appl Eng Agric. 2010;26:109–13.

62. Shetty PH, Bhat R V. A physical method for segregation of fumonisin-contaminated maize. Food Chem. 1999;66:371–4.
63. Busman M, Butchko RAE, Proctor RH. LC-MS/MS method for the determination of the fungal pigment bikaverin in maize kernels as an indicator of ear rot. Food Addit Contam Part A. 2012;29:1736–42.
64. Lazzaro I, Busman M, Battilani P, Butchko RAE. FUM and BIK gene expression contribute to describe fumonisin and bikaverin synthesis in *Fusarium verticillioides*. Int J Food Microbiol. 2012;160:94–8.
65. Butchko RAE, Brown DW, Busman M, Tudzynski B, Wiemann P. Lae1 regulates expression of multiple secondary metabolite gene clusters in *Fusarium verticillioides*. Fungal Genet Biol. 2012;49:602–12.
66. Zila CT, Samayoa LF, Santiago R, Butrón A, Holland JB. A genome-wide association study reveals genes associated with Fusarium ear rot resistance in a maize core diversity panel. G3. 2013;3:2095–104.
67. Perez-Brito D, Jeffers D, Gonzalez-de-Leon D, Khairallah M, Cortes-Cruz M, Velazquez-Cardelas G, et al. QTL mapping of *Fusarium moniliforme* ear rot resistance in high land maize, Mexico. Agrociencia. 2001;35:181–96.
68. Brown PJ, Upadyayula N, Mahone GS, Tian F, Bradbury PJ, Myles S, et al. Distinct genetic architectures for male and female inflorescence traits of maize. PLoS Genet. 2011;7:e1002383.
69. Cook JP, McMullen MD, Holland JB, Tian F, Bradbury P, Ross-Ibarra J, et al. Genetic architecture of maize kernel composition in the nested association mapping and inbred association panels. Plant Physiol. 2012;158:824–34.
70. Blandino M, Reyneri A. Effect of maize hybrid maturity and grain hardness on fumonisin and zearalenone contamination. Ital J Agron. 2008;2:107–17.

CHAPTER 2

LEVERAGING VARIATION IN SYMPTOMATOLOGY TO REDUCE FUMONISIN CONTAMINATION IN MAIZE GRAIN

Introduction

In maize (*Zea mays* L), the filamentous ascomycete fungus *Fusarium verticillioides* causes Fusarium ear rot (FER) and produces the mycotoxin (toxic fungal secondary metabolite) fumonisin, which can compromise human and animal health and reduce yields (1,2). The environmental conditions of the tropics and sub-tropics are conducive to *F. verticillioides* infection and subsequent fumonisin contamination in maize (3–5). In addition, food systems in these regions provide minimal regulation of mycotoxins, leading to high levels of fumonisin exposure (6,3).

Although fumonisin cannot be completely removed from foodstuffs, pre- and post-harvest interventions can reduce fumonisin levels. Breeding varieties resistant to fumonisin contamination is one strategy, as this trait is highly heritable and thus can be effectively selected for (7–10). Agronomic practices such as irrigation and crop rotation can minimize infection and fumonisin accumulation by *F. verticillioides* in the field (11,12). At the post-harvest stage, chemical and heat treatments can remove fumonisin from maize products (13,14), while visual and spectral methods can remove the small proportion of kernels with the highest levels of fumonisin from bulk grain samples (15,16). Identifying proxies for fumonisin, which is costly to quantification, can potentially aid grain sorting efforts and alleviate breeding expenses (9,17,18).

Spatiotemporal interactions among abiotic and biotic factors, plant development and physiology, and pathogen populations affect pathogenesis and its manifestation of external and internal symptoms (3,19,4). Under experimental conditions, the mode of inoculum introduction further influences inference on disease

severity and genetic variation in resistance (20,21). Employing multi-environment trials and diverse inoculation methods may be necessary for understanding the biological basis of resistance.

In this study, 50 maize inbred breeding lines were inoculated with *F. verticillioides* using two methods representing distinct infection pathways: inundative and point inoculation. Under inundative inoculation (10), liquid inoculum is injected into the silk channel and underneath the husk, thereby making widespread contact with the kernels and other tissues. The point method (22) initiates infection at a single location by penetrating the ear with a spore-coated toothpick, providing the fungus access to both cob and kernel tissues. The inundative method may simulate infection via the silk channel, while the point method may simulate infection promoted by insect damage. I leveraged these two inoculation strategies to dissect the symptomatology of *F. verticillioides*-infected maize grain and to identify kernel traits as proxies for fumonisin contamination.

Materials and methods

Field design and inoculation

Fifty maize inbred lines (Table 2.1) with varying levels of resistance to Fusarium ear rot (FER) and fumonisin contamination (8,23,22,24–26) were grown at the Central Crops Research Station in Clayton, NC in 2015 with two completely randomized replicates. No seeds germinated in one plot, resulting in 99 total plots. Each plot was split into two subplots by point inoculating half of the primary ears (22,21) and inundatively inoculating the other half (10). Forty-five of the lines had two replicates from both inoculation methods. Because of suboptimal germination, four lines had two inundative replicates and one under point inoculation, and one line had one replication per inoculation method. There were 194 subplots total.

With the point method, one toothpick coated with spores from local toxigenic *F. verticillioides* isolates was inserted into the middle of each developing primary ear approximately two weeks after silking, and the toothpick remained in the ear until harvest. Six local *F. verticillioides* isolates (NC-36D, NC-40A, NC-40J, NC-N16, NC-N17, and NC-40N) selected for high fumonisin production *in vitro* were used for inundative inoculation. The isolates were cultured individually on potato dextrose agar. Conidia were collected by rinsing the plates with distilled water, and the conidial suspension was diluted to a final inoculum concentration of approximately 1×10^6 conidia mL^{-1}. Approximately two weeks after silking, 5 mL of conidial suspension was injected into the silk channel of each primary ear with a vaccinator, and one week later another 5 mL of inoculum was injected under the husk leaves.

Disease phenotyping

Primary ears were harvested from each subplot at maturity, dried, and then visually evaluated for FER. FER was scored based on the percentage of the kernels presenting symptoms on a 1-100% scale with 5% increments (10). The average FER score of all the ears in each subplot was then calculated. In order to account for the qualitative variation in FER symptomatology, each ear was assigned a symptom type: asymptomatic, blush, starburst, purple, or moldy (Fig. 2.1). Blush kernels had pink discoloration of the kernel crown; starburst kernels were characterized by white or pink streaks radiating from the kernel crown; purple kernels had severe purple or brownish discoloration, and moldy kernels were severely degraded and had matted fungal growth (Fig. 2.1). Each subplot was assigned a main symptom type based on the most frequent symptom type of the ears in the subplot. Subplots with equal representation from more than on symptom type were labeled “multiple”. Subplots with less than 10% average FER were considered asymptomatic.

Ears were then shelled and bulked per subplot. The bulk density of grain from each subplot was calculated as the weight of a random 250 mL volume of kernels. All kernels in each bulked subplot were ground into a fine powder with a Waring 7010 two-speed laboratory blender (Waring Commercial, Inc., Torrington, CT). A 10 g subsample from each ground bulk was put in a 25 mL centrifuge tube. To extract fumonisin, 20 mL of 90% methanol was added to each 25 mL tube, resulting in a two-fold dilution factor at this step. The tubes were then shaken with a Lab-Line Environ Orbitol Shaker (Lab-Line Instruments, Inc., Melrose Park, IL) at 150 rpm for approximately five minutes. The samples settled for 15 minutes, after which 0.5 mL of supernatant from each sample was transferred to a 15 mL centrifuge tube. To dilute to supernatant to a final 40-fold dilution, 9.5 mL of distilled water was added to each 15 mL tube. Fumonisin was quantified with fumonisin-specific enzyme-linked immunosorbent assay (ELISA) kits (Helica Biosystems, Inc., Santa Ana, CA). Absorbance at 450 nm of the ELISA plates was read using a BioTek μQuant™ microplate spectrophotometer (BioTek Instruments, Inc., Winooski, VT) paired with Gen5™ software (BioTek Instruments, Inc., Winooski, VT). Samples that had fumonisin levels predicted to be above the highest standard provided by the ELISA kits, 6 $\mu g\ g^{-1}$ (ppm), were serially diluted until their predicted fumonisin levels were within the standard curve. The ratio of fumonisin to FER (FUM:FER) was calculated as FUM/(FER+1). One was added to all FER data to adjust 0% FER scores in the denominator.

Bikaverin was extracted from ground bulk samples as described by Busman et al. (18). A 0.2 g subsample from each ground bulk and 1 mL of 1:1 acetonitrile/ethyl acetate were added to a 2 mL centrifuge tube, and the tubes were occasionally mixed for three hours. The supernatant from each sample was then transferred to a clean 2 mL centrifuge tube. Stock solution of 10 ppm bikaverin was prepared by dissolving

pure bikaverin (AdipoGen Corp., San Diego, CA) in 1:1 acetonitrile/ethyl acetate. Five other bikaverin standards were prepared by diluting the stock solution further with 1:1 acetonitrile/ethyl acetate to final concentrations of 0.25, 0.5, 1, 2.5, and 5 ppm. One hundred µL of the six bikaverin standards and 90 unknown extracts were transferred to 96-well glass-coated microplates. Absorbance at 518 nm was read using a BioTek Synergy 2 multi-mode plate reader (BioTek Instruments, Inc., Winooski, VT) paired with Gen5™ software (BioTek Instruments, Inc., Winooski, VT).
Seven maize lines were selected for further analysis at the symptom type level (Table 2.1). Six of the lines had two paired subplot samples. One line had two pairs of subplot samples from both field replications. From each of the 16 total subplot samples, approximately 25 asymptomatic kernels and 25 symptomatic kernels were randomly selected. This yielded a total of 44 samples representative of four symptom type classes: asymptomatic, blush, starburst, purple. These subplot samples had very few moldy kernels, so the "moldy" category was not included in these experiments. The bulk density of each 25-kernel sample was calculated as the weight divided by the bulk volume of the 25 kernels. Approximately five kernels were randomly selected from each sample, weighed, and ground to a fine powder using an IKA® Tube Mill (IKA® Works, Inc., Wilmington, NC). Fumonisin was extracted and quantified using the same ELISA kit protocols described previously (Helica Biosystems, Inc., Santa Ana, CA). Approximately 10 kernels were randomly selected from each sample and ground to a fine powder using an IKA® Tube Mill (IKA® Works, Inc., Wilmington, NC). Bikaverin was extracted and quantified using the protocol described previously.

Data transformation

The raw FER, fumonisin, bulk density, bikaverin, and FUM:FER data were not normally distributed (Fig. 2.2). Box-Cox transformations were performed using JMP®

(27) software to normalize the data, where $\lambda=0$ for FUM, FUM:FER, and bikaverin; $\lambda=0.2$ for FER, and $\lambda=2$ for bulk density (Fig. 2.2). The raw fumonisin, bulk density, and bikaverin discrete symptom type data were also Box-Cox-transformed, where $\lambda=0$, 2, and 0.4, respectively. Because Box-Cox transformation of bulk density returned negative values, one was added to all Box-Cox-transformed bulk density values to positivize the data.

Linear models and heritability

All models described in this section were analyzed using JMP® software. Subplot Box-Cox-transformed FER, fumonisin, bulk density, bikaverin, and FUM:FER under the two inoculation methods were compared with one-tailed and two-tailed t-tests. A likelihood ratio test with a χ^2 distribution was used to compare the composition of symptom types under the two inoculation methods. General linear models assuming a binomial distribution and employing a logit link function were fit with the absence or presence of each symptom type as the response and inoculation method as a fixed effect. Correlations among Box-Cox-transformed FER, fumonisin, bulk density, and bikaverin for all subplot data combined and by inoculation method were calculated. Box-Cox-transformed FER, fumonisin, bulk density, bikaverin, and FUM:FER versus symptom type for all subplot data combined and by inoculation method were assessed with ANOVA and pairwise two-tailed t-tests.

Mixed linear models including Box-Cox-transformed fumonisin, bulk density, and bikaverin as separate response variables were fit with Box-Cox-transformed FER and symptom type as fixed effects for all subplot data combined and by inoculation method. Mixed linear models were fit including Box-Cox-transformed FER, fumonisin, bikaverin, bulk density, and FUM:FER as separate response variables with (1) inoculation method and line as fixed effects and field replication and

block[replication] as random variables for all subplot data combined and (2) line as a fixed effect and replication and block[replication] as random effects by inoculation method.

Multivariate mixed linear models were fit including Box-Cox-transformed FER, fumonisin, bikaverin, and bulk density as the response with (1) inoculation method and line as fixed effects and field replication and block[replication] as random variables for all subplot data combined and (2) line as a fixed effect and replication and block[replication] as random effects by inoculation method. Least-square (LS) means of lines were then extracted from combined and inoculation method-specific models to calculate genetic correlations among FER, fumonisin, bikaverin, and bulk density.

Random linear models were fit with Box-Cox-transformed FER, fumonisin, bikaverin, bulk density, and FUM:FER as separate response variables and line, replication, and block[replication] as random effects for all subplot data combined and by inoculation method. Broad-sense heritability (H) was estimated as $\sigma^2_G/(\sigma^2_G+\sigma^2_e/r)$, where r is the number of replications, and σ^2_e and σ^2_G are the error and genetic variance components, respectively (18). H was calculated for all traits for all subplot data combined and by inoculation method.

The following describe analyses conducted on data from discrete symptom type samples. Box-Cox-transformed fumonisin, bulk density, and bikaverin versus symptom type were assessed with ANOVA. Box-Cox-transformed fumonisin, bulk density, and bikaverin among symptom types were compared with pairwise two-tailed t-tests. Box-Cox-transformed bulk density and bikaverin of samples with raw fumonisin contamination < 2 ppm versus samples with fumonisin ≥ 2 ppm were compared with one-tailed and two-tailed t-tests.

Predictions

Principal component analysis (PCA) was conducted using JMP® software. Three PCA models including Box-Cox-transformed bulk density, FER, and bikaverin were constructed for all subplot data combined and by inoculation method. The first two principal components (PC) were extracted, and each observation was assigned to one of the four Cartesian quadrants of the first two PCs. The composition of points in the four quadrants versus fumonisin group (< 2 ppm and ≥ 2 ppm) was assessed with a likelihood ratio test with a χ^2 distribution. General linear models assuming a binomial distribution and employing a logit link function were fit with the absence or presence in each quadrant as the response and fumonisin group as a fixed effect.

Linear discriminant analysis (LDA) was conducted using the MASS package (28) in R version 3.3.1 (29). LDA models with Box-Cox-transformed FER, bulk density, and bikaverin as covariates were constructed to discriminate subplot samples with fumonisin contamination below and above five thresholds: 2, 4, 6, 8, and 10 ppm. LDA models were applied to all subplot data combined and by inoculation method. LDA models with transformed bulk density were constructed to discriminate discrete symptom type samples with fumonisin below 2 ppm from samples with fumonisin greater than or equal to 2 ppm for all data combined and by inoculation method. All LDA models were five-fold cross-validated with ten replications.

The bulk density grand mean of all discrete symptom type samples (approximately 0.59 g mL^{-1}) was calculated and used as a threshold to separate samples into two groups: samples with bulk density below the threshold ("low-density") and samples with bulk density greater than or equal to the threshold ("high-density"). The fumonisin content of each sample was calculated as the fumonisin concentration multiplied by the weight. The fumonisin content and weight of samples from the same subplot were added to calculate the total weight and fumonisin content

of each subplot. Within each subplot, samples were assigned to low- and high-density groups and the fumonisin content and weight of each group were calculated. Percentages of fumonisin content and weight of the two density groups versus the total of the subplot were then calculated.

Results

FER, fumonisin, bulk density, and bikaverin are correlated

For both inoculation methods, a wide range of qualitative and quantitative phenotypes was observed (Fig. 2.2). All samples had detectable levels of fumonisin and only two samples (1% of total) were asymptomatic, demonstrating that both inoculation methods were successful and yielded few escapes (Table 2.2). FER, fumonisin, and bikaverin were positively phenotypically and genetically correlated with each other and negatively correlated with bulk density (Figs. 2.3-6).

Disease severity is greater under inundative inoculation

Inundative inoculation yielded higher FER, fumonisin, FUM:FER, and bikaverin and more greatly reduced bulk density than point inoculation (Fig. 2.7). Phenotypic and genetic correlations among FER, fumonisin, bikaverin, and bulk density were greater under inundative inoculation (Figs. 2.4-6).

The composition of symptom types was significantly different between the two inoculation methods (likelihood ratio test, χ^2=38.083, P<0.0001) (Fig. 2.7), with a greater representation of severe and pigmented symptom types under inundative inoculation (Fig. 2.7, Table 2.2). Specifically, the inundative method yielded a greater proportion of purple and blush and fewer starburst subplot samples than point inoculation (Fig. 2.7, Table 2.2). A uniform spread of symptom types was observed under point inoculation (Fig. 2.7).

External symptomatology tracks fumonisin contamination and bulk density

The following results refer to subplot samples. Symptom type was significantly associated with FER, fumonisin, and bikaverin (Table 2.3). Blush and starburst samples tended to have the highest FER scores (Table 2.3). Although purple samples had low FER on average, they had the highest fumonisin contamination and FUM:FER (Table 2.3). Asymptomatic samples had the lowest fumonisin overall, and although ANOVA indicated that bulk density did not significantly differ among symptom types, pairwise two-tailed t-tests revealed that asymptomatic samples had higher bulk density than any of the symptomatic groups (Table 2.3). Bikaverin differed significantly among symptom types under point inoculation only (Table 2.3), but this result is driven by the one blush sample – if this sample was removed from the model, symptom type was not significantly associated with bikaverin (P=0.35).

FER was significantly associated with fumonisin and bulk density in all models and with bikaverin in the combined and point inoculation-specific models (Table 2.4). After controlling for FER, fumonisin was significantly and marginally associated with symptom type in the combined and point inoculation-specific models, respectively; bulk density was marginally and significantly associated with symptom type in the combined and inundative-specific analyses, and bikaverin was marginally and significantly associated with symptom type in the combined and point inoculation models, respectively (Table 2.4). The purple symptom type had the highest fumonisin levels after controlling for FER in combined and point inoculation analyses. Although purple and moldy samples had the lowest FER scores (Table 2.3), they had the lowest bulk density after controlling for FER severity (Table 2.4).

In the discrete symptom type samples, ANOVA indicated that symptom types differed significantly with respect to bulk density and fumonisin (Table 2.5). Purple

kernels had the highest fumonisin contamination and lowest bulk density, while asymptomatic kernels had the lowest fumonisin and highest bulk density (Fig. 2.8, Table 2.5). The blush and starburst symptom types were intermediate with respect to fumonisin and bulk density (Fig. 2.8, Table 2.5). Although ANOVA of bikaverin vs. symptom type was only marginally significant, pairwise t-tests indicated that purple and starburst kernels had higher bikaverin than blush kernels (Table 2.5). Samples over the regulatory limit of 2 ppb fumonisin (10) had marginally significantly higher bikaverin than legal fumonisin samples (< 2 ppm) (one-tailed t-test, t-ratio=1.47, P=0.07).

Genetic variation detected for resistance to *F. verticillioides* infection is higher under inundative inoculation

In the mixed models of FER, fumonisin, bulk density, and FUM:FER versus inoculation method, line, replication, and block[replication], both inoculation method and line were significantly associated with the response (Table 2.6). Line was significantly associated with FER, fumonisin, bulk density, and FUM:FER in the combined and inundative models and was significantly associated with bulk density and marginally associated with FER and fumonisin under point inoculation (Table 2.6). Inoculation method but not line was significantly associated with bikaverin (Table 2.6).

Broad-sense heritability (H) for FER, fumonisin, bulk density, and FUM:FER was highest under inundative inoculation (Table 2.7). Bulk density had the highest heritability of the five traits in combined and point-specific analyses, and fumonisin was the most heritable trait under inundative inoculation (Table 2.7). There was genetic variation for bikaverin only under point inoculation, with H=0.20 (Table 2.7).

Prediction of fumonisin contamination is poor in bulked samples

PCA including Box-Cox-transformed FER, bulk density, and bikaverin demonstrated limited but significant (likelihood ratio test, χ^2=12.600, P=0.0056) separation of subplot samples with levels of fumonisin over the regulatory limit (≥ 2 ppm, "illegal") from "legal" samples (< 2 ppm fumonisin) (Fig. 2.9, Table 2.8). The first two PCs explained 76% of the total variance in the subplot data. LDA to discriminate illegal subplot samples from legal samples based on five fumonisin thresholds using Box-Cox-transformed FER, bulk density, and bikaverin as covariates had poor accuracy, which may have been due to the small proportion of subplot samples with low levels of fumonisin (Fig. 2.10).

Bulk density accurately predicts fumonisin in discrete symptom type samples

Sixteen subplots were selected for analyses at the symptom type level. From each subplot, 25 asymptomatic and 25 symptomatic kernels were selected. The kernels within each symptomatic set all exhibited the sample symptom type (blush, starburst, or purple). The asymptomatic and symptomatic kernel sets will be referred to as the "discrete symptom type" samples in this section.

Box-Cox-transformed bulk density was positively associated with Box-Cox-transformed fumonisin (R^2=0.72, P<0.0001) in discrete symptom type samples. Bulk density was lower in discrete symptom type samples with "illegal" levels fumonisin (≥ 2 ppm) than in "legal" samples with < 2 ppm fumonisin (one- and two-tailed t-tests, P<0.0001) (Fig. 2.11).

A bulk density threshold based on the grand mean of bulk density for all discrete symptom type samples (0.59 g mL^{-1}) was used to classify low-density (bulk density < 0.59 g mL^{-1}) and high-density (bulk density ≥ 0.59 g mL^{-1}) samples. Low-density samples represented a significantly lower proportion of the total subplot

sample weight (one- and two-tailed t-tests, $P<0.0001$) and a higher proportion of the fumonisin in the subplot than high-density samples (one- and two-tailed t-tests, $P<0.0001$). The low-density samples accounted for approximately one quarter of the total sample weight (3.78 ± 0.35 g) but contained more than 98% of the total fumonisin content on average (1.07 ± 0.20 ng fumonisin), compared to high-density samples that composed more than 75% of the total weight (11.71 ± 0.55 g) but less than 2% of the total fumonisin content (0.007 ± 0.002 ng fumonisin) (Fig. 2.12). LDA models using Box-Cox-transformed bulk density to discriminate samples with legal fumonisin contamination (< 2 ppm) from illegal samples (≥ 2 ppm) had high accuracy, sensitivity, and specificity in all analyses (Table 2.9).

Discussion

In the context of breeding, inundative inoculation may be more useful than the point method, yielding higher disease severity, phenotypic and genetic correlations among indicators of *F. verticillioides* infection, and broad-sense heritabilities. Clements et al. (21) demonstrated that injection of liquid spore suspension into the silk channel resulted in the greatest disease severity and was the only method conducive to fumonisin accumulation and capable of differentiating maize hybrids. In contrast, here point inoculation did induce fumonisin accumulation and revealed marginally significant genetic effects. In addition, the interaction between inoculation method and genotype was not significant ($P>0.05$) for any of the disease severity traits, demonstrating that rankings of genotypic resistance do not differ between the two inoculation methods. However, these two inoculation methods may expose different types of resistance mechanisms. For example, silk-mediated resistance may be induced under inundative inoculation, while the cob might be more important under point inoculation.

Although point inoculation may be suboptimal for breeding, the wide phenotypic variation resulting from combining the two inoculation methods allowed for a more detailed dissection of symptomatology than previous studies. Our characterization of symptom types complements published findings wherein visibly moldy kernels had more fumonisin than starburst kernels (19,4) by further dividing external symptomatology into two moderate and two extreme types. External symptom severity clearly tracks internal symptom severity with respect to bulk density and fumonisin contamination.

Unlike the inundative method, point inoculation results in fumonisin levels comparable to those found in naturally infected grain (3,19,4,30,31). Point infection may simulate insect damage to the cob and thus may be useful for identifying sources of resistance to insect-mediated infection and fumonisin contamination. Given that insect damage is an important avenue for *F. verticillioides* infection and that it has been shown to be the major contributor to FER severity and fumonisin contamination in previous studies (19,4), it would be of interest to identify sources of resistance that may reduce the spread of the pathogen via the cob.

Zummo and Scott (32) demonstrated that *F. verticillioides* infection was greatest in the cob sclerenchyma and placenta tissues and that kernels were most frequently infected through the pedicel. Because the toothpick is inserted into the cob, the point method may further encourage the fungus to first colonize the cob followed by the kernels via the pedicel. In addition, I demonstrate that a large proportion of point-inoculated samples exhibited the starburst symptom type, which has been shown to be the result of fungal dissolution of pericarp cell walls and intracellular hyphal extension (33). The combination of (1) the preference of *F. verticillioides* to infect the cob and pedicel, (2) the low oxygen environment of the endosperm (34), and (3) the rich starch reserves in the lower pericarp adjacent to the pedicel (35) may explain the

pathogenesis underlying the starburst symptom type, which was characteristic of point-inoculated samples.

Under inundative inoculation, *F. verticillioides* makes widespread contact with the developing kernel and cob tissues. Inundatively inoculated samples showed greater reductions in bulk density and higher FER, fumonisin, bikaverin, and FUM:FER than point-inoculated samples and the majority exhibited the purple symptom type. The correlation among disease phenotypes was also higher under inundative inoculation. Parsons and Munkvold (4) found that fumonisin contamination was more strongly correlated with the percentage of visibly moldy kernels than with starburst symptoms, suggesting that the higher proportion of purple kernels under inundative inoculation could explain the higher correlation between fumonisin and FER. The larger inoculum load of the inundative method could allow for rapid and extensive infection of kernels by the fungus.

Reduction of fumonisin content, an expensive and time-intensive trait to phenotype, can be accomplished via indirect selection for resistance to FER (23). In addition, bulk density and bikaverin levels have the potential to serve as proxies for fumonisin contamination, as demonstrated by previous findings and the results presented here. Kernel weight has been associated with FER severity and fumonisin contamination (36) and sorting based on buoyancy in saline solution has been shown to drastically reduce fumonisin content in maize grain (37). Maize varieties with higher grain hardness and density tend to have lower levels of fumonisin (9,17). Bikaverin, a red fungal pigment produced by many *Fusarium* spp., has also been used as an indicator of FER (18) and its biosynthesis is co-regulated with that of fumonisin (38).

In this study, bulk density was found to be an effective indicator of disease severity and fumonisin contamination. Reduced bulk density may be directly due to

kernel tissue degradation by *F. verticillioides*. However, trends in bulk density under *F. verticillioides* inoculation may be confounded by innate grain characteristics (39) and agronomic factors (40,41). Bulk density has the potential to substantially lower fumonisin levels in maize grain at the breeding and post-harvest stages. High phenotypic and genetic correlations indicate that reduction of FER and fumonisin content could potentially be accomplished via indirect selection of bulk density under *F. verticillioides* inoculation. Using discrete symptom type samples, I demonstrate that LDA using only bulk density can accurately predict fumonisin legality status (< 2 ppm or ≥ 2 ppm) and that a simple bulk density threshold can remove more than 98% of the fumonisin from only a quarter of the total sample weight. In addition, these findings are the first to employ a low-cost method of extraction and quantification of bikaverin that was significantly phenotypically and genetically correlated with FER and bulk density.

Tables and figures

Table 2.1. Fifty maize inbred lines included in experiments.

Line	Line
14CL1161-1	NCG1502[C]
14CL1162-1	NCG1503
14CL1164-1	NCG1504
B73	NCG1505[C]
CML373xNC320*[A]	NCG1506
FR1064	NCG1507[C]
GE440	NCG1508[C]
GEMS-0002	NCG1509
GEMS-0224	NCG1510
NC301	NCG1511
NC303	NCG1512
NC408	NCG1513
NC422	NCG1514
NC446	NCG1515
NC508[B]	NCG1516
NC524	NCG1517
NC526[C]	NCG1518
NC530	NCG1519
NC534	NCG1520
NC536	NCG1521[C]
NC538[B]	NCG1522
NC540[B]	NCG1523
NC542	NCG1524
NC544	NCG1525
NCG1501	P.3737xNC320*3[B,C]

[A]One replication per inoculation method; [B]Two replications under inundative and one under point inoculation; [C]Included in discrete symptom type analyses

Table 2.2. Binomial GLM summaries of symptom type (absence/presence) vs. inoculation method.

Response	**LR χ^2**	**P-value**	**Inundative**		**Point**	
			Present	**Absent**	**Present**	**Absent**
Asymptomatic	2.9	0.09^{MS}	0%, N=0	100%, N=99	2%, N=2	98%, N=93
Blush	13.8	0.0002**	14%, N=14	86%, N=85	1%, N=1	99%, N=94
Starburst	13.0	0.0003**	8%, N=8	92%, N=91	27%, N=26	73%, N=69
Purple	6.5	0.01*	49%, N=49	51%, N=50	32%, N=30	68%, N=65
Moldy	0.3	0.60^{NS}	23%, N=23	77%, N=76	20%, N=19	80%, N=76

LR=likelihood ratio; NS=not significant; MS=marginally significant (P<0.1); *0.05>P>0.01; **0.01>P>0.0001

Table 2.3. Box-Cox-transformed FER, fumonisin, bikaverin, bulk density, and FUM:FER least square means of the five symptom types and model summaries for combined and inoc. method-specific ANOVA of disease phenotype vs. symptom type.

Combined						
Statistic	**N**	**FER**	**Fumonisin**	**Bulk den.**	**Bikaverin**	**FUM:FER**
Asym. LS mean	2	0 ± 8.3 C	66 ± 11 C	0.76 ± 0.026 A	1.52 ± 0.26 A	3.70 ± 0.51 AB
Blush LS mean	15	50 ± 3.0 A	98 ± 3.9 AB	0.69 ± 0.009 B	1.18 ± 0.10 A	3.53 ± 0.19 AB
Starburst LS mean	34	46 ± 2.0 A	91 ± 2.6 AB	0.69 ± 0.006 B	1.27 ± 0.06 A	3.32 ± 0.12 B
Purple LS mean	79	38 ± 1.3 B	95 ± 1.7 A	0.69 ± 0.004 B	1.27 ± 0.04 A	3.73 ± 0.08 A
Moldy LS mean	42	35 ± 1.9 B	89 ± 2.3 B	0.70 ± 0.005 B	1.24 ± 0.06 A	3.45 ± 0.11 AB
Model R^2	172	0.23***	0.07*	0.04^{NS}	0.01^{NS}	0.05^{NS}
Inundative						
Statistic	**N**	**FER**	**Fumonisin**	**Bulk den.**	**Bikaverin**	**FUM:FER**
Asym. LS mean	0	NA	NA	NA	NA	NA
Blush LS mean	14	52 ± 2.5 A	99 ± 3.8 A	0.686 ± 0.010 A	1.25 ± 0.10 A	3.51 ± 0.18 A
Starburst LS mean	8	50 ± 3.4 A	98 ± 5.0 A	0.683 ± 0.013 A	1.36 ± 0.13 A	3.54 ± 0.24 A
Purple LS mean	49	41 ± 1.4 B	96 ± 2.0 A	0.682 ± 0.005 A	1.35 ± 0.05 A	3.70 ± 0.10 A
Moldy LS mean	23	39 ± 2.1 B	96 ± 3.0 A	0.690 ± 0.008 A	1.29 ± 0.08 A	3.68 ± 0.15 A
Model R^2	94	0.20**	0.005^{NS}	0.01^{NS}	0.01^{NS}	0.01^{NS}
Point						
Statistic	**N**	**FER**	**Fumonisin**	**Bulk den.**	**Bikaverin**	**FUM:FER**
Asym. LS mean	2	0 ± 9.0 C	66 ± 11 C	0.756 ± 0.024 A	1.52 ± 0.24 A	3.70 ± 0.53 AB
Blush LS mean	1	21 ± 12.7 ABC	86 ± 15 ABC	0.723 ± 0.034 AB	0.16 ± 0.33 B	3.83 ± 0.76 AB
Starburst LS mean	26	44 ± 2.5 A	89 ± 3.0 AB	0.693 ± 0.007 B	1.24 ± 0.07 A	3.25 ± 0.15 B
Purple LS mean	30	34 ± 2.3 B	93 ± 2.8 A	0.698 ± 0.006 B	1.14 ± 0.06 A	3.76 ± 0.14 A
Moldy LS mean	19	31 ± 2.9 B	81 ± 3.5 BC	0.706 ± 0.008 B	1.17 ± 0.08 A	3.20 ± 0.17 B
Model R^2	78	0.31***	0.13*	0.09^{NS}	0.15*	0.11^{NS}

LS means and standard errors (±) are reported in each symptom type/disease trait cell. Groups not connected by the same letter are significantly different (two-tailed t-test, $P<0.05$). Levels of significance of ANOVA for Box-Cox-transformed FER, fumonisin, bikaverin, bulk density, and FUM:FER vs. symptom type are denoted next to model R^2 values as: *$0.05>P\geq0.01$; **$0.01>P\geq0.0001$; ***$P<0.0001$; NS=not significant. LS means are colored by a yellow to red (relatively low to high) heat map.

Table 2.4. Box-Cox-transformed fumonisin, bulk density, and bikaverin LS means of the five symptom types, model summaries, and P-values of FER and symptom type fixed effects for combined and inoculation method-specific models of disease phenotype vs. FER and symptom type.

Combined				
Statistic	**N**	**Fumonisin**	**Bulk density**	**Bikaverin**
Asym. LS mean	2	92.6 ± 9.7 AB	0.689 ± 0.023 AB	1.88 ± 0.27 A
Blush LS mean	15	90.1 ± 3.4 AB	0.706 ± 0.008 A	1.09 ± 0.10 B
Starburst LS mean	34	87.5 ± 2.3 B	0.701 ± 0.005 A	1.22 ± 0.06 B
Purple LS mean	79	95.8 ± 1.5 A	0.686 ± 0.003 B	1.28 ± 0.04 B
Moldy LS mean	42	91.2 ± 2.1 AB	0.690 ± 0.005 AB	1.27 ± 0.06 B
Model R^2		0.33***	0.33***	0.09**
FER P-value		<0.0001***	<0.0001***	0.0002**
Sym. type P-value		0.0364*	0.0975^{MS}	0.0867^{MS}
Inundative				
Statistic	**N**	**Fumonisin**	**Bulk density**	**Bikaverin**
Asym. LS mean	0	NA	NA	NA
Blush LS mean	14	91.4 ± 3.4 A	0.707 ± 0.009 A	1.20 ± 0.11 A
Starburst LS mean	8	92.6 ± 4.3 A	0.699 ± 0.011 AB	1.32 ± 0.14 A
Purple LS mean	49	97.9 ± 1.7 A	0.678 ± 0.004 B	1.36 ± 0.05 A
Moldy LS mean	23	98.1 ± 2.7 A	0.680 ± 0.007 B	1.32 ± 0.09 A
Model R^2		0.31^{NS}	0.36***	0.04^{NS}
FER P-value		<0.0001***	<0.0001***	0.1283^{NS}
Sym. type P-value		0.3178^{NS}	0.0237*	0.6117^{NS}
Point				
Statistic	**N**	**Fumonisin**	**Bulk density**	**Bikaverin**
Asym. LS mean	2	84.7 ± 10.7 AB	0.713 ± 0.023 A	1.69 ± 0.25 A
Blush LS mean	1	93.8 ± 13.8 AB	0.796 ± 0.030 A	0.25 ± 0.33 C
Starburst LS mean	26	84.7 ± 2.9 B	0.704 ± 0.006 A	1.18 ± 0.07 B
Purple LS mean	30	93.6 ± 2.5 A	0.696 ± 0.006 A	1.15 ± 0.06 B
Moldy LS mean	19	83.5 ± 3.2 B	0.700 ± 0.007 A	1.20 ± 0.08 B
Model R^2		0.30***	0.28**	0.21**
FER P-value		<0.0001***	<0.0001***	0.0306*
Sym. type P-value		0.0743^{MS}	0.8586^{NS}	0.0098**

LS means and standard errors (±) are reported in each symptom type/disease trait cell. Groups not connected by the same letter are significantly different (two-tailed t-test, P<0.05). Levels of significance of ANOVA and fixed effects from models with Box-Cox-transformed fumonisin, bulk density, and bikaverin as separate responses and Box-Cox-transformed FER and symptom type as fixed effects are denoted next to model R2 and fixed effect P-values as: *0.05>P≥0.01; **0.01>P≥0.0001; ***P<0.0001; MS=marginally significant (P<0.1); NS=not significant. LS means are colored by a yellow to red (relatively low to high) heat map.

Table 2.5. Raw bulk density and fumonisin symptom type means and model summaries of Box-Cox-transformed bulk density and fumonisin vs. symptom type in discrete symptom type samples.

Combined				
Statistic	**N**	**Bulk den. (g mL^{-1})**	**Fumonisin (ppm)**	**Bikaverin (ppm)**
Asym. mean	16	0.67 ± 0.005 A	0.111 ± 0.009 C	3.374 ± 0.634 AB
Blush mean	5	0.64 ± 0.018 AB	8.726 ± 7.404 B	0.982 ± 0.202 B
Starburst mean	9	0.61 ± 0.015 B	2.657 ± 1.288 B	3.804 ± 0.688 A
Purple mean	14	0.46 ± 0.014 C	309.181 ± 55.117 A	4.724 ± 0.857 A
Model R^2	44	0.86***	0.89***	0.16 ^{MS}
Inundative				
Statistic	**N**	**Bulk den. (g mL^{-1})**	**Fumonisin (ppm)**	**Bikaverin (ppm)**
Asym. mean	8	0.67 ± 0.008 A	0.118 ± 0.013 C	3.252 ± 0.938 A
Blush mean	4	0.62 ± 0.009 B	1.337 ± 0.601 B	0.795 ± 0.098 A
Starburst mean	3	0.63 ± 0.022 B	2.182 ± 1.559 B	3.485 ± 0.948 A
Purple mean	7	0.45 ± 0.018 C	279.889 ± 81.423 A	3.966 ± 1.107 A
Model R^2	22	0.92***	0.93***	0.20^{NS}
Point				
Statistic	**N**	**Bulk den. (g mL^{-1})**	**Fumonisin (ppm)**	**Bikaverin (ppm)**
Asym. mean	8	0.67 ± 0.007 A	0.104 ± 0.014 C	3.496 ± 0.916 A
Blush mean	1	0.71 ± 0 A	38.283 ± 0 A	1.731 ± 0 A
Starburst mean	6	0.60 ± 0.021 B	2.895 ± 4.556 B	3.964 ± 0.970 A
Purple mean	7	0.47 ± 0.021 C	338.473 ± 79.047 A	5.482 ± 1.329 A
Model R^2	22	0.85***	0.91***	0.09^{NS}

Raw bulk density, fumonisin, and bikaverin means and standard errors (±) are reported in each symptom type/disease trait cell. Groups not connected by the same letter are significantly different (two-tailed t-test, $P<0.05$) with respect to Box-Cox-transformed bulk density or fumonisin. Levels of significance of ANOVA of Box-Cox-transformed fumonisin and bulk density vs. symptom type are denoted next to model R^2 values as: MS=marginally significant ($P<0.1$); *$0.05>P\geq0.01$; **$0.01>P\geq0.0001$; ***$P<0.0001$. Means are colored by a yellow to red (relatively low to high) heat map.

Table 2.6. Mixed linear model summaries with Box-Cox-transformed FER, fumonisin (FUM), bulk density (DEN), bikaverin (BIK), and FUM:FER as the response. Combined analyses included inoculation method and line as fixed effects and field replicate as a random effect. Inoculation method-specific analyses included line as a fixed effect and replication as random. P-values of fixed effects and percent variances explained by replication and error are reported.

Analysis	**Response**	**R^2**	**Inoculation method**	**Line**	**Rep**	**Block [Rep]**	**Error**
Combined	FER	0.62	<0.0001***	<0.0001***	0	12.1	87.9
	FUM	0.65	<0.0001***	<0.0001***	0	3.6	96.4
	DEN	0.61	0.0003**	0.04*	0	0	100
	BIK	0.22	0.0056**	0.93^{NS}	0	1.1	99.9
	FUM:FER	0.29	0.0039**	0.003**	0	0	100
Inundative	FER	0.84		0.0006**	10.1	0.3	89.6
	FUM	0.82		<0.0001***	0	12.6	87.4
	DEN	0.84		<0.0001***	0	4.9	95.1
	BIK	0.29		0.83^{NS}	0	0	100
	FUM:FER	0.81		0.0005**	1.2	4.5	94.3
Point	FER	0.77		0.12^{NS}	8.1	21.9	70.0
	FUM	0.75		0.12^{NS}	0	27.3	72.7
	DEN	0.75		0.09^{MS}	0.7	0	93.3
	BIK	0.70		0.23^{NS}	0	23.2	76.8
	FUM:FER	0.80		0.04*	0	36.4	63.6

Fixed effect P-value significance denoted as: *0.05>P≥0.01; **0.01>P≥0.0001; ***P<0.0001; MS=marginally significant (P<0.1); NS=not significant.

Table 2.7. Random linear model summaries with Box-Cox-transformed FER, fumonisin (FUM), bulk density (DEN), bikaverin (BIK), and FUM:FER as the response and line, rep, and block[rep] as random effects for combined and inoculation method-specific data. Variance components of the random effects within each model and broad-sense heritability (H) of each trait are reported.

Analysis	Response	Line	Rep	Block[Rep]	Error	H
Combined	FER	46.89	0	10.99	113.02	0.45
	FUM	94.46	0	0	138.41	0.58
	DEN	0.00069	0	0	0.00063	0.69
	BIK	0	0	0	127.39	0
	FUM:FER	0.15	0	0	0.37	0.46
Inundative	FER	68.05	4.26	4.38	32.79	0.81
	FUM	126.41	0	12.16	52.02	0.83
	DEN	0.00096	0	0	0.00044	0.81
	BIK	0	0	0	136.79	0
	FUM:FER	0.25	0.0018	0.020	0.18	0.74
Point	FER	46.81	9.88	32.29	122.49	0.43
	FUM	55.77	0	0	177.37	0.39
	DEN	0.00040	0	0	0.00076	0.51
	BIK	12.11	0	0	95.13	0.20
	FUM:FER	0.13	0.0075	0.035	0.41	0.38

Table 2.8. Summaries of likelihood ratio (LR) tests comparing the density of legal fumonisin (< 2 ppm) and illegal fumonisin (≥ 2 ppm) subplot samples in each of the four quadrants of the PC2 vs. PC1 plot.

Quad.	LR χ^2	FUM < 2 ppm		FUM ≥ 2 ppm	
		Present	Absent	Present	Absent
I	3.1^{NS}	9% (2)	91% (20)	24% (41)	76% (127)
II	9.9**	59% (13)	41% (9)	25% (42)	75% (126)
III	0.02^{NS}	23% (5)	77% (17)	21% (36)	79% (132)
IV	4.8*	9% (2)	91% (20)	29% (49)	71% (119)

LR test significance is denoted next to χ^2 values as *0.05>P≥0.01; **0.01>P≥0.0001; NS=not significant. The number of and percent of total samples within each of the quadrants with fumonisin < 2ppm or ≥ 2 ppm are shown.

Table 2.9. Specificity, sensitivity, false positive, and false negative rates of LDA models using Box-Cox-transformed bulk density as a covariate to discriminate discrete symptom type samples with legal fumonisin (FUM) levels (< 2 ppm) from illegal samples (≥ 2 ppm) in combined and inoculation method-specific analyses.

		Predicted FUM	
Analysis	**Actual FUM**	**≥ 2 ppm**	**< 2 ppm**
Combined	≥ 2 ppm	0.80	0.03
	< 2 ppm	0.20	0.97
Inundative	≥ 2 ppm	0.78	0.03
	< 2 ppm	0.22	0.97
Point	≥ 2 ppm	0.84	0.01
	< 2 ppm	0.16	0.99

Figure 2.1. Photographic examples of kernels exhibiting the five FER symptom types.

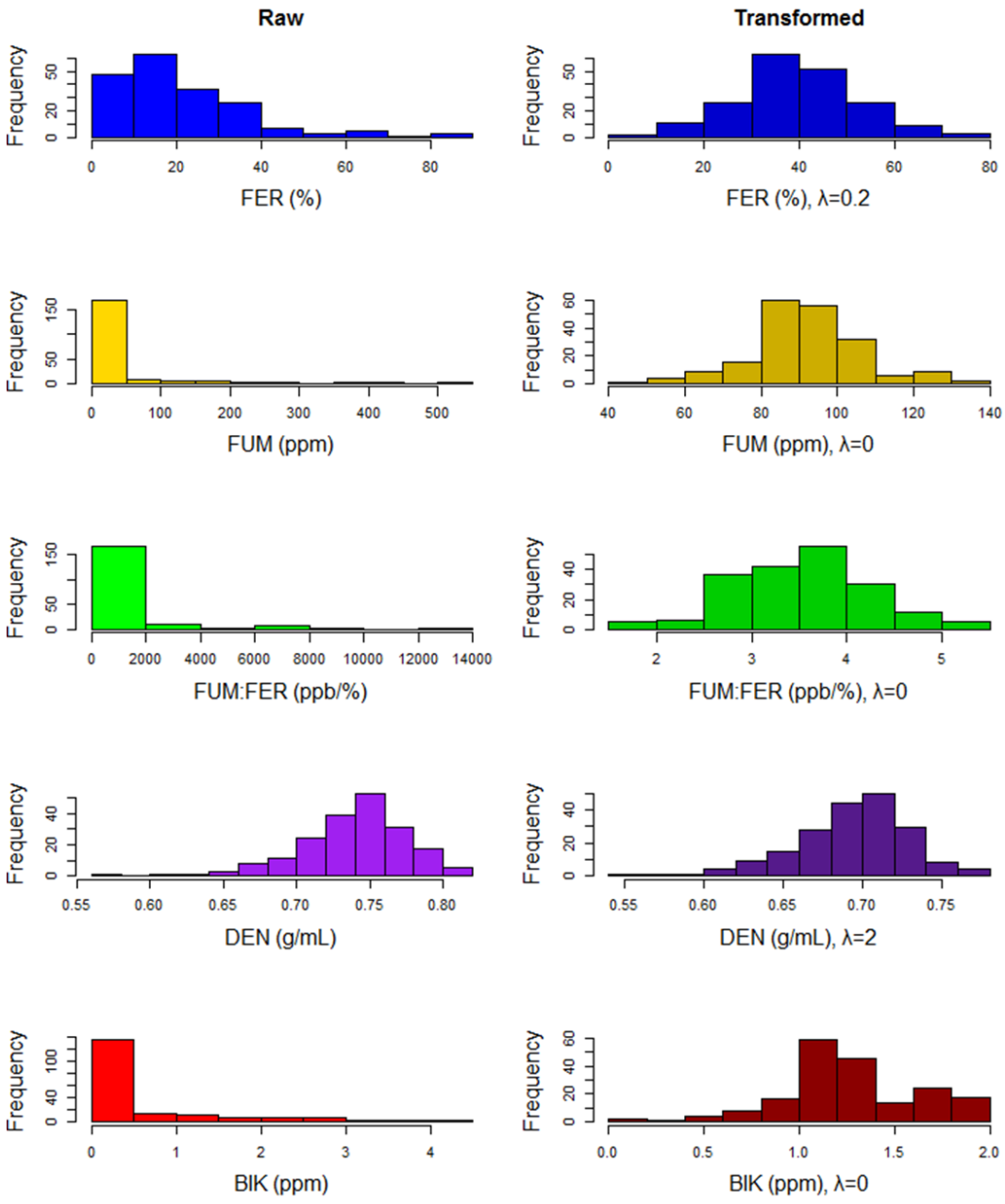

Figure 2.2. Histograms of raw and Box-Cox-transformed FER, fumonisin (FUM), FUM:FER, bulk density (DEN), and bikaverin (BIK) subplot data. The best λ values estimated by the Box-Cox method and used for exponential transformation of the raw data are shown in the y-axis.

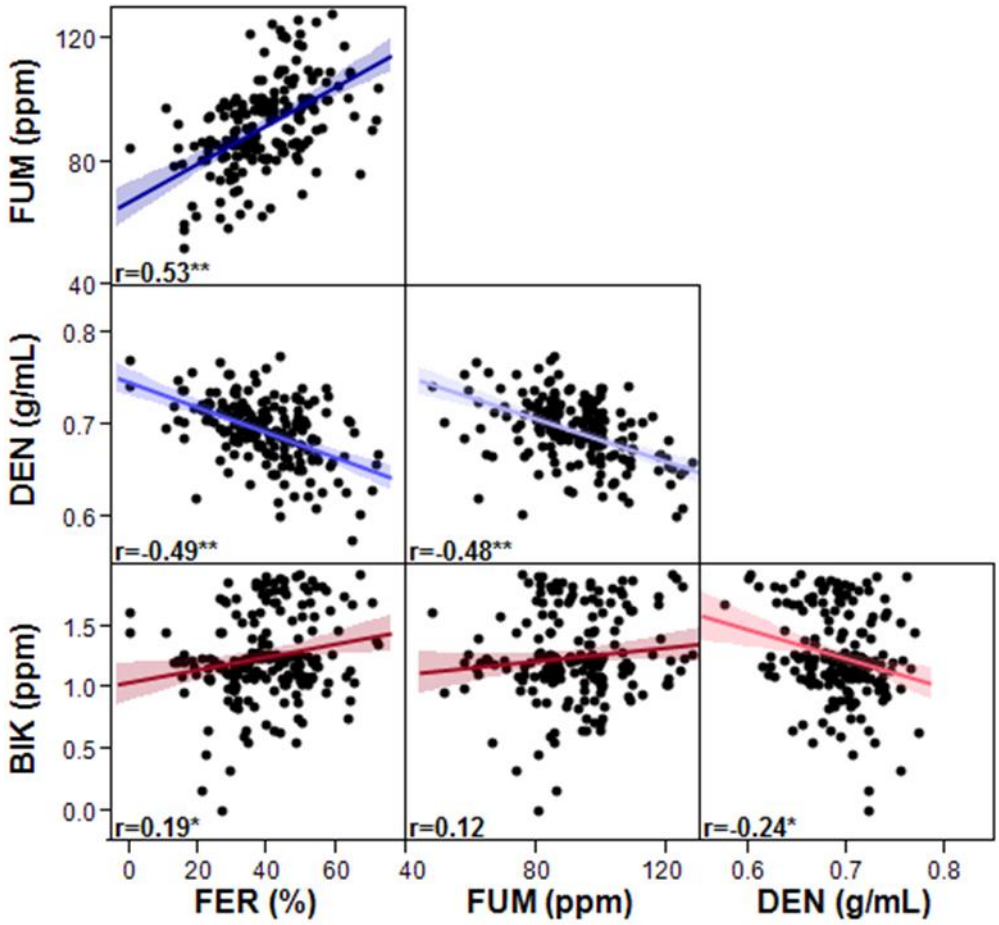

Figure 2.3. Phenotypic correlation matrix of Box-Cox-transformed FER, fumonisin (FUM), bulk density (DEN), and bikaverin (BIK) in all subplot samples combined. Regression lines are colored according to the direction and magnitude of correlation coefficients. Negative correlations are colored red; positive correlations are colored blue, and the darkness of the color is proportional to the relative magnitude of the correlation. Shading around the regression lines indicates the 95% confidence interval of the model fit. Correlation coefficients (r) are reported with significance denoted as: *0.01>P≥0.0001; **P<0.0001.

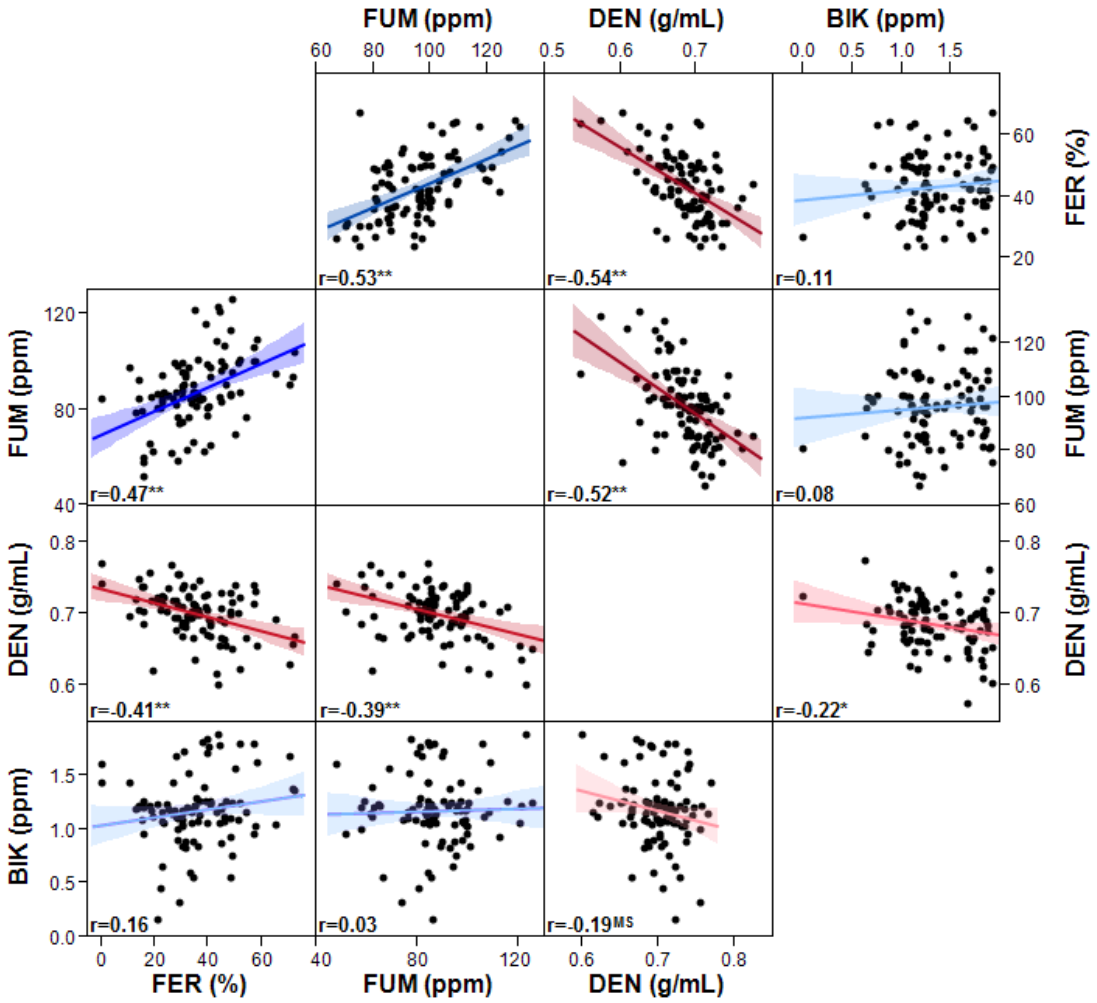

Figure 2.4. Phenotypic correlation matrices of Box-Cox-transformed FER, fumonisin (FUM), bulk density (DEN), and bikaverin (BIK), with inundative inoculation subplot data in the above-diagonal and point-inoculation subplot data in the below-diagonal. Regression lines are colored according to the direction and magnitude of correlation coefficients. Negative correlations are colored red; positive correlations are colored blue, and the darkness of the color is proportional to the relative magnitude of the correlation. Shading around the regression lines indicates the 95% confidence interval of the model fit. Correlation coefficients (r) are reported with significance denoted as: *0.05>P≥0.01; **0.01>P≥0.0001; ***P<0.0001; MS=marginally significant (P<0.1).

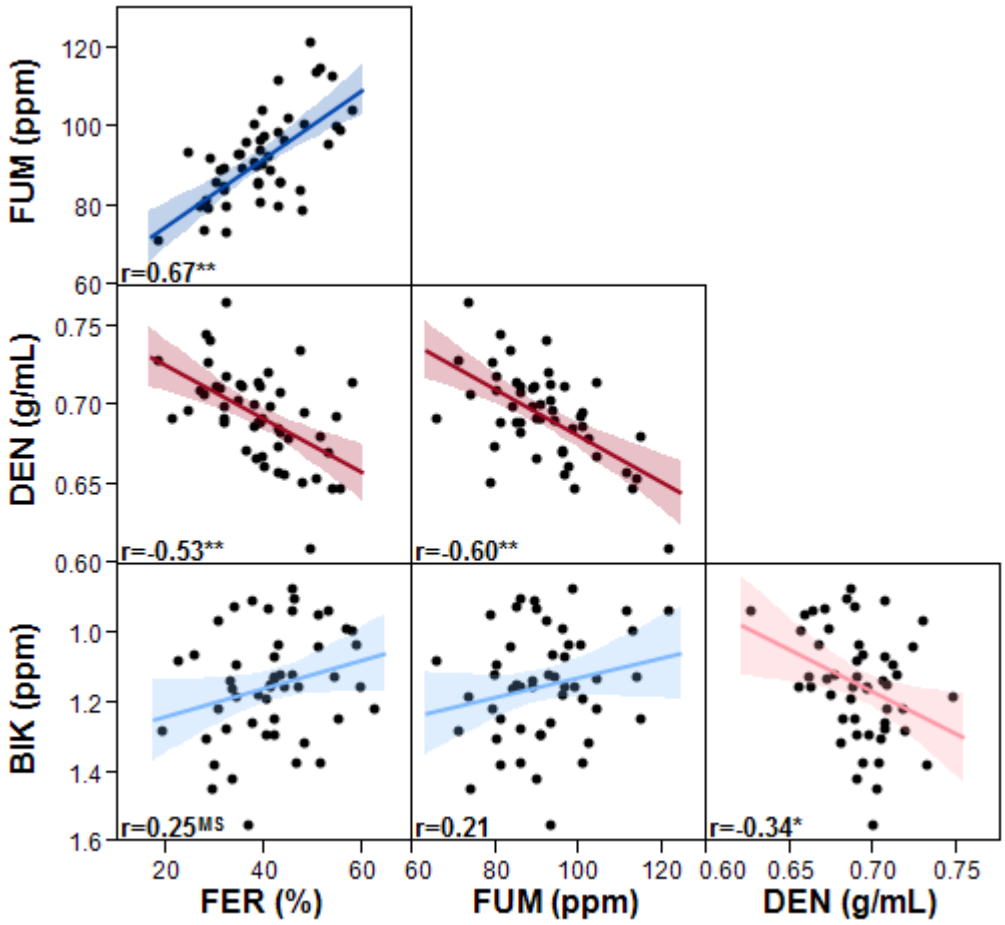

Figure 2.5. Genetic correlation matrix of Box-Cox-transformed FER, fumonisin (FUM), bulk density (DEN), and bikaverin (BIK) in all subplot samples combined. Regression lines are colored according to the direction and magnitude of correlation coefficients. Negative correlations are colored red; positive correlations are colored blue, and the darkness of the color is proportional to the relative magnitude of the correlation. Shading around the regression lines indicates the 95% confidence interval of the model fit. Correlation coefficients (r) are reported with significance denoted as: *0.05>P≥0.01; **0.01>P≥0.0001; ***P<0.0001; MS=marginally significant (P<0.1).

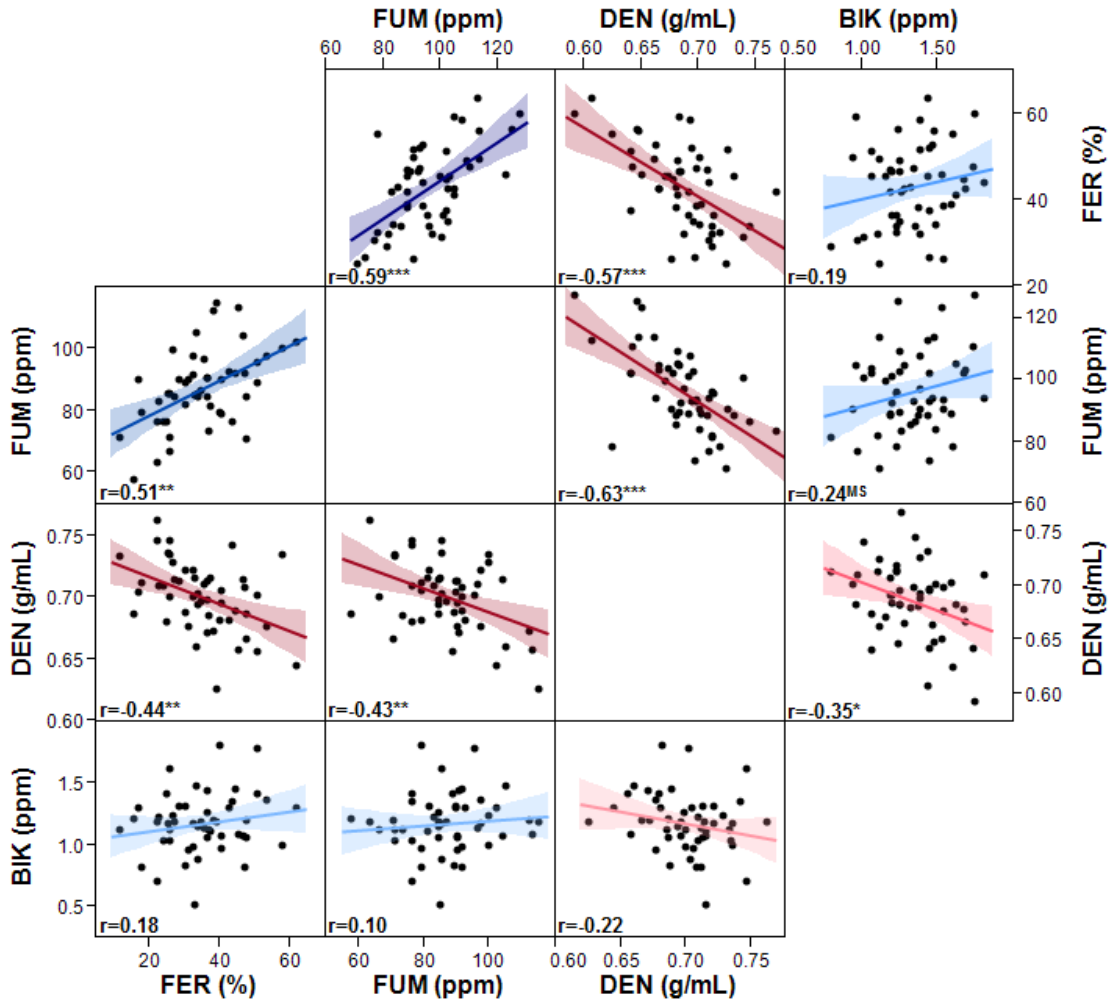

Figure 2.6. Genetic correlation matrices of Box-Cox-transformed FER, fumonisin (FUM), bulk density (DEN), and bikaverin (BIK), with inundative inoculation subplot data in the above-diagonal and point-inoculation subplot data in the below-diagonal. Regression lines are colored according to the direction and magnitude of correlation coefficients. Negative correlations are colored red; positive correlations are colored blue, and the darkness of the color is proportional to the relative magnitude of the correlation. Shading around the regression lines indicates the 95% confidence interval of the model fit. Correlation coefficients (r) are reported with significance denoted as: *0.05>P≥0.01; **0.01>P≥0.0001; ***P<0.0001; MS=marginally significant (P<0.1).

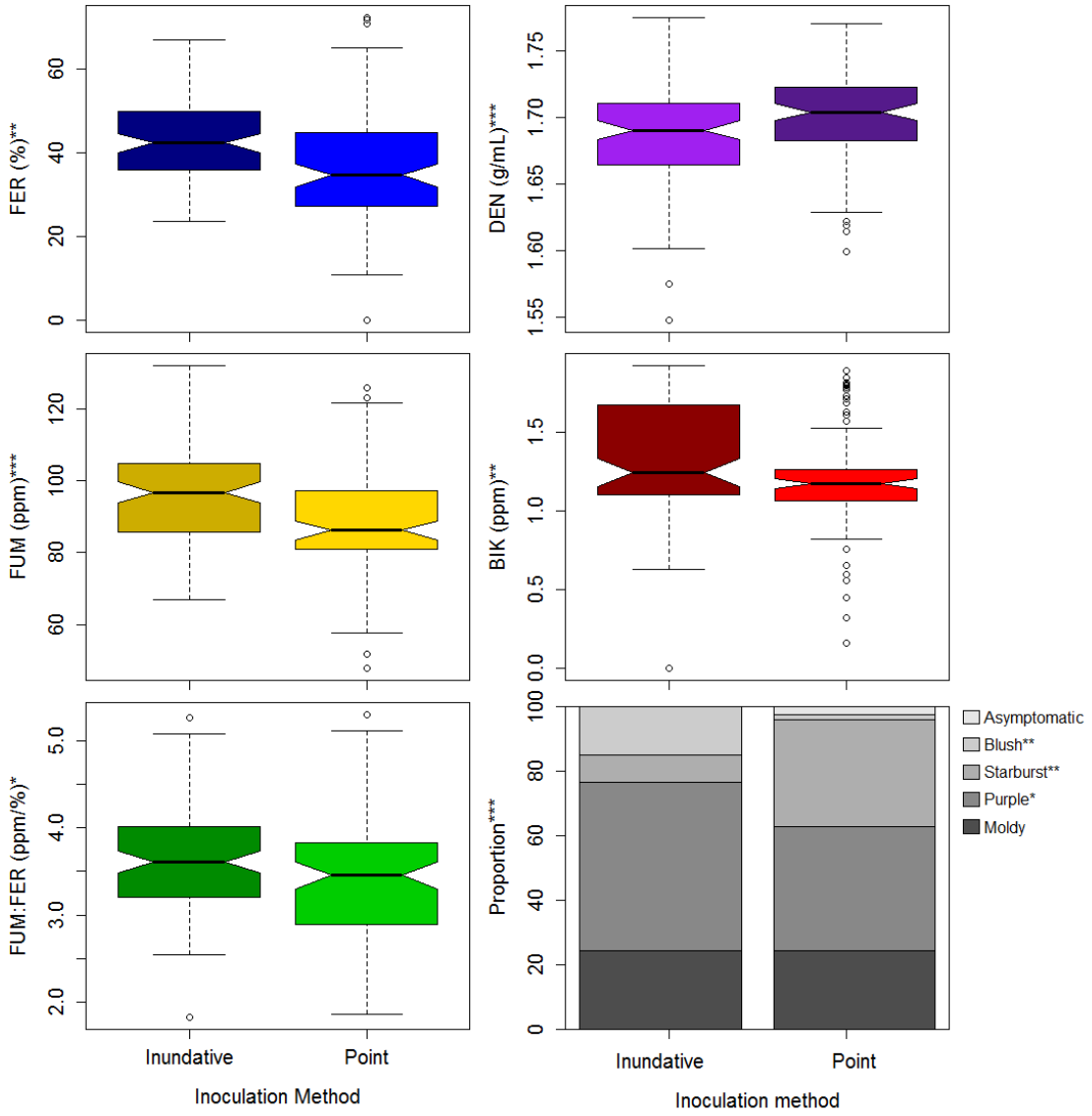

Figure 2.7. Box plots of Box-Cox-transformed FER, fumonisin (FUM), FUM:FER, bulk density (DEN), and bikaverin (BIK) and mosaic plot of symptom type proportions under inundative and point inoculation. Levels of significance of (1) two-tailed t-tests comparing FER, FUM, FUM:FER, DEN, and BIK vs. inoculation method, (2) likelihood ratio test comparing symptom type composition vs. inoculation method, and (3) binomial models comparing the absence/presence of each symptom type vs. inoculation method are denoted on the y-axes and next to each symptom type in the legend as: *0.05>P≥0.01;**0.01>P≥0.0001; ***P<0.0001. The darkness of the color inside of the box-plots is proportional to the relative magnitude of the mean.

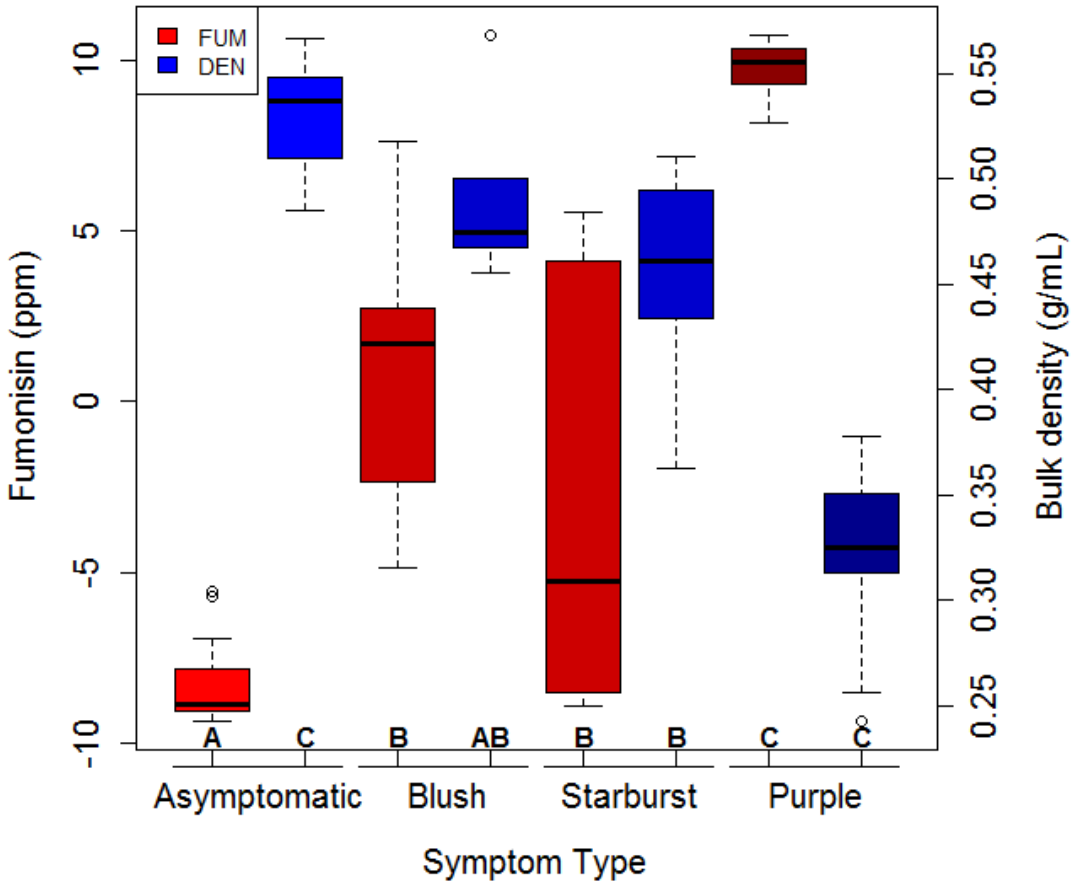

Figure 2.8. Boxplots of Box-Cox-transformed fumonisin and bulk density in the four discrete symptom types. Symptom types not connected by the same letter are significantly different (two-tailed t-test, $P<0.05$). Fumonisin box-plots are colored in red and bulk density box-plots in blue, with the darkness of the color proportional to the relative magnitude of the mean.

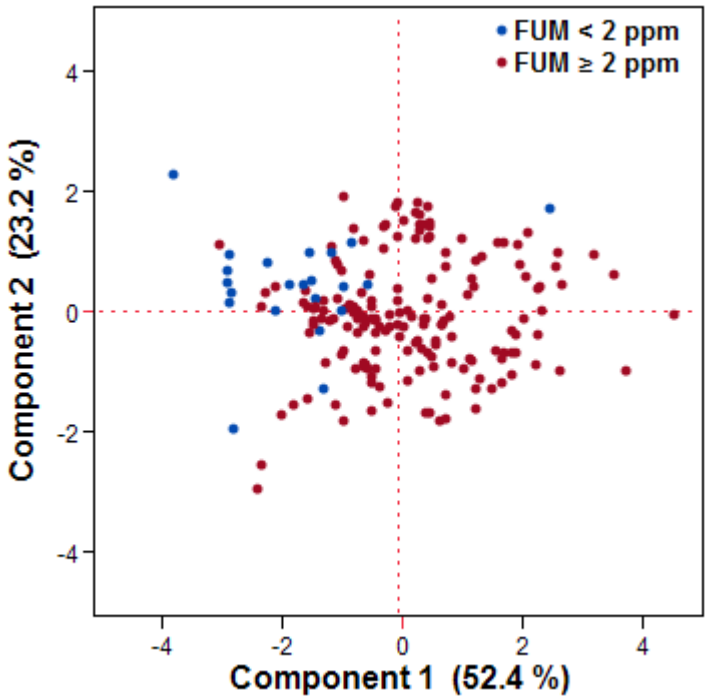

Figure 2.9. The first two principal components (PC) of PCA including Box-Cox-transformed FER, bulk density, and bikaverin for all subplot data combined explain 75.6% of the total variance.

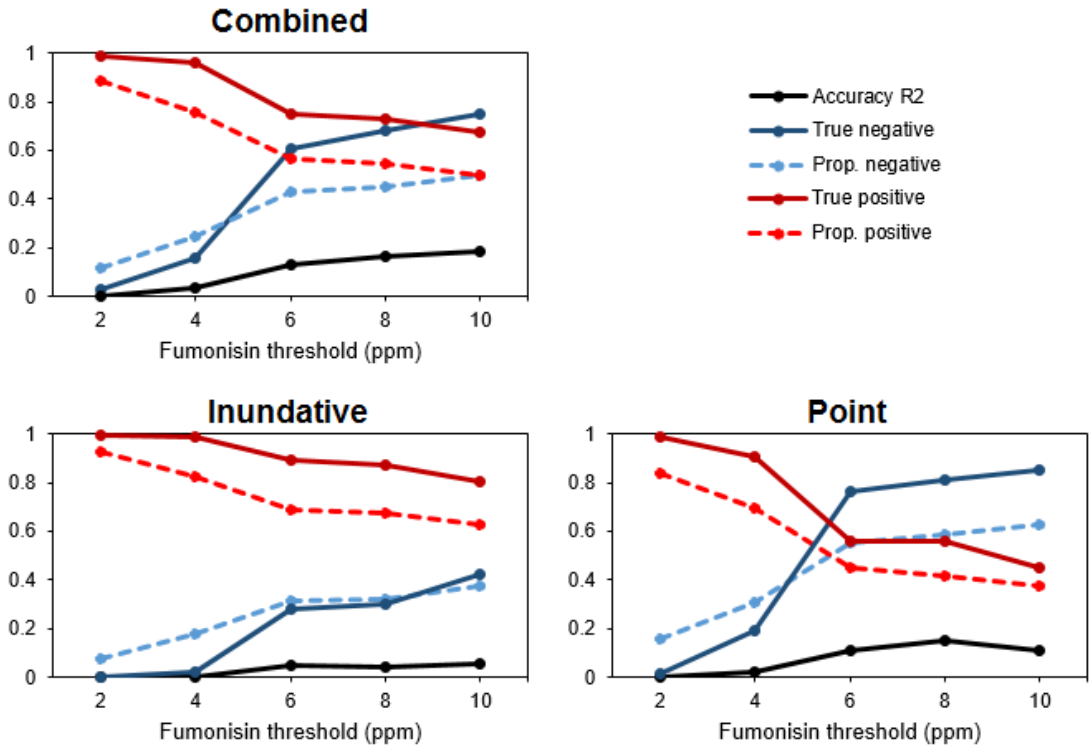

Figure 2.10. Summaries of LDA results using Box-Cox-transformed FER, bulk density, and bikaverin to discriminate between subplot samples above and below five different fumonisin thresholds for combined and inoculation method-specific models.

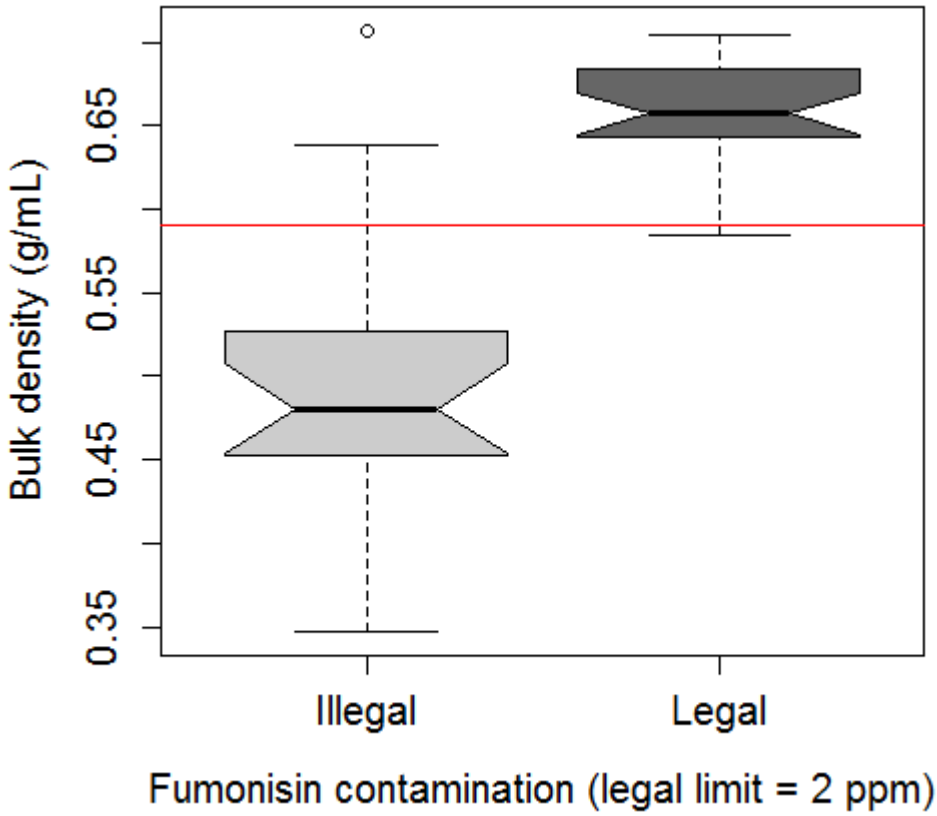

Figure 2.11. Raw bulk density of discrete symptom type samples with fumonisin levels above and below the legal limit (2 ppm fumonisin). The red horizontal line indicates the bulk density grand mean. The darkness of the gray color inside of the box-plots is proportional to the relative magnitude of the mean.

Figure 2.12. Percent of total subsample weight and fumonisin content in high-density (bulk density ≥ 0.59 g mL-1) and low-density (bulk density < 0.59 g mL-1) discrete symptom type samples. High density average proportions are colored in dark gray and low-density average proportions in light gray.

REFERENCES

1. Wild CP, Gong YY. Mycotoxins and human disease: A largely ignored global health issue. Carcinogenesis. 2009;31:71–82.
2. Mueller DS, Wise KA, Sisson AJ, Allen TW, Bergstrom GC, Bosley DB, et al. Corn yield loss estimates due to diseases in the United States and Ontario, Canada from 2012 to 2015. Plant Health Prog. 2016;17:211–22.
3. Mutiga SK, Were V, Hoffmann V, Harvey JW, Milgroom MG, Nelson RJ. Extent and drivers of mycotoxin contamination: inferences from a survey of Kenyan maize mills. Phytopathology. 2014;104:1221–31.
4. Parsons MW, Munkvold GP. Effects of planting date and environmental factors on Fusarium ear rot symptoms and fumonisin B1 accumulation in maize grown in six North American locations. Plant Pathol. 2012;61:1130–42.
5. Schjøth JE, Visconti A, Sundheim L. Fumonisins in maize in relation to climate, planting time and hybrids in two agroecological zones in Zambia. Mycopathologia. 2009;167:209–19.
6. Kimanya ME, De Meulenaer B, Roberfroid D, Lachat C. Fumonisin exposure through maize in complementary foods is inversely associated with linear growth of infants in Tanzania. Mol Nutr Food Res. 2010;54:1659–67.
7. Bolduan C, Miedaner T, Schipprack W, Dhillon BS, Melchinger AE. Genetic variation for resistance to ear rots and mycotoxins contamination in early European maize inbred lines. Crop Sci. 2009;49:2019–28.
8. Eller MS, Holland JB, Payne GA. Breeding for improved resistance to fumonisin contamination in maize. Toxin Rev. 2008;27:371–89.
9. Presello DA, Iglesias J, Botta G, Eyhérabide GH. Severity of Fusarium ear rot and concentration of fumonisin in grain of Argentinian maize hybrids. Crop Prot. 2007;26:852–5.
10. Robertson-Hoyt LA, Jines MP, Balint-kurti PJ, Kleinschmidt CE, White DG, Payne GA, et al. QTL mapping for Fusarium ear rot and fumonisin contamination resistance in two maize populations. Crop Sci. 2006;46:1734–43.
11. Munkvold GP. Cultural and genetic approaches to managing mycotoxins in maize. Annu Rev Phytopathol. 2003;41:99–116.
12. Arino A, Herrera M, Juan T, Estopanan G, Carraminana JJ, Rota C, et al. Influence of agricultural practices on the contamination of maize by fumonisin mycotoxins. J Food Prot. 2009;72:898–902.
13. Humpf H-U, Voss KA. Effects of thermal food processing on the chemical structure and toxicity of fumonisin mycotoxins. Mol Nutr Food Res. 2004;48:255–69.
14. Dombrink-Kurtzman MA, Dvorak TJ, Barron ME, Rooney LW. Effect of nixtamalization (alkaline cooking) on fumonisin-contaminated corn for production of masa and tortillas. J Agric Food Chem. 2000;48:5781–6.

15. Stasiewicz MJ, Falade TDO, Mutuma M, Mutiga SK, Harvey JJW, Fox G, et al. Multi-spectral kernel sorting to reduce aflatoxins and fumonisins in Kenyan maize. Food Control. 2017;78:203–14.
16. Afolabi CG, Bandyopadhyay R, Leslie JF, Ekpo EJA. Effect of sorting on incidence and occurrence of fumonisins and *Fusarium verticillioides* on maize from Nigeria. J Food Prot. 2006;69:2019–23.
17. Blandino M, Reyneri A. Effect of maize hybrid maturity and grain hardness on fumonisin and zearalenone contamination. Ital J Agron. 2008;2:107–17.
18. Busman M, Butchko RAE, Proctor RH. LC-MS/MS method for the determination of the fungal pigment bikaverin in maize kernels as an indicator of ear rot. Food Addit Contam Part A. 2012;29:1736–42.
19. Parsons MW, Munkvold GP. Associations of planting date, drought stress, and insects with Fusarium ear rot and fumonisin B1 contamination in California maize. Food Addit Contam. 2010;27:591–607.
20. Munkvold GP, Carlton WM. Influence of inoculation method on systemic *Fusarium moniliforme* infection of maize plants grown from infected seeds. Plant Dis. 1997;81:211–6.
21. Clements MJ, Kleinschmidt CE, Maragos CM, Pataky JK, White DG. Evaluation of inoculation techniques for Fusarium ear rot and fumonisin contamination of corn. Plant Dis. 2003;87:147–53.
22. Zila CT, Samayoa LF, Santiago R, Butrón A, Holland JB. A genome-wide association study reveals genes associated with Fusarium ear rot resistance in a maize core diversity panel. G3. 2013;3:2095–104.
23. Horne DW, Eller MS, Holland JB. Responses to recurrent index selection for reduced Fusarium ear rot and lodging and for increased yield in maize. Crop Sci. 2016;56:85–94.
24. Clements MJ, Maragos CM, Pataky JK, White DG. Sources of resistance to fumonisin accumulation in grain and Fusarium ear and kernel rot of corn. Phytopathology. 2004;94:251–60.
25. Hung HY, Holland JB. Diallel analysis of resistance to Fusarium ear rot and fumonisin contamination in maize. Crop Sci. 2012;52:2173–81.
26. Zila CT, Ogut F, Romay MC, Gardner CA, Buckler ES, Holland JB. Genome-wide association study of Fusarium ear rot disease in the U.S.A. maize inbred line collection. BMC Plant Biol. 2014;14:372.
27. JMP®. Version Pro 12. SAS Institute Inc. 1989-2007.
28. Venables W, Ripley B. Modern Applied Statistics with S. 4th ed. New York: Springer; 2002.
29. R Core Team. R: A Language and Environment for Statistical Computing. Version 3.3.1. R Foundation for Statistical Computing. 2017.
30. Pearson TC, Wicklow DT, Brabec DL. Characteristics and sorting of white food corn contaminated with mycotoxins. Appl Eng Agric. 2010;26:109–13.
31. Shelby RA, White DG, Bauske EM. Differential fumonisin production in maize hybrids. Plant Dis. 1994;78:582–4.
32. Zummo N, Scott GE. Cob and kernel infection by *Aspergillus flavus* and *Fusarium moniliforme* in inoculated, field-grown maize ears. Plant Dis. 1990;74:627–31.

33. Duncan KE, Howard RJ. Biology of maize kernel infection by *Fusarium verticillioides*. MPMI. 2010;23:6–16.
34. Rolletschek H, Koch K, Wobus U, Borisjuk L. Positional cues for the starch/lipid balance in maize kernels and resource partitioning to the embryo. Plant J. 2005;69–83.
35. Bihmidine S, Hunter CT III, Johns CE, Koch KE, Braun DM. Regulation of assimilate import into sink organs: update on molecular drivers of sink strength. Front Plant Sci. 2013;4:1–15.
36. Presello DA, Botta G, Iglesias J, Eyhérabide GH. Effect of disease severity on yield and grain fumonisin concentration of maize hybrids inoculated with *Fusarium verticillioides*. Crop Prot. 2008;27:572–6.
37. Shetty PH, Bhat R V. A physical method for segregation of fumonisin-contaminated maize. Food Chem. 1999;66:371–4.
38. Lazzaro I, Busman M, Battilani P, Butchko RAE. FUM and BIK gene expression contribute to describe fumonisin and bikaverin synthesis in *Fusarium verticillioides*. Int J Food Microbiol. 2012;160:94–8.
39. Fox G, Manley M. Hardness methods for testing maize kernels. J Agric Food Chem. 2009;57:5647–57.
40. Blandino M, Reyneri A, Vanara F. Influence of nitrogen fertilization on mycotoxin contamination of maize kernels. Crop Prot. 2008;27:222–30.
41. Miller JD. Factors that affect the occurrence of fumonisin. Environ Health Perspect. 2001;109:321–4.

CHAPTER 3

GENETIC ANALYSIS OF RESISTANCE TO *FUSARIUM VERTICILLIOIDES* INFECTION AND FUMONISIN CONTAMINATION IN FOUR MAIZE RECOMBINANT INBRED LINE FAMILIES

Introduction

The filamentous ascomycete fungus *Fusarium verticillioides* causes Fusarium ear rot (FER) and produces the mycotoxin fumonisin in maize (Zea mays L), reducing yields and compromising human and animal health (1,2). Ear rots and mycotoxin contamination accounted for approximately 10% of maize yield losses in the United States and Ontario, Canada from 2012-2015 (1), and fumonisin contamination in naturally infected maize hybrids has been reported above the regulatory limit of 2 μg g^{-1} (ppm) across the US (3,4). Fumonisin exposure is especially concerning in tropical and sub-tropical regions of the world, such as sub-Saharan Africa (5–8) and central America (9,10), where environmental conditions are conducive to *F. verticillioides* infection (FVI) but where monitoring and control of fumonisin contamination in the food system are limited or nonexistent (2,3).

Resistances to FER and fumonisin contamination are quantitatively controlled, moderately to highly heritable, and genetically correlated, allowing for efficient selection and durable resistance (11–15). Variation in external symptomatology has been associated with differential fumonisin accumulation (4), suggesting that qualitative measures of symptom severity are important components of resistance. FVI and fumonisin levels have also been negatively associated with kernel density and hardness (16–21). For example, flint (hard endosperm) varieties, which are preferred in the mycotoxin-prone tropics (22), have been shown to be more resistant to mycotoxin contamination than dent (soft endosperm) lines (20,23,24). However,

modern breeding programs have been employing dent-by-flint crosses to increase yields (20,25). Understanding the diverse modes of pathogenesis, the role of kernel density in resistance, and their shared genetic control can potentially inform breeding decisions.

The genetic and phenotypic resources available for maize research are extensive. The maize nested association mapping (NAM) population, composed of 25 recombinant inbred line (RIL) families derived from 25 diverse inbred lines crossed to one recurrent parent (B73), is a powerful tool for dissecting the genetic architecture of quantitatively inherited traits (26). We employed quantitative, qualitative, external, and internal phenotypes of FVI severity – including FER severity and symptom variation, fumonisin contamination, and kernel bulk density – to dissect the symptomatology and genetic basis of resistance to FVI and fumonisin accumulation in four tropical flint-by-temperate dent (B73) NAM RIL families.

Materials and methods

Field design and inoculation

Four RIL families (CML333xB73, CML52xB73, CML69xB73, NC358xB73) from the maize NAM population were grown at the Central Crops Research Station in Clayton, NC from 2012-2015 in an augmented incomplete block design. The four non-B73 parents originate from breeding programs in Mexico and North Carolina, regions that are prone to mycotoxin contamination (9,3). RILs were replicated once per year and randomized within family, and the two parental lines of each family were randomized in each 20-plot block. In 2012, all RILs from the CML52xB73 and NC358xB73 families and 40 RILS each from the CML333XB73 and CML69xB73 families were grown. Days to silk (DTS) was phenotyped for each plot as described by Buckler et al. (27). One toothpick coated with spores from local toxigenic *F.*

verticillioides isolates was inserted into the middle of each developing primary ear approximately ten days after silking, and the toothpick remained in the ear until harvest (28).

Disease phenotyping

Primary ears were harvested from each plot at maturity, dried, and then visually evaluated for FER. FER was scored based on the percentage of the kernels presenting symptoms on a 1-100% scale with 5% increments (12). The average FER score of all the ears in each plot was then calculated. In order to account for the qualitative variation in FER symptomatology, each ear was assigned a symptom type: asymptomatic, blush, starburst, purple, or moldy (Fig. 3.1). Blush kernels had pink discoloration of the kernel crown; starburst kernels were characterized by white or pink streaks radiating from the kernel crown; purple kernels had severe purple or brownish discoloration, and moldy kernels were severely degraded and had matted fungal growth (Fig. 3.1). Each subplot was assigned a main symptom type based on the most frequent symptom type of the ears in the subplot. Subplots with equal representation from more than on symptom type were labeled “multiple”. Subplots with less than 10% average FER were considered asymptomatic.

Ears were then shelled and bulked per plot. From each plot, a random 250-mL volume of kernels was weighed, and kernel bulk density ($BDEN_{inoc}$) was calculated as the weight of the kernels divided by 250 mL. The kernels were ground into a fine powder with a Waring 7010 two-speed laboratory blender (Waring Commercial, Inc., Torrington, CT). A 10-g subsample from each ground bulk was put in a 25 mL centrifuge tube. To extract fumonisin, 20 mL of 90% methanol was added to each 25 mL tube, resulting in a two-fold dilution factor at this step. The tubes were then shaken with a Lab-Line Environ Orbitol Shaker (Lab-Line Instruments, Inc., Melrose

Park, IL) at 150 rpm for approximately five minutes. The samples settled for 15 minutes, after which 0.5 mL of supernatant from each sample was transferred to a 15 mL centrifuge tube. To dilute the supernatant to a final 40-fold dilution, 9.5 mL of distilled water was added to each 15 mL tube. Fumonisin (FUM) was quantified with FUM-specific enzyme-linked immunosorbent assay (ELISA) kits (Helica Biosystems, Inc., Santa Ana, CA). Absorbance at 450 nm of the ELISA plates was read using a BioTek μQuant™ microplate spectrophotometer (BioTek Instruments, Inc., Winooski, VT) paired with Gen5™ software (BioTek Instruments, Inc., Winooski, VT). Samples that had FUM levels predicted to be above the highest standard provided by the ELISA kits, 6 ppm, were serially diluted until their predicted FUM levels were within the standard curve. To approximate samples that had non-detectable FUM levels (< 0.1 ppm), uniform random values between 0 and 0.1 ppm were assigned to these samples (29). The ratio of FUM to FER (FUM:FER) was calculated as FUM/(FER+1). One was added to all FER data to adjust 0% FER scores in the denominator.

Symptom type sampling and phenotyping

We sought to test whether external symptom severity was associated with *F. verticillioides* colonization and fumonisin contamination. From plots harvested in 2013, we pooled kernels exhibiting the five symptom types (asymptomatic, blush, starburst, purple, and moldy) from each family. Each family/symptom type sample was composed of approximately 25 kernels. The samples were ground with a mortar and pestle. The ground samples were then used for evaluation of *F. verticillioides* colonization and fumonisin contamination. As described by Boutigny et al. (30), DNA was extracted from samples and quantitative PCR (qPCR) was used to quantify the relative amounts of maize and *F. verticillioides* DNA in the sample. The coefficient of infection was defined as (*Fvert/maize*)*100, where *Fvert* and *maize* are the relative

amounts of *F. verticillioides* and maize DNA, respectively (30). Fumonisin was extracted and quantified as described previously.

Entry-means and heritability estimation

Because the raw $BDEN_{inoc}$, FER, FUM, and FUM:FER data were not normally distributed, they were Box-Cox transformed using JMP® software (31). The lme4 package (32) in R version 3.3.1 (33) was used to estimate entry-means for $BDEN_{inoc}$, FER, FUM, and FUM:FER within and among the four families. With the lme4 package, mixed linear models were fit with Box-Cox-transformed $BDEN_{inoc}$, FER, FUM, and FUM:FER as separate response variables as $y_{ijkl} = \mu + Y_i + B[Y]_{j[i]} + G_k + GY_{ik} + F_l + e_{ijkl}$, where y is the response; μ is the grand mean; year (Y), block[year] ($B[Y]$), entry (G), and entry*year (GY) are random effects; DTS (F) is a fixed effect, and e is the error. DTS was included in the mixed models because of its correlation with $BDEN_{inoc}$, FER, FUM, and FUM:FER (Table 3.1). Variance components from each model were extracted and used to calculate broad-sense heritability (H) as $\sigma^2_G/(\sigma^2_G + (\sigma^2_{GY}/y) + (\sigma^2_e/b))$, where σ^2_G, σ^2_{GY}, and σ^2_e are the entry, entry*year, and error variances, respectively, and y and b are the number of years and blocks per year, respectively (34).

We also sought to assess associations between kernel bulk density under non-inoculated conditions ($BDEN_{uninoc}$) and FVI. Total kernel volume, cob weight, and ear weight data from these four families were accessed from Panzea (35). Total kernel bulk density was calculated as $BDEN_{uninoc} = (EarWeight - CobWeight)/TotalKernelVolume$. A random linear model was fit for $BDEN_{uninoc}$ using the lme4 package as $y_{ij} = \mu + L_i + G_j + e_{ij}$, where y is the response; μ is the grand mean; location (L) and entry (G) are random effects, and e is the error.

Trait correlation analyses

Pairwise correlations among plot phenotypes and among trait BLUPs were calculated within families using JMP® software. Plot phenotypes included DTS and Box-Cox-transformed $BDEN_{inoc}$, FER, FUM, and FUM:FER. Trait BLUPs included $BDEN_{inoc}$, $BDEN_{uninoc}$, FER, FUM, and FUM:FER. To assess differences in $BDEN_{inoc}$, FER, FUM, and FUM:FER among the five symptom types (asymptomatic, blush, starburst, purple, and moldy) within and among families, ANOVA was performed on plot phenotypes (Box-Cox-transformed) and pairwise differences between symptom types were assessed with two-tailed t-tests using JMP® software.

Comparison of disease severity among families

To test the effect of family on $BDEN_{inoc}$, FER, FUM, and FUM:FER, analysis of variance (ANOVA) was performed using JMP® software, and pairwise differences between families were assessed with two-tailed t-tests. A likelihood ratio χ^2 test was used to compare the composition of symptom types among families with JMP® software.

QTL mapping

The NAM population had been genotyped using genotyping-by-sequencing (GBS) technology (36). A subset of 7,386 GBS markers with 0.2 cM resolution was selected by Olukolu et al. (37) The 7,386 markers were extracted for the CML333xB73, CML52xB73, CML69xB73, and NC358xB73 NAM families and used for stepwise regression.

Stepwise regression models were fit in TASSEL version 5.2.37 (38) to identify markers associated with $BDEN_{inoc}$, $BDEN_{uninoc}$, FER, FUM, FUM:FER, and the absence/presence of asymptomatic, blush, starburst, purple, and moldy symptom

types. For the single-family models, a marker significance threshold of 0.001 was used (39). For the joint-family models, marker effects were nested within family and the significance threshold was set to 0.0001 (39). QTL were defined by the confidence intervals (CIs) of markers selected by stepwise regression (38).

Analysis of pleiotropic effects

Stepwise QTL were considered colocalized if their CIs overlapped, and the overlapping region defined the colocalized QTL. In addition to identifying colocalized QTL, we sought to test pleiotropy among traits across all associated QTL. There were 1396 markers within the QTL selected by stepwise regression, and each marker was regressed against each of the 10 traits within each family using GLM in TASSEL. Family-specific marker effects on the 10 traits were used for pleiotropic analyses.

Because this study only included four families, we did not have the power to test QTL-specific pleiotropy as described by Buckler et al. (27). To test general pleiotropy across the 1396 QTL-associated markers, we correlated all pairwise combinations of marker effects. We also assessed whether pleiotropy differed among families by correlating all pairwise combinations of marker effects within families.

Comparison of QTL mapped in this study and previously described loci

Several studies have previously identified loci associated with resistance to ear rots, FER, and FUM via linkage mapping, genome-wide association studies (GWAS), and meta-QTL analysis (12,14,25,28,40–45). In order to address whether the QTL mapped in this study colocalized with previously described loci, we gathered QTL, meta-QTL, and GWAS hits from nine publications (12,14,25,28,40–45). Five publications provided bin locations for the associated loci (12,25,40,42,43). For loci mapped in this study and in studies that did not provide bin locations (14,28,41,44,45),

we identified the bins wherein these loci were located (based on their physical or genetic positions) using MaizeGDB (46). We then compared the number of loci located in the 85 bins to identify putative "hot spots" of resistance to FVI and fumonisin contamination.

Candidate gene analysis

We sought to identify candidate genes and biological processes associated with FVI hotspots (Fig. 3.3). The AGP v2 gene atlas (47) was downloaded from MaizeGDB (46). We then identified genes within the confidence intervals of our QTL that were mapped to FVI hotspot bins. We used agriGO (48) to assign gene ontology (GO) terms to these genes and to perform singular enrichment analysis (SEA) on the resulting GO term list. We accessed annotations for significantly enriched GO terms (FDR-adjusted $P<0.1$) with QuickGO (49).

We also tested whether the expression of genes within hot spot QTL were correlated with FER. We accessed data on FER from Zila et al. (28) and gene expression from Kremling et al. (in press) for the maize core diversity panel, composed of 282 diverse inbred lines (50). The expression dataset included expression data for 37,127 genes from 8 different tissues (Kremling et al., in press). To control for population structure effects on correlations between FER and gene expression, we fit a mixed model (FER as the response) including only a kinship matrix and extracted the FER residuals in TASSEL (38). We then correlated tissue-specific gene expression to the FER residuals and identified genes whose tissue-specific expression was significantly correlated with FER residuals ($P<0.05$). From the list of FER-correlated genes, we extracted genes that were within our hot spot QTL and conduced GO term analyses with these genes as described previously.

Results

Symptomatology differs among families

To assess differences in symptomatology, we compared qualitative (e.g. symptom type) and quantitative (e.g. FUM, FER) plot-level phenotypes of disease severity among families. $BDEN_{inoc}$, FER, FUM, and FUM:FER differed significantly among families (Table 3.2a, Fig. 3.2). Families that had higher $BDEN_{inoc}$ tended to have lower FER, FUM, and FUM:FER on average (Table 3.2b). The CML333xB73 family was unique in that it had the highest average FER, but the highest $BDEN_{inoc}$ and lowest FUM and FUM:FER (Table 3.2b). This may be due to the fact that this family had the greatest proportion of plots exhibiting the most moderate disease phenotype (22% of the plots were scored as blush) (Fig. 3.2).

The composition of symptom types significantly differed among families. The majority of plots (57-75%) in all families exhibited the starburst and purple symptom types (Fig. 3.2). The CML52xB73 family had the largest proportion of asymptomatic (20%) and starburst (44%) plots (Fig. 3.2). The proportion of starburst plots was greatest in the CML69xB73 (35%) and NC358xB73 (40%) families (Fig. 3.2). Approximately 9% of plots presented multiple symptoms in all families (Fig. 3.2).

External symptom severity tracks kernel bulk density, fumonisin content, and *F. verticillioides* infection

$BDEN_{inoc}$ tracked external symptom severity, with asymptomatic plots having the highest $BDEN_{inoc}$, followed by blush, starburst, purple, and moldy plots in descending order (Table 3.3). By definition, asymptomatic plots had the lowest FER and highest FUM:FER (Table 3.3). Differences in FER and FUM:FER among symptom types varied from family to family; in general, moldy and starburst plots had the highest FER scores and purple and moldy plots had high FUM:FER (Table 3.3).

Symptom types differed significantly with respect to FUM, with moldy plots having the highest FUM (Table 3.3). However, asymptomatic and starburst plots also had high levels of FUM (Table 3.3). The high FUM in starburst plots may be due to their high FER severity. The unexpectedly high FUM in asymptomatic plots may be the result of the symptom type scoring method, which was conducted with the kernels still attached to the cob; the kernels may have had symptoms present below the visible area. In addition, symptomatology within and among ears was highly heterogeneous at the plot level, and thus may confound inferences on relationships between symptom severity and FUM.

To directly test the link between external symptomatology and FUM, we phenotyped sets of kernels representing discrete symptom types (approx. 15 kernels/symptom type), including kernels that were completely asymptomatic. Fumonisin contamination and *F. verticillioides* infection (coefficient of infection, as determined by qPCR) differed marginally ($P<0.1$) and significantly ($P<0.05$), respectively, among discrete symptom type samples (Table 3.4). Purple samples had the highest fumonisin content; moldy and starburst samples were intermediate, and blush and asymptomatic samples had the lowest fumonisin levels (Table 3.4.). With respect to infection severity, purple and moldy samples had higher coefficients of infection than asymptomatic, blush, and starburst samples (Table 3.4). In addition, fumonisin contamination was positively correlated with the coefficient of infection ($r=0.505$, $P=0.037$).

Indicators of *F. verticillioides* infection severity, fumonisin contamination, and kernel bulk density are correlated

We assessed correlations among indicators of FVI severity and fumonisin contamination at the plot and entry-means levels. In all families, FUM and FER were

positively correlated with each other and negatively with $BDEN_{inoc}$ in the plot and/or entry-mean analyses (Tables 3.1 and 3.5). As expected given that FUM:FER is a ratio, FUM:FER was positively correlated with FUM and negatively with FER in all analyses (Tables 3.1 and 3.5). At the plot level, $BDEN_{inoc}$ was negatively correlated with FUM:FER in the CML333xB73 family (Table 3.1). However, $BDEN_{inoc}$ was positively correlated with FUM:FER the CML52xB73 plots, which may be the result of the high proportion of asymptomatic plots in that family (Table 3.1).

We also correlated FVI BLUPs with BLUPs of $BDEN_{uninoc}$. As expected under the hypothesis that denser lines have less reduced bulk density under inoculation, $BDEN_{uninoc}$ and $BDEN_{inoc}$ were positively correlated in all families (Table 3.5). $BDEN_{uninoc}$ was negatively correlated with FER in the CML52xB73 and CML69xB73 families (Table 3.5). Unlike the correlations between FUM and $BDEN_{inoc}$, FUM was not significantly correlated with $BDEN_{uninoc}$ in any family (Table 3.5). Similar to its correlation with $BDEN_{inoc}$, FUM:FER was positively correlated with $BDEN_{uninoc}$ in the CML52xB73 family (Table 3.5). The positive correlation between $BDEN_{uninoc}$ and FUM:FER in the CML333xB73 family was opposite to that of $BDEN_{inoc}$ and FUM:FER (Table 3.5).

Broad-sense heritability and GxE differs by family and trait

To investigate genetic and environmental effects on FVI and fumonisin contamination, broad-sense heritabilities (H) were compared with the effects of genotype, environment, and their interaction (GxE) on FVI traits within and among families. H was highest for FER (76-91%) and $BDEN_{inoc}$ (81-97%) and lowest for FUM (22-70%) and FUM:FER (40-67%) (Table 3.6). Compared to the other families, the CML52xB73 family had the highest H for FER, FUM, and FUM:FER and the CML333xB73 family had the highest H for $BDEN_{inoc}$ (Table 3.6).

The variance explained by entry, year, and GxE varied by trait and by family (Table 3.6). GxE was highest for $BDEN_{inoc}$ in the CML69xB73 (32% of variance) and NC358xB73 (56% of variance) families and accounted for less than 20% of the variance in all other trait-family combinations (Table 3.6). Although GxE was low for FUM and FUM:FER in all families, year accounted for more than half of the variation and entry explained less than 10% (Table 3.6).

QTL are unique to traits

Stepwise regression selected 87 QTL associated with the nine FVI traits (69 QTL) and $BDEN_{uninoc}$ (18 QTL) in single and joint family models (Table 3.7). Eighteen QTL were selected in the joint models, and 23, 13, 21, and 12 QTL were mapped in the CML333xB73, CML52xB73, CML69xB73, and NC358xB73 families, respectively (Table 3.7). FER, $BDEN_{inoc}$, and $BDEN_{uninoc}$ had the greatest number of associated QTL (FER=26, $BDEN_{inoc}$=20, $BDEN_{uninoc}$=18), while the remaining traits had 3-5 QTL each (Table 3.7). No QTL were significantly associated with the moldy symptom type. The majority of QTL were unique to one trait (63/87, 72%), but more than half (49/87, 56%) of the single-trait QTL were found in multiple families (Table 3.8).

Kernel bulk density QTL colocalize with QTL for FVI

Four regions colocalized for multiple traits within families (Table 3.8). In the CML333xB73 family, QTL for FUM and FER colocalized on chromosome 1 at 50.84-52.22 Mbp, and QTL for FER and FUM:FER colocalized on chromosome 7 at 14.15-23.75 Mbp (Table 3.8). QTL for FER and $BDEN_{inoc}$ colocalized on chromosome 4 at 17.99-21.01 Mbp in the CML69xB73 family (Table 3.8). In the CML52xB73 family,

QTL for FER and FUM:FER colocalized on chromosome 6 at 154.53-155.09 Mbp (Table 3.8).

Six multi-trait regions were shared among families (Table 3.8). $BDEN_{inoc}$ and the starburst symptom type had overlapping QTL on chromosome 1 at 269.07-270.42 Mbp from the CML52xB73 and CML69xB73 families and on chromosome 2 at 27.6-29.68 Mbp from the CML333xB73 and NC358xB73 families (Table 3.8). QTL associated with $BDEN_{inoc}$ and FER overlapped on chromosome 4 at 178.16-179.87 Mbp in the CML69xB73 and NC358xB73 families (Table 3.8). QTL for FER, $BDEN_{inoc}$, and $BDEN_{uninoc}$ from all analyses overlapped on chromosome 5 at 84.89-169.85 Mbp (Table 3.8). A blush symptom type QTL mapped in the NC358xB73 family and a CML52xB73 QTL for FUM:FER overlapped at 17.02-18.22 Mbp on chromosome 8 (Table 3.8). Two QTL on chromosome 9 showed co-localization of $BDEN_{uninoc}$ and FUM or FER. Specifically, the QTL overlapped at 88.65-99.1 Mbp in the combined and CML69xB73 analyses and at 146.59-147.19 Mbp in the CML333xB73 and NC358xB73 families (Table 3.8).

Eight trait-specific regions were shared among single-family and joint analyses (Table 3.8). Two regions associated with $BDEN_{inoc}$ in the joint and CML333xB73 family analyses overlapped on chromosome 2 at 193.18-193.4 Mbp and on chromosome 8 at 146.16-148.34 Mbp (Table 3.8). FER QTL mapped in the NC358xB73 and joint family models overlapped on chromosome 5 at 207.26-208.11 Mbp (Table 3.8). The CML69xB73 and joint family models had overlapping regions associated with FER on chromosome 6 at 130.72-133.8 Mbp and on chromosome 7 at 141.01-141.49 Mbp (Table 3.8). QTL for the blush symptom type from the joint and CML333xB73 analyses overlapped on chromosome 5 at 202.56-203.39 Mbp (Table 3.8). Chromosome 10 at 141.55-143.13 Mbp was associated with the asymptomatic type in the CML52xB73 and joint analyses (Table 3.8). One region associated with

$BDEN_{inoc}$ was identified in two single-family (CML52xB73 and NC358xB73) analyses and in the joint model on chromosome 3 at 7.79-8.56 Mbp (Table 3.8).

Marker effects on FVI severity, fumonisin contamination, and kernel bulk density are correlated

We correlated family-specific marker effects (from markers within QTL mapped in this study) on the 10 phenotypes within and among families. Of the 225 pairwise combinations of marker effect correlations (45 trait-trait marker effect combinations*5 family-specific/combined sets), 199 were significant ($P<0.05$) (Table 3.9).

Marker effect correlations among the quantitatively-measured phenotypes ($BDEN_{inoc}$, $BDEN_{uninoc}$, FER, FUM, FUM:FER) were consistent across families and mirrored phenotypic correlations (Table 3.9). Marker effects on $BDEN_{inoc}$ and $BDEN_{uninoc}$ were positively correlated with each other, negatively correlated with marker effects on FER and FUM, and positively correlated with marker effects on FUM:FER (Table 3.9). Marker effects on FUM were positively correlated with FER and FUM:FER marker effects, and marker effects on FER and FUM:FER were negatively correlated (Table 3.9).

Marker effect correlations among the quantitative phenotypes (absence/presence of symptom types) were highly variable across families (Table 3.9). However, marker effects on the absence/presence of similar symptom types were generally positively correlated. For example, the two mild symptom types (blush and starburst) had positively correlated marker effects with each other and negatively correlated marker effects with purple, one of the most severe symptom types (Table 3.9).

Correlations between marker effects on quantitative and qualitative phenotypes were similar to their associations at the phenotypic level. For example, purple and blush plots tended to have low FER, and marker effects on the absence/presence of the purple and blush symptom type were generally negatively correlated with marker effects on FER (Table 3.9). We also found that discrete purple and moldy samples had high fumonisin levels and high coefficients of infection, and similarly, marker effects on FUM were positively correlated with marker effects on the absence/presence of the purple and moldy symptom types (Table 3.9).

FVI QTL are located in regions previously implicated in resistance to ear rots and fumonisin contamination

The majority of FVI (60/69) and $BDEN_{uninoc}$ (15/18) QTL identified in this study colocalized with previously described loci associated with ear rots, FER, and/or FUM at the bin level (Fig. 3.4). Bins 5.07, 8.08-9, 9.00, and 10.06-10.07 were unique to this study (Fig. 3.4). To identify hot spots for resistance to FVI and fumonisin contamination, we compared the number of loci (associated with ear rots, FER, FUM, and/or FVI) mapped among the bins. Bins that had a greater number of loci than one standard deviation (3.92) above the average (4.17) were considered hot spots. Nine bins fit this criterion: 2.08, 3.06, 4.03, 4.08-9, 5.04-5, 7.02, 8.03, and 10.03 (Fig. 3.4). Seven of these hot spot bins contained QTL mapped in this study (Fig. 3.4, Table 3.8).

Genes involved in cell wall organization and seed protein storage are associated with resistance to FVI

Twelve QTL mapped in this study were located in FVI hot spot bins (Table 3.8), and we sought to identify processes that were enriched in these hot-spot QTL (Fig. 3.3). There were 1,596 genes within these QTL, and we conducted GO term SEA

analysis on this list of genes. One cellular component and three molecular function GO terms were significantly enriched. GO:0016757 and GO:0016762 define the molecular functions of glycosyl transferase activity and xyloglucan:xyloglucosyl transferase activity, respectively; both are involved in cell wall organization (49). GO:0045735 corresponds to the molecular function of nutrient reservoir activity, specifically the accumulation of seed storage proteins (49). GO:0048046 is defined as an apoplast cellular component (49).

Of the 1,596 genes within hot spot QTL, the tissue-specific expression of 357 of these genes was significantly correlated with FER in the maize core diversity panel. GO term analysis on these 357 genes revealed two significantly enriched GO terms (GO:0045735, GO:0048046) involved in the apoplast and nutrient reservoir activity, which were also enriched in hot spot QTL before filtering for FER-gene expression correlations, as described previously. There were eight genes associated with these two GO terms (Table 3.10). One gene (ereb82) encodes an APETALA2-ethylene-responsive element binding protein (AP2-EREBP) transcription factor and has been shown to be highly expressed in the outer husk (47). Two genes encode germin-like proteins (GRMZM2G049930, GRMZM2G071390) (51), which have high expression the primary root and first leaf (47). Two genes encode xyloglucan:xyloglucosyl transferases (51), one which is highly expressed in the immature cob and embryo 16-18 days after pollination (DAP) (GRMZM2G319798) and the other has high expression in the immature leaf and primary root (GRMZM2G364748) (47). Two genes are highly expressed in the endosperm 20-24 DAP; GRMZM2G404688 encodes a trypsin/factor XIIA inhibitor and AF546188.1_FG001 encodes an α-zein protein (51).

Discussion

Here we show that quantitative indicators of *F. verticillioides* infection, such as FER, FUM, and $BDEN_{inoc}$ were correlated. These correlations support previous findings, wherein FER and FUM were both phenotypically and genetically correlated (12) and wherein kernel traits related to density and hardness were associated with reduced FER and FUM (16,52). Although few loci were shared among our quantitative phenotypes, marker effects on these phenotypes were correlated across loci and mirrored correlations at the phenotypic level. Horne et al. (13) previously demonstrated that resistance to fumonisin contamination can be accomplished via indirect selection for FER resistance, and our results support the feasibility of employing kernel bulk density as a proxy for fumonisin contamination and *F. verticillioides* infection severity (21,52).

However, marker effects on FUM and $BDEN_{uninoc}$ varied among families, showing that innate kernel characteristics that influence bulk density are not necessarily indicative of resistance to fumonisin contamination. In addition, symptomatology and marker effect correlations between symptom types and the other traits were family-specific, further demonstrating the diverse modes of resistance and symptomatology. For example, although the CML333xB73 family had high FER scores, it had low FUM and high DEN_{uninoc}. The relatively mild symptomatology (blush symptom type) of the CML333xB73 family may indicate this family's unique ability of limiting fungal infection to the kernel crown.

Broad-sense heritability for FER was high across families (77-91%), comparable to heritabilites reported in the literature (11,28). In previous studies, FER was less heritable than FUM (11,12). The relatively lower heritability for FUM (22-70% broad-sense heritability) in our experiments may be due to the inoculation method (insertion of spore-coated toothpick into the developing ear), which has been shown to have poor ability to differentiate hybrids with respect to FUM (53).

However, we were able to detect significant genotypic effects on FUM and identify QTL associated with FUM. In addition, this inoculation method yielded FUM levels similar to those found in naturally-infected grain (6,4). Mycotoxin resistance and kernel composition are influenced by environmental conditions and management practices (12,4,23,43,54–57), which may explain the environmental and GxE effects on FUM and $BDEN_{inoc}$ reported here.

The majority of QTL in this study were located in regions of the genome previously implicated in resistance to *F. verticillioides* (12,14,25,28,40–44), and the loci reported here and in other studies were overrepresented in certain hot spots. Genes involved in the apoplast and seed storage protein accumulation were enriched in these hot spots. *F. verticillioides* primarily colonizes maize kernel tissues intercellularly via the apoplast (58), and our candidate genes involved in the apoplast (xyloglucan:xyloglucosyl transferases) may be involved in detection of fungal entry or in strengthening the cell wall (59,60). Seed storage proteins, such as zeins and germins, confer hardness to the endosperm (61) and have been associated with resistance to *F. verticillioides* in maize kernels (62), respectively. We also identified an AP2-EREBP-transcription factor as a candidate gene, which is part of a family of transcription factors that are involved in signaling during pathogenesis in Arabidopsis (63) and have pleiotropic effects on plant architecture and yield components, such as total kernel weight, in wheat (64). Our analyses of FER versus gene expression employed expression data from uninoculated experiments, which may reveal constitutive defense mechanisms.

This experiment employed four tropical flint-by-temperate dent RIL families from the NAM, demonstrating the link between kernel density-related characteristics and resistance to *F. verticillioides* infection and fumonisin production. In addition, the candidate genes identified here were located in bins previously associated with

resistance to FER in a tropical-by-temperate association panel (25). It is important to document the dynamics of these types of population crosses because breeding programs located in tropical regions where infection by mycotoxigenic fungi is prevalent frequently employ temperate-by-tropical crosses to improve yield (20,25). Our results complement previous findings, wherein quality-related kernel traits, such as density, were positively associated with mycotoxin resistance at the phenotypic and genetic levels (1,20,65). However, the family-specific nature of correlations and colocalizations in this study implies that distinct modes of pathogenesis exist within tropical germplasm, which can be leveraged for breeding resistance. We recommend that breeders take into account the trade-offs among yield capacity, stress tolerance, and mycotoxin resistance.

Tables and figures

Table 3.1. Pairwise correlations among days to silking (DTS), inoculated kernel bulk density ($BDEN_{inoc}$), Fusarium ear rot (FER), fumonisin (FUM), and FUM:FER of plots within the four families.

Family	Pheno 1	Pheno 2	N	Correlation	p-value
CML333xB73	$BDEN_{inoc}$	DTS	256	-0.090	0.1514
CML333xB73	$BDEN_{inoc}$	FER	256	-0.464	<.0001***
CML333xB73	FER	DTS	493	-0.014	0.7603
CML333xB73	FUM	$BDEN_{inoc}$	257	-0.350	<.0001***
CML333xB73	FUM	DTS	453	-0.172	0.0002**
CML333xB73	FUM	FER	453	0.169	0.0003**
CML333xB73	FUM	FUM:FER	453	0.936	<.0001***
CML333xB73	FUM:FER	$BDEN_{inoc}$	256	-0.153	0.014*
CML333xB73	FUM:FER	DTS	453	-0.170	0.0003**
CML333xB73	FUM:FER	FER	453	-0.182	0.0001**
CML52xB73	$BDEN_{inoc}$	DTS	319	0.146	0.009**
CML52xB73	$BDEN_{inoc}$	FER	321	-0.472	<.0001***
CML52xB73	FER	DTS	703	0.130	0.0005**
CML52xB73	FUM	$BDEN_{inoc}$	320	-0.122	0.0289*
CML52xB73	FUM	DTS	507	-0.302	<.0001***
CML52xB73	FUM	FER	508	0.084	0.06
CML52xB73	FUM	FUM:FER	508	0.895	<.0001***
CML52xB73	FUM:FER	$BDEN_{inoc}$	320	0.116	0.0387*
CML52xB73	FUM:FER	DTS	506	-0.269	<.0001***
CML52xB73	FUM:FER	FER	508	-0.359	<.0001***
CML69xB73	$BDEN_{inoc}$	DTS	303	0.066	0.2543
CML69xB73	$BDEN_{inoc}$	FER	302	-0.552	<.0001***
CML69xB73	FER	DTS	512	0.041	0.3572
CML69xB73	FUM	$BDEN_{inoc}$	303	-0.301	<.0001***
CML69xB73	FUM	DTS	473	-0.581	<.0001***
CML69xB73	FUM	FER	472	-0.014	0.7627
CML69xB73	FUM	FUM:FER	472	0.946	<.0001***
CML69xB73	FUM:FER	$BDEN_{inoc}$	302	0.017	0.7692
CML69xB73	FUM:FER	DTS	472	-0.574	<.0001***
CML69xB73	FUM:FER	FER	472	-0.333	<.0001***
NC358xB73	$BDEN_{inoc}$	DTS	242	-0.110	0.0872
NC358xB73	$BDEN_{inoc}$	FER	241	-0.593	<.0001***
NC358xB73	FER	DTS	622	-0.024	0.5494
NC358xB73	FUM	$BDEN_{inoc}$	241	-0.192	0.0027**
NC358xB73	FUM	DTS	431	-0.534	<.0001***
NC358xB73	FUM	FER	429	0.212	<.0001***
NC358xB73	FUM	FUM:FER	429	0.936	<.0001***
NC358xB73	FUM:FER	$BDEN_{inoc}$	240	0.110	0.0896
NC358xB73	FUM:FER	DTS	429	-0.526	<.0001***
NC358xB73	FUM:FER	FER	429	-0.138	0.0041**

Correlation significance denoted as: *0.1>P≥0.05; **0.05>P≥0.0001; ***P<0.0001
$BDEN_{inoc}$, FER, FUM, and FUM:FER plot data were Box-Cox transformed

Table 3.2. (A) ANOVA summaries of inoculated kernel bulk density ($BDEN_{inoc}$), Fusarium ear rot (FER), fumonisin (FUM), and FUM:FER versus family and (B) pairwise t-tests comparing $BDEN_{inoc}$, FER, FUM, and FUM:FER between families.

Trait	(A) ANOVA						(B) Mean comparisons				
	Source	DF	SS	MS	F	p-value	Family	N	Mean	SE	Sig. group
$BDEN_{inoc}$	Family	3	0.40	0.13	40.88	<.0001***	CML333xB73	257	0.74005	0.00332	A
	Error	1119	3.63	0.00			CML52xB73	321	0.72338	0.00354	B
	Total	1122	4.02				CML69xB73	303	0.7156	0.00328	B
	R^2	0.099					NC358xB73	242	0.68412	0.00423	C
FER	Family	3	30704.40	10234.80	16.41	<.0001***	CML333xB73	493	43.0372	1.269	A
	Error	2329	1452661.50	623.70			CML52xB73	706	34.4091	1.0525	B
	Total	2332	1483365.90				CML69xB73	512	40.0382	1.231	A
	R^2	0.021					NC358xB73	622	43.2665	1.1979	A
FUM	Family	3	741.10	247.03	9.51	<.0001***	CML333xB73	455	24.239	5.322	B
	Error	1865	48449.87	25.98			CML52xB73	509	11.769	2.385	B
	Total	1868	49190.97				CML69xB73	474	31.276	5.053	A
	R^2	0.015					NC358xB73	431	32.615	4.213	A
FUM:FER	Family	3	1.63	0.54	10.91	<.0001***	CML333xB73	453	0.51326	0.09555	C
	Error	1858	92.32	0.05			CML52xB73	508	0.5975	0.0755	B
	Total	1861	93.94				CML69xB73	472	0.99794	0.12741	AB
	R^2	0.017					NC358xB73	429	1.18623	0.2265	A

ANOVA significance of family is denoted as: ***P<0.0001

Families not connected by the same letter are significantly different (two-tailed t-test P<0.05)

$BDEN_{inoc}$, FER, FUM, and FUM:FER plot data were Box-Cox transformed for analyses, but the means and standard errors reported here were back-transformed

Table 3.3. ANOVA model summaries (families combined and individually) and symptom type means and standard errors for inoculated kernel bulk density ($BDEN_{inoc}$), FER, fumonisin (FUM), and FUM:FER in bulked plot samples.

Family	Symptom type	$BDEN_{inoc}$	FER	FUM	FUM:FER
Combined	Asymptomatic	0.69 ±0.003 A	19.58 ±0.44 E	2.67 ±0.21 A	0.96 ±0.009 A
	Blush	0.68 ±0.005 A	56.59 ±1.88 C	0.79 ±0.43 C	0.73 ±0.017 C
	Starburst	0.66 ±0.003 B	65.54 ±0.75 B	1.84 ±0.18 B	0.75 ±0.008 C
	Purple	0.64 ±0.003 C	50.51 ±0.82 D	1.40 ±0.23 BC	0.78 ±0.009 B
	Moldy	0.58 ±0.013 D	76.14 ±2.64 A	3.44 ±0.86 A	0.79 ±0.038 BC
	Model R^2	0.16	0.38	0.01	0.1
	Model p-value	<0.0001***	<0.0001***	0.0002**	<0.0001***
CML333xB73	Asymptomatic	0.713 ±0.007 A	19.73 ±1.36 C	1.50 ±0.59 AB	0.91 ±0.02 A
	Blush	0.691 ±0.005 B	58.68 ±2.20 B	1.06 ±0.47 AB	0.74 ±0.02 B
	Starburst	0.685 ±0.006 B	70.49 ±1.49 A	1.80 ±0.37 A	0.73 ±0.02 B
	Purple	0.658 ±0.006 C	54.04 ±1.79 B	0.10 ±0.49 B	0.71 ±0.02 B
	Moldy	0.601 ±0.021 D	77.95 ±3.77 A	2.35 ±1.45 AB	0.73 ±0.07 B
	Model R^2	0.19	0.3	0.02	0.05
	Model p-value	<0.0001***	<0.0001***	0.0427*	0.0001**
CML52xB73	Asymptomatic	0.688 ±0.005 A	18.09 ±0.68 D	2.13 ±0.31 A	0.94 ±0.01 A
	Blush	0.606 ±0.020 B	46.78 ±7.61 BC	-0.69 ±2.08 AB	0.7 0±0.07 BC
	Starburst	0.660 ±0.004 B	59.81 ±1.32 B	1.27 ±0.28 B	0.74 ±0.01 C
	Purple	0.655 ±0.008 B	41.05 ±1.57 C	0.76 ±0.44 AB	0.78 ±0.02 B
	Moldy	0.503 ±0.039 C	84.19 ±5.38 A	1.03 ±1.99 AB	0.66 ±0.08 BC
	Model R^2	0.19	0.5	0.01	0.17
	Model p-value	<0.0001***	<0.0001***	0.113	<0.0001***
CML69xB73	Asymptomatic	0.693 ±0.004 A	21.47 ±0.79 C	3.86 ±0.33 AB	0.99 ±0.01 A
	Blush	0.659 ±0.016 AB	46.36 ±6.61 B	1.03 ±1.82 BC	0.78 ±0.07 BC
	Starburst	0.657 ±0.005 C	67.74 ±1.40 A	2.06 ±0.39 C	0.75 ±0.02 C
	Purple	0.644 ±0.006 B	54.22 ±1.63 B	1.68 ±0.48 C	0.78 ±0.02 BC
	Moldy	0.588 ±0.021 B	72.49 ±5.74 A	5.43 ±1.58 A	0.88 ±0.07 AB
	Model R^2	0.17	0.38	0.03	0.11
	Model p-value	<0.0001***	<0.0001***	0.015*	<0.0001***
NC358xB73	Asymptomatic	0.692 ±0.006 A	20.88 ±0.85 D	3.32 ±0.56 A	0.97 ±0.02 A
	Blush	0.654 ±0.016 AB	56.06 ±4.60 BC	-0.55 ±1.3 B	0.67 ±0.05 D
	Starburst	0.617 ±0.006 C	66.45 ±1.68 A	2.41 ±0.41 A	0.77 ±0.02 CD
	Purple	0.623 ±0.006 B	51.19 ±1.40 C	2.67 ±0.40 A	0.82 ±0.02 B
	Moldy	0.562 ±0.029 B	68.74 ±7.55 AB	5.51 ±1.80 A	0.89 ±0.08 ABC
	Model R2	0.17	0.33	0.02	0.09
	Model p-value	<0.0001***	<0.0001***	0.0502	<0.0001***

$BDEN_{inoc}$, FER, FUM, and FUM:FER were Box-Cox transformed
Pairwise correlation significance is denoted as: **0.05>P≥0.0001; ***P<0.0001

Table 3.4. Model summaries of ANOVA of fumonisin and *F. verticillioides* infection vs. symptom type, and means and standard errors of discrete symptom type kernel samples.

Symptom type	Fumonisin	*F. vert.* infection
Asymptomatic	3.33 ±0.04 B	68.59 ±5.39 B
Blush	28.22 ±15.92 B	81.57 ±9.82 B
Starburst	33.98 ±28.57 AB	72.02 ±5.42 B
Moldy	40.42 ±24.39 AB	150.10 ±5.02 A
Purple	100.08 ±30.67 A	136.34 ±6.88 A
Model R^2	0.4	0.94
Model p-value	0.09	<0.0001

Levels not connected by the same letter are significantly different (two-tailed t-test, $P<0.05$)

Table 3.5. Pairwise correlations among line-means of kernel bulk density without ($BDEN_{uninoc}$) and with inoculation ($BDEN_{inoc}$), Fusarium ear rot (FER), fumonisin (FUM), and FUM:FER within the four families.

Family	BLUP 1	BLUP 2	N	Correlation	p-value
CML333xB71	$BDEN_{uninoc}$	$BDEN_{inoc}$	133	0.261	0.0024**
CML333xB69	$BDEN_{uninoc}$	FER	186	-0.058	0.4314
CML333xB70	$BDEN_{uninoc}$	FUM	186	0.122	0.0982
CML333xB71	$BDEN_{uninoc}$	FUM:FER	186	0.150	0.0417*
CML333xB72	$BDEN_{inoc}$	FER	139	-0.533	<.0001***
CML333xB73	$BDEN_{inoc}$	FUM	139	-0.307	0.0002**
CML333xB73	FUM	FER	192	0.279	<.0001***
CML333xB73	FUM:FER	$BDEN_{inoc}$	139	0.026	0.7631
CML333xB73	FUM:FER	FER	192	-0.334	<.0001***
CML333xB73	FUM:FER	FUM	192	0.797	<.0001***
CML52xB73	$BDEN_{uninoc}$	$BDEN_{inoc}$	176	0.367	<.0001***
CML52xB73	$BDEN_{uninoc}$	FER	186	-0.305	<.0001***
CML52xB73	$BDEN_{uninoc}$	FUM	185	-0.008	0.9137
CML52xB73	$BDEN_{uninoc}$	FUM:FER	185	0.191	0.0091**
CML52xB73	$BDEN_{inoc}$	FER	177	-0.460	<.0001***
CML52xB73	$BDEN_{inoc}$	FUM	177	-0.181	0.0157*
CML52xB73	FUM	FER	186	0.174	0.0178*
CML52xB73	FUM:FER	$BDEN_{inoc}$	177	0.139	0.0642
CML52xB73	FUM:FER	FER	186	-0.479	<.0001***
CML52xB73	FUM:FER	FUM	186	0.745	<.0001***
CML69xB73	$BDEN_{uninoc}$	$BDEN_{inoc}$	170	0.378	<.0001***
CML69xB73	$BDEN_{uninoc}$	FER	183	-0.224	0.0023**
CML69xB73	$BDEN_{uninoc}$	FUM	181	-0.145	0.0517
CML69xB73	$BDEN_{uninoc}$	FUM:FER	181	-0.003	0.9654
CML69xB73	$BDEN_{inoc}$	FER	178	-0.539	<.0001***
CML69xB73	$BDEN_{inoc}$	FUM	178	-0.278	0.0002**
CML69xB73	FUM	FER	189	0.212	0.0034**
CML69xB73	FUM:FER	$BDEN_{inoc}$	178	0.048	0.5249
CML69xB73	FUM:FER	FER	189	-0.384	<.0001***
CML69xB73	FUM:FER	FUM	189	0.807	<.0001***
NC358xB73	$BDEN_{uninoc}$	$BDEN_{inoc}$	139	0.349	<.0001***
NC358xB73	$BDEN_{uninoc}$	FER	171	-0.102	0.1854
NC358xB73	$BDEN_{uninoc}$	FUM	163	-0.004	0.9556
NC358xB73	$BDEN_{uninoc}$	FUM:FER	163	0.070	0.377
NC358xB73	$BDEN_{inoc}$	FER	145	-0.576	<.0001***
NC358xB73	$BDEN_{inoc}$	FUM	145	-0.248	0.0027**
NC358xB73	FUM	FER	171	0.117	0.128
NC358xB73	FUM:FER	$BDEN_{inoc}$	145	0.153	0.0665
NC358xB73	FUM:FER	FER	171	-0.458	<.0001***
NC358xB73	FUM:FER	FUM	171	0.792	<.0001***

Pairwise correlation significance is denoted as: *0.1>P≥0.05; **0.05>P≥0.0001; ***P<0.0001

Table 3.6. Mixed model summaries and broad-sense heritabilities of Fusarium ear rot (FER), fumonisin (FUM), inoculated kernel bulk density ($BDEN_{inoc}$), and FUM:FER within and among the four families.

Family	Trait	Random effects			Fixed effects			H
		Effect	Variance	SD	Effect	Estimate	SE	
Combined	FER	Entry*Year	6.03E+01	7.76E+00	Int.	4.3E+01	1.1E+01	0.89
		Entry	2.14E+02	1.46E+01	DTS	2.3E-01	1.4E-01	
		Block[Year]	3.36E+01	5.80E+00				
		Year	9.01E+01	9.49E+00				
		Error	2.80E+02	1.67E+01				
	FUM	Entry*Year	2.21E+00	1.49E+00	Int.	5.9E+00	3.0E+00	0.32
		Entry	5.39E-01	7.34E-01	DTS	-5.3E-02	2.4E-02	
		Block[Year]	1.17E+00	1.08E+00				
		Year	1.89E+01	4.34E+00				
		Error	8.52E+00	2.92E+00				
	$BDEN_{inoc}$	Entry*Year	1.52E-04	1.23E-02	Int.	-3.5E-01	-3.5E-02	0.91
		Entry	1.51E-03	3.89E-02	DTS	9.3E-05	4.9E-04	
		Block[Year]	3.02E-04	1.74E-02				
		Year	3.76E-05	6.13E-03				
		Error	1.55E-03	3.93E-02				
	FUM:FER	Entry*Year	2.35E-03	4.85E-02	Int.	-8.8E-02	1.3E-01	0.49
		Entry	1.59E-03	3.99E-02	DTS	-1.6E-03	1.1E-03	
		Block[Year]	2.07E-03	4.55E-02				
		Year	3.50E-02	1.87E-01				
		Error	1.91E-02	1.38E-01				
CML333xB73	FER	Entry*Year	6.94E+01	8.33E+00	Int.	6.0E+01	2.5E+01	0.90
		Entry	2.54E+02	1.59E+01	DTS	3.9E-02	3.5E-01	
		Block[Year]	0.00E+00	0.00E+00				
		Year	1.71E+01	4.14E+00				
		Error	2.60E+02	1.61E+01				
	FUM	Entry*Year	5.48E+00	2.34E+00	Int.	-3.2E+00	5.3E+00	0.21
		Entry	5.63E-01	7.50E-01	DTS	6.8E-02	6.4E-02	
		Block[Year]	0.00E+00	0.00E+00				
		Year	2.06E+01	4.54E+00				
		Error	7.27E+00	2.70E+00				
	$BDEN_{inoc}$	Entry*Year	1.14E-04	1.07E-02	Int.	-2.0E-01	6.3E-02	0.95
		Entry	1.92E-03	4.38E-02	DTS	-1.7E-03	8.9E-04	
		Block[Year]	0.00E+00	0.00E+00				
		Year	3.63E-05	6.03E-03				
		Error	9.09E-04	3.02E-02				
	FUM:FER	Entry*Year	6.25E-03	7.91E-02	Int.	-3.5E-01	2.3E-01	0.36
		Entry	1.65E-03	4.06E-02	DTS	1.5E-03	2.8E-03	
		Block[Year]	0.00E+00	0.00E+00				
		Year	3.53E-02	1.88E-01				
		Error	1.72E-02	1.31E-01				
CML52xB73	FER	Entry*Year	4.08E+01	6.39E+00	Int.	1.1E+01	1.9E+01	0.90
		Entry	2.13E+02	1.46E+01	DTS	5.3E-01	2.3E-01	
		Block[Year]	2.28E+01	4.78E+00				
		Year	1.38E+02	1.17E+01				
		Error	2.87E+02	1.69E+01				
	FUM	Entry*Year	2.43E-01	4.93E-01	Int.	6.9E+00	3.6E+00	0.56
		Entry	7.32E-01	8.55E-01	DTS	-7.3E-02	4.1E-02	
		Block[Year]	8.81E-01	9.39E-01				
		Year	1.04E+01	3.23E+00				
		Error	1.07E+01	3.27E+00				
	$BDEN_{inoc}$	Entry*Year	0.00E+00	0.00E+00	Int.	-3.5E-01	5.4E-02	0.92
		Entry	1.19E-03	3.45E-02	DTS	3.2E-04	7.3E-04	
		Block[Year]	1.42E-04	1.19E-02				
		Year	1.20E-05	3.47E-03				
		Error	2.23E-03	4.72E-02				
	FUM:FER	Entry*Year	0.00E+00	0.00E+00	Int.	-3.9E-02	1.6E-01	0.50
		Entry	1.08E-03	3.29E-02	DTS	-2.2E-03	1.8E-03	
		Block[Year]	7.05E-04	2.66E-02				
		Year	2.34E-02	1.53E-01				
		Error	2.35E-02	1.53E-01				

Table 3.6. (continued)

Family	Trait	Random effects			Fixed effects			H
		Effect	Variance	SD	Effect	Estimate	SE	
CML69xB73	FER	Entry*Year	1.21E+02	1.10E+01	Int.	5.5E+01	2.8E+01	0.77
		Entry	1.45E+02	1.21E+01	DTS	8.2E-02	3.8E-01	
		Block[Year]	1.92E+01	4.38E+00				
		Year	9.36E+01	9.68E+00				
		Error	2.90E+02	1.70E+01				
	FUM	Entry*Year	4.92E+00	2.22E+00	Int.	8.6E+00	4.9E+00	0.23
		Entry	5.71E-01	7.55E-01	DTS	-8.6E-02	5.4E-02	
		Block[Year]	4.14E-01	6.43E-01				
		Year	2.58E+01	5.08E+00				
		Error	5.09E+00	2.26E+00				
	$BDEN_{inoc}$	Entry*Year	9.49E-04	3.08E-02	Int.	-3.5E-01	7.6E-02	0.73
		Entry	1.37E-03	3.71E-02	DTS	1.0E-04	1.1E-03	
		Block[Year]	6.27E-05	7.92E-03				
		Year	8.30E-05	9.11E-03				
		Error	5.48E-04	2.34E-02				
	FUM:FER	Entry*Year	5.03E-03	7.09E-02	Int.	-2.1E-03	2.2E-01	0.42
		Entry	1.72E-03	4.15E-02	DTS	-2.7E-03	2.5E-03	
		Block[Year]	1.27E-03	3.56E-02				
		Year	5.32E-02	2.31E-01				
		Error	1.47E-02	1.21E-01				
NC358xB73	FER	Entry*Year	4.25E+01	6.52E+00	Int.	-1.2E+01	2.4E+01	0.89
		Entry	1.80E+02	1.34E+01	DTS	1.1E+00	3.4E-01	
		Block[Year]	2.61E+01	5.11E+00				
		Year	1.50E+02	1.22E+01				
		Error	2.70E+02	1.64E+01				
	FUM	Entry*Year	1.34E+00	1.16E+00	Int.	1.7E+00	4.9E+00	0.38
		Entry	4.78E-01	6.91E-01	DTS	1.9E-02	5.7E-02	
		Block[Year]	0.00E+00	0.00E+00				
		Year	2.51E+01	5.01E+00				
		Error	7.70E+00	2.77E+00				
	$BDEN_{inoc}$	Entry*Year	2.11E-03	4.60E-02	Int.	-1.4E-01	1.0E-01	0.45
		Entry	8.74E-04	2.96E-02	DTS	-3.5E-03	1.5E-03	
		Block[Year]	5.85E-05	7.65E-03				
		Year	2.83E-04	1.68E-02				
		Error	4.64E-04	2.15E-02				
	FUM:FER	Entry*Year	3.53E-03	5.94E-02	Int.	-9.5E-02	2.1E-01	0.44
		Entry	1.49E-03	3.86E-02	DTS	-1.1E-03	2.6E-03	
		Block[Year]	0.00E+00	0.00E+00				
		Year	3.70E-02	1.92E-01				
		Error	1.53E-02	1.24E-01				

Table 3.7. Stepwise model summaries for each trait in combined and single families.

Family	Trait	Chr.	Left	Right	df	SS	MS	F	p-value	BIC	mBIC	AIC	Model R^2
CML333xB73	Blush	5	202372898	203392355	1	5.36E+00	5.36E+00	30.43	1.15E-07	-316.11	694.58	-322.57	0.141
		Error	--	--	185	3.26E+01	1.76E-01	--	--	--	--	--	--
		mean	--	--	1	1.94E+01	1.94E+01	109.97	1.73E-20	-316.11	694.58	-322.57	0.141
	$BDEN_{inoc}$	2	22854482	35311519	1	1.09E-02	1.09E-02	20.09	1.58E-05	-1017.70	-256.54	-1032.30	0.394
		2	193177081	195188506	1	1.42E-02	1.42E-02	26.00	1.15E-06	-1017.70	-256.54	-1032.30	0.394
		8	146156391	151773181	1	6.47E-03	6.47E-03	11.89	7.57E-04	-1017.70	-256.54	-1032.30	0.394
		8	173075636	175784078	1	8.83E-03	8.83E-03	16.22	9.43E-05	-1017.70	-256.54	-1032.30	0.394
		Error	--	--	133	7.24E-02	5.44E-04	--	--	--	--	--	--
		mean	--	--	1	3.41E+00	3.41E+00	6269.15	9.10E-114	-1017.70	-256.54	-1032.30	0.394
	FER	1	88897	3026161	1	1.99E+03	1.99E+03	24.28	1.90E-06	852.95	1954.84	827.15	0.423
		1	50843507	57347172	1	1.87E+03	1.87E+03	22.90	3.57E-06	852.95	1954.84	827.15	0.423
		2	37754001	39891173	1	1.39E+03	1.39E+03	17.03	5.63E-05	852.95	1954.84	827.15	0.423
		2	226246821	226664978	1	1.30E+03	1.30E+03	15.83	1.01E-04	852.95	1954.84	827.15	0.423
		3	171730137	182742189	1	1.13E+03	1.13E+03	13.82	2.69E-04	852.95	1954.84	827.15	0.423
		7	14152199	14804088	1	9.80E+02	9.80E+02	11.97	6.76E-04	852.95	1954.84	827.15	0.423
		9	1244225	2627062	1	1.32E+03	1.32E+03	16.08	8.91E-05	852.95	1954.84	827.15	0.423
		Error	--	--	178	1.46E+04	8.19E+01	--	--	--	--	--	--
		mean	--	--	1	6.16E+04	6.16E+04	752.92	7.51E-66	852.95	1954.84	827.15	0.423
	FUM	1	47813030	52221146	1	1.14E+00	1.14E+00	20.85	9.11E-06	-528.54	492.16	-538.21	0.144
		7	107154252	108353941	1	7.16E-01	7.16E-01	13.14	3.75E-04	-528.54	492.16	-538.21	0.144
		Error	--	--	183	9.97E+00	5.45E-02	--	--	--	--	--	--
		mean	--	--	1	2.52E+03	2.52E+03	46238.48	6.03E-222	-528.54	492.16	-538.21	0.144
	FUM:FER	7	14804088	23748237	1	3.37E-03	3.37E-03	15.36	1.25E-04	-1558.40	-553.98	-1564.90	0.077
		Error	--	--	184	4.04E-02	2.20E-04	--	--	--	--	--	--
		mean	--	--	1	7.98E-01	7.98E-01	3633.92	4.12E-123	-1558.40	-553.98	-1564.90	0.077
	Starburst	7	4823956	5828359	1	3.89E+00	3.89E+00	17.48	4.48E-05	-272.32	738.37	-278.79	0.086
		Error	--	--	185	4.12E+01	2.23E-01	--	--	--	--	--	--
		mean	--	--	1	6.20E+00	6.20E+00	27.85	3.65E-07	-272.32	738.37	-278.79	0.086
	$BDEN_{uninoc}$	3	137231734	154792291	1	3.38E-02	3.38E-02	14.60	1.85E-04	-1060.00	6.09	-1090.00	0.438
		5	6948413	7883990	1	3.60E-02	3.60E-02	15.53	1.18E-04	-1060.00	6.09	-1090.00	0.438
		5	164440127	172756497	1	3.02E-02	3.02E-02	13.02	4.03E-04	-1060.00	6.09	-1090.00	0.438
		5	215194661	217759022	1	5.27E-02	5.27E-02	22.72	3.95E-06	-1060.00	6.09	-1090.00	0.438
		8	95667409	98116975	1	1.07E-01	1.07E-01	46.15	1.69E-10	-1060.00	6.09	-1090.00	0.438
		9	120045550	126147403	1	6.31E-02	6.31E-02	27.24	5.10E-07	-1060.00	6.09	-1090.00	0.438
		9	146587518	148495053	1	3.99E-02	3.99E-02	17.23	5.19E-05	-1060.00	6.09	-1090.00	0.438
		Error	--	--	173	4.01E-01	2.32E-03	--	--	--	--	--	--
		mean	--	--	1	1.62E+01	1.62E+01	7008.88	6.51E-142	-1060.00	6.09	-1090.00	0.438
CML52xB73	Asym	10	141547773	143125860	1	2.51E+00	2.51E+00	12.82	4.44E-04	-278.40	664.08	-284.74	0.069
		Error	--	--	174	3.41E+01	1.96E-01	--	--	--	--	--	--
		mean	--	--	1	2.49E+00	2.49E+00	12.68	4.76E-04	-278.40	664.08	-284.74	0.069
	$BDEN_{inoc}$	1	265764266	270418769	1	1.01E-02	1.01E-02	14.39	2.09E-04	-1195.90	-276.23	-1208.40	0.245
		3	7785135	9391912	1	1.41E-02	1.41E-02	20.01	1.44E-05	-1195.90	-276.23	-1208.40	0.245
		5	84885005	129645630	1	1.32E-02	1.32E-02	18.69	2.67E-05	-1195.90	-276.23	-1208.40	0.245
		Error	--	--	163	1.15E-01	7.04E-04	--	--	--	--	--	--
		mean	--	--	1	5.14E+00	5.14E+00	7301.10	2.79E-137	-1195.90	-276.23	-1208.40	0.245
	FER	3	161576393	166829493	1	1.51E+03	1.51E+03	14.82	1.67E-04	834.54	1825.73	818.69	0.278
		5	206058644	206658699	1	1.18E+03	1.18E+03	11.59	8.26E-04	834.54	1825.73	818.69	0.278
		6	154345567	155086056	1	2.30E+03	2.30E+03	22.60	4.21E-06	834.54	1825.73	818.69	0.278
		8	137311246	139916747	1	1.31E+03	1.31E+03	12.85	4.41E-04	834.54	1825.73	818.69	0.278
		Error	--	--	171	1.74E+04	1.02E+02	--	--	--	--	--	--
		mean	--	--	1	6.71E+04	6.71E+04	658.33	1.60E-60	834.54	1825.73	818.69	0.278
	FUM:FER	2	186831881	189497979	1	2.76E-03	2.76E-03	13.28	3.56E-04	-1467.20	-498.42	-1479.90	0.187
		6	154530689	156104230	1	3.70E-03	3.70E-03	17.79	3.99E-05	-1467.20	-498.42	-1479.90	0.187
		8	17017893	18482735	1	2.36E-03	2.36E-03	11.35	9.35E-04	-1467.20	-498.42	-1479.90	0.187
		Error	--	--	171	3.55E-02	2.08E-04	--	--	--	--	--	--
		mean	--	--	1	4.01E-01	4.01E-01	1931.05	4.35E-95	-1467.20	-498.42	-1479.90	0.187
	$BDEN_{uninoc}$	2	171109445	176426230	1	0.03248	0.03248	11.29651	9.57E-04	-1.01E+03	-5.90E+01	-1.02E+03	0.14261
		9	106856548	113420650	1	0.04543	0.04543	15.79902	1.04E-04	-1.01E+03	-5.90E+01	-1.02E+03	0.14261
		Error	--	--	172	0.49455	0.00288	--	--	--	--	--	--
		mean	--	--	1	28.71946	28.71946	9988.423	2.81E-154	-1.01E+03	-5.90E+01	-1.02E+03	0.14261

Table 3.7. (continued)

Family	Trait	Chr.	Left	Right	df	SS	MS	F	p-value	BIC	mBIC	AIC	Model R^2
CML69xB73	Asym	7	127285223	131013932	1	2.11E+00	2.11E+00	13.48	3.16E-04	-334.51	663.73	-340.95	0.069
		Error	--	--	183	2.87E+01	1.57E-01	--	--	--	--	--	--
		mean	--	--	1	1.22E+00	1.22E+00	7.79	5.80E-03	-334.51	663.73	-340.95	0.069
	$BDEN_{inoc}$	1	22029001	24689765	1	1.51E-02	1.51E-02	28.98	2.45E-07	-1279.20	-312.65	-1294.90	0.336
		4	17330826	21710411	1	1.31E-02	1.31E-02	25.16	1.34E-06	-1279.20	-312.65	-1294.90	0.336
		5	171150903	175669412	1	9.02E-03	9.02E-03	17.27	5.17E-05	-1279.20	-312.65	-1294.90	0.336
		8	100566541	102748623	1	6.05E-03	6.05E-03	11.58	8.36E-04	-1279.20	-312.65	-1294.90	0.336
		Error	--	--	167	8.72E-02	5.22E-04	--	--	--	--	--	--
		mean	--	--	1	3.07E+00	3.07E+00	5879.98	4.31E-132	-1279.20	-312.65	-1294.90	0.336
	FER	1	276934002	280825668	1	1.05E+03	1.05E+03	15.91	9.75E-05	808.77	1914.45	779.83	0.454
		4	17986822	21013671	1	1.64E+03	1.64E+03	24.90	1.45E-06	808.77	1914.45	779.83	0.454
		4	178497329	179870074	1	1.16E+03	1.16E+03	17.61	4.31E-05	808.77	1914.45	779.83	0.454
		5	80166258	156764314	1	1.34E+03	1.34E+03	20.32	1.20E-05	808.77	1914.45	779.83	0.454
		6	93144004	95724368	1	9.62E+02	9.62E+02	14.56	1.88E-04	808.77	1914.45	779.83	0.454
		6	130721405	133529499	1	1.18E+03	1.18E+03	17.79	3.95E-05	808.77	1914.45	779.83	0.454
		7	141486076	142429440	1	2.30E+03	2.30E+03	34.83	1.82E-08	808.77	1914.45	779.83	0.454
		8	169208747	169829320	1	9.61E+02	9.61E+02	14.55	1.89E-04	808.77	1914.45	779.83	0.454
		Error	--	--	175	1.16E+04	6.61E+01	--	--	--	--	--	--
		mean	--	--	1	5.47E+04	5.47E+04	827.39	3.13E-68	808.77	1914.45	779.83	0.454
	FUM	9	88651842	96557796	1	7.33E-01	7.33E-01	15.47	1.20E-04	-546.64	432.97	-553.04	0.079
		Error	--	--	180	8.53E+00	4.74E-02	--	--	--	--	--	--
		mean	--	--	1	3.00E+03	3.00E+03	63308.21	3.21E-231	-546.64	432.97	-553.04	0.079
	Purple	4	167128403	172797675	1	3.04E+00	3.04E+00	14.09	2.34E-04	-270.90	743.58	-280.56	0.145
		7	167973298	169095061	1	3.04E+00	3.04E+00	14.07	2.36E-04	-270.90	743.58	-280.56	0.145
		Error	--	--	182	3.93E+01	2.16E-01	--	--	--	--	--	--
		mean	--	--	1	5.54E+00	5.54E+00	25.66	9.95E-07	-270.90	743.58	-280.56	0.145
	Starburst	1	269068613	273487121	1	2.99E+00	2.99E+00	13.66	2.89E-04	-268.27	746.20	-277.93	0.135
		2	59197257	113031412	1	3.41E+00	3.41E+00	15.54	1.15E-04	-268.27	746.20	-277.93	0.135
		Error	--	--	182	3.99E+01	2.19E-01	--	--	--	--	--	--
		mean	--	--	1	2.73E+00	2.73E+00	12.47	5.25E-04	-268.27	746.20	-277.93	0.135
	$BDEN_{uninoc}$	1	7719999	9378393	1	0.02189	0.02189	12.21201	6.03E-04	-1.10E+03	-1.22E+02	-1.12E+03	0.17971
		5	64119272	150355506	1	0.02035	0.02035	11.35329	9.29E-04	-1.10E+03	-1.22E+02	-1.12E+03	0.17971
		9	134160053	137848869	1	0.02689	0.02689	14.9964	1.53E-04	-1.10E+03	-1.22E+02	-1.12E+03	0.17971
		Error	--	--	173	0.31016	0.00179	--	--	--	--	--	--
		mean	--	--	1	17.47039	17.47039	9744.677	4.87E-154	-1.10E+03	-1.22E+02	-1.12E+03	0.17971
NC358xB73	Asym	10	25976272	77678052	1	2.72E+00	2.72E+00	20.40	1.15E-05	-352.58	608.44	-358.95	0.103
		Error	--	--	177	2.36E+01	1.33E-01	--	--	--	--	--	--
		mean	--	--	1	2.47E-01	2.47E-01	1.85	1.75E-01	-352.58	608.44	-358.95	0.103
	Blush	8	16800171	18215366	1	1.23E+00	1.23E+00	13.76	2.77E-04	-424.60	536.41	-430.98	0.072
		Error	--	--	177	1.58E+01	8.90E-02	--	--	--	--	--	--
		mean	--	--	1	3.19E+00	3.19E+00	35.88	1.14E-08	-424.60	536.41	-430.98	0.072
	$BDEN_{inoc}$	3	6864389	8563589	1	1.48E-02	1.48E-02	25.93	1.11E-06	-1067.50	-280.94	-1079.40	0.287
		4	178164694	178497329	1	9.94E-03	9.94E-03	17.47	5.09E-05	-1067.50	-280.94	-1079.40	0.287
		8	159326028	161514221	1	7.99E-03	7.99E-03	14.05	2.60E-04	-1067.50	-280.94	-1079.40	0.287
		Error	--	--	141	8.02E-02	5.69E-04	--	--	--	--	--	--
		mean	--	--	1	4.70E+00	4.70E+00	8251.92	5.18E-127	-1067.50	-280.94	-1079.40	0.287
	FER	5	168673498	169849055	1	2.71E+03	2.71E+03	28.88	2.45E-07	825.03	1812.34	812.31	0.248
		5	206778711	208114393	1	2.76E+03	2.76E+03	29.39	1.95E-07	825.03	1812.34	812.31	0.248
		9	141508232	147189867	1	1.21E+03	1.21E+03	12.85	4.38E-04	825.03	1812.34	812.31	0.248
		Error	--	--	174	1.63E+04	9.38E+01	--	--	--	--	--	--
		mean	--	--	1	8.15E+04	8.15E+04	868.38	1.51E-69	825.03	1812.34	812.31	0.248
	FUM:FER	9	207097	3318481	1	2.24E-03	2.24E-03	11.79	7.48E-04	-1448.30	-542.71	-1454.50	0.066
		Error	--	--	168	3.19E-02	1.90E-04	--	--	--	--	--	--
		mean	--	--	1	7.00E-01	7.00E-01	3682.88	3.44E-116	-1448.30	-542.71	-1454.50	0.066
	Starburst	2	27599883	29679728	1	3.24E+00	3.24E+00	13.86	2.64E-04	-251.72	709.29	-258.10	0.073
		Error	--	--	177	4.14E+01	2.34E-01	--	--	--	--	--	--
		mean	--	--	1	1.30E+01	1.30E+01	55.51	3.95E-12	-251.72	709.29	-258.10	0.073
	$BDEN_{uninoc}$	1	203237687	206745740	1	8.29E-02	8.29E-02	34.65	2.09E-08	-1020.00	-91.70	-1030.00	0.212
		8	1559423	3276836	1	2.71E-02	2.71E-02	11.31	9.54E-04	-1020.00	-91.70	-1030.00	0.212
		Error	--	--	168	0.40203	0.00239	--	--	--	--	--	--
		mean	--	--	1	2.71E+01	2.71E+01	11313.08	4.78E-156	-1020.00	-91.70	-1030.00	0.212

Table 3.7. (continued)

Family	Trait	Chr.	Left	Right	df	SS	MS	F	p-value	BIC	mBIC	AIC	Model R^2
Combined	Asym	10	141262497	143125860	4	3.79E+00	9.47E-01	6.62	3.13E-05	-1369.00	3551.07	-1405.70	0.075
		Error	--	--	719	1.03E+02	1.43E-01	--	--	--	--	--	--
		Family	--	--	3	1.01E+00	3.37E-01	2.36	7.06E-02	-1369.00	3551.07	-1405.70	0.075
		mean	--	--	1	7.50E-01	7.50E-01	5.24	2.23E-02	-1369.00	3551.07	-1405.70	0.075
	Blush	2	179721294	180683300	4	2.04E+00	5.11E-01	6.03	9.02E-05	-1726.80	3258.22	-1781.80	0.200
		5	202562693	203392355	4	5.86E+00	1.47E+00	17.28	1.54E-13	-1726.80	3258.22	-1781.80	0.200
		Error	--	--	715	6.06E+01	8.48E-02	--	--	--	--	--	--
		Family	--	--	3	4.07E+00	1.36E+00	15.98	4.58E-10	-1726.80	3258.22	-1781.80	0.200
		mean	--	--	1	5.81E-01	5.81E-01	6.85	9.04E-03	-1726.80	3258.22	-1781.80	0.200
	$BDEN_{inoc}$	1	17256105	21804718	4	2.04E-02	5.10E-03	7.84	3.68E-06	-4412.00	43.97	-4536.10	0.282
		2	193400572	195781723	4	2.44E-02	6.10E-03	9.36	2.42E-07	-4412.00	43.97	-4536.10	0.282
		3	6687212	8789496	4	2.83E-02	7.08E-03	10.87	1.64E-08	-4412.00	43.97	-4536.10	0.282
		5	183303798	186075125	4	2.80E-02	6.99E-03	10.73	2.11E-08	-4412.00	43.97	-4536.10	0.282
		5	205258663	205938633	4	1.61E-02	4.03E-03	6.19	7.00E-05	-4412.00	43.97	-4536.10	0.282
		8	148339315	155973496	4	1.57E-02	3.93E-03	6.04	9.15E-05	-4412.00	43.97	-4536.10	0.282
		Error	--	--	594	3.87E-01	6.51E-04	--	--	--	--	--	--
		Family	--	--	3	3.11E-03	1.04E-03	1.59	1.90E-01	-4412.00	43.97	-4536.10	0.282
		mean	--	--	1	2.95E+00	2.95E+00	4527.31	4.68E-280	-4412.00	43.97	-4536.10	0.282
	FER	5	141537763	169849055	4	3.04E+03	7.60E+02	6.81	2.22E-05	3524.78	8616.92	3433.09	0.185
		5	207258755	208114393	4	4.08E+03	1.02E+03	9.14	3.38E-07	3524.78	8616.92	3433.09	0.185
		6	130721405	133795910	4	4.55E+03	1.14E+03	10.20	4.92E-08	3524.78	8616.92	3433.09	0.185
		7	141014394	145817515	4	3.20E+03	8.00E+02	7.17	1.17E-05	3524.78	8616.92	3433.09	0.185
		Error	--	--	704	7.85E+04	1.12E+02	--	--	--	--	--	--
		Family	--	--	3	3.04E+03	1.01E+03	9.10	6.51E-06	3524.78	8616.92	3433.09	0.185
		mean	--	--	1	8.14E+04	8.14E+04	729.19	8.93E-111	3524.78	8616.92	3433.09	0.185
	Purple	2	149474697	155746493	4	5.94E+00	1.49E+00	6.19	6.70E-05	-992.92	3927.13	-1029.60	0.051
		Error	--	--	719	1.73E+02	2.40E-01	--	--	--	--	--	--
		Family	--	--	3	4.38E+00	1.46E+00	6.08	4.36E-04	-992.92	3927.13	-1029.60	0.051
		mean	--	--	1	4.44E+01	4.44E+01	184.87	1.23E-37	-992.92	3927.13	-1029.60	0.051
	$BDEN_{uninoc}$	1	200794862	214954217	4	8.79E-02	2.20E-02	8.16	1.99E-06	-4050.00	886.09	-4150.00	0.195
		5	6859778	7527027	4	6.79E-02	1.70E-02	6.30	5.56E-05	-4050.00	886.09	-4150.00	0.195
		8	89350950	103389182	4	9.34E-02	2.33E-02	8.66	7.98E-07	-4050.00	886.09	-4150.00	0.195
		9	96557796	99098669	4	8.04E-02	2.01E-02	7.47	6.88E-06	-4050.00	886.09	-4150.00	0.195
		Error	--	--	684	1.84E+00	2.69E-03	--	--	--	--	--	--
		mean	--	--	1	1.85E+01	1.85E+01	6867.77	0.00E+00	-4050.00	886.09	-4150.00	0.195
		Family	--	--	3	2.29E-02	7.62E-03	2.83	3.77E-02	-4050.00	886.09	-4150.00	0.195

Table 3.8. QTL descriptions, including physical positions, associated traits, and families in which the QTL were mapped.

Chr.	Left (bp)	Right (bp)	Bin	Associated traits	Families	Type
1	88897	3026161	1-1.01	FER	Z007	Single trait, single family
1	7719999	9378393	1.01	$BDEN_{uninoc}$	Z007	Single trait, single family
1	17256105	21804718	1.02	$BDEN_{inoc}$	Combined	Single trait, single family
1	22029001	24689765	1.02	$BDEN_{inoc}$	Z009	Single trait, single family
1	50843507	52221146	1.03-1.04	FER, FUM	Z007	Multi-trait, single family
1	203237687	206745740	1.07	$BDEN_{uninoc}$	Combined, Z021	Single trait, multi-family
1	269068613	270418769	1.10	$BDEN_{inoc}$, Starburst	Z008, Z009	Multi-trait, multi-family
1	276934002	280825668	1.10	FER	Z009	Single trait, single family
2	27599883	29679728	2.03-2.04	$BDEN_{inoc}$, Starburst	Z007, Z021	Multi-trait, multi-family
2	37754001	39891173	2.04	FER	Z007	Single trait, single family
2	59197257	113031412	2.04-2.05	Starburst	Z009	Single trait, single family
2	149474697	155746493	2.05-2.06	Purple	Combined	Single trait, single family
2	171109445	176426230	2.06	$BDEN_{uninoc}$	Z008	Single trait, single family
2	179721294	180683300	2.06	Blush	Combined	Single trait, single family
2	186831881	189497979	2.06-2.07	FUM:FER	Z008	Single trait, single family
2	193400572	195188506	2.07	$BDEN_{inoc}$	Combined, Z007	Single trait, multi-family
2	226246821	226664978	2.09	FER	Z007	Single trait, single family
3	7785135	8563589	3.02	$BDEN_{inoc}$	Combined, Z008, Z021	Single trait, multi-family
3	137231734	154792291	3.05	$BDEN_{uninoc}$	Z007	Single trait, multi-family
3	161576393	166829493	3.05	FER	Z008	Single trait, single family
3	171730137	182742189	3.06*	FER	Z007	Single trait, single family
4	17986822	21013671	4.03*	$BDEN_{inoc}$, FER	Z009	Multi-trait, single family
4	167128403	172797675	4.06-4.07	Purple	Z009	Single trait, single family
4	178164694	179870074	4.07-4.08*	$BDEN_{inoc}$, FER	Z009, Z021	Multi-trait, multi-family
5	6948413	7527027	5.01	$BDEN_{uninoc}$	Combined, Z007	Single trait, multi-family
5	84885005	169849055	5.04*	$BDEN_{inoc}$, $BDEN_{uninoc}$, FER	All	Multi-trait, multi-family
5	171150903	175669412	5.04-5.05*	$BDEN_{inoc}$	Z009	Single trait, single family
5	183303798	186075125	5.05*	$BDEN_{inoc}$	Combined	Single trait, single family

Families denoted as: Z007=CML333xB73; Z008=CML52xB73; Z009=CML69xB73; Z021=NC358xB73

*denotes "hot spot" FVI bins; ^ denotes bins unique to this study

Table 3.8. (continued)

Chr.	Left (bp)	Right (bp)	Bin	Associated traits	Families	Type
5	202562693	203392355	5.06	Blush	Combined, Z007	Single trait, multi-family
5	205258663	205938633	5.07^	$BDEN_{inoc}$	Combined	Single trait, single family
5	206058644	206658699	5.07^	FER	Z008	Single trait, single family
5	207258755	208114393	5.07^	FER	Combined, Z021	Single trait, multi-family
5	215194661	217759022	5.08-5.09	$BDEN_{uninoc}$	Z007	Single trait, single family
6	93144004	95724368	6.02	FER	Z009	Single trait, single family
6	130721405	133529499	6.05	FER	Combined, Z009	Single trait, multi-family
6	154530689	155086056	6.06	FER, FUM:FER	Z008	Multi-trait, single family
7	4823956	5828359	7.01	Starburst	Z007	Single trait, single family
7	14152199	23748237	7.02*	FER, FUM:FER	Z007	Multi-trait, single family
7	107154252	108353941	7.02*	FUM	Z007	Single trait, single family
7	127285223	131013932	7.02-7.03*	Asymptomatic	Z009	Single trait, single family
7	141486076	142429440	7.03	FER	Combined, Z009	Single trait, multi-family
7	167973298	169095061	7.04-7.05	Purple	Z009	Single trait, single family
8	1559423	3276836	8.00-8.01	$BDEN_{uninoc}$	Z021	Single trait, single family
8	17017893	18215366	8.02	Blush, FUM:FER	Z008, Z021	Multi-trait, multi-family
8	95667409	98116975	8.03*	$BDEN_{uninoc}$	Combined, Z007	Single trait, multi-family
8	100566541	102748623	8.03*	$BDEN_{inoc}$	Z009	Single trait, single family
8	137311246	139916747	8.05	FER	Z008	Single trait, single family
8	148339315	151773181	8.06	$BDEN_{inoc}$	Combined, Z007	Single trait, multi-family
8	159326028	161514221	8.06	$BDEN_{inoc}$	Z021	Single trait, single family
8	169208747	169829320	8.08^	FER	Z009	Single trait, single family
8	173075636	175784078	8.09^	$BDEN_{inoc}$	Z007	Single trait, single family
9	207097	3318481	9.00-9.01	FUM:FER	Z021	Single trait, single family
9	1244225	2627062	9.00^	FER	Z007	Single trait, single family
9	88651842	99098669	9.03	FUM, $BDEN_{uninoc}$	Combined, Z009	Single trait, single family
9	106856548	113420650	9.04	$BDEN_{uninoc}$	Z008	Single trait, single family
9	120045550	126147403	9.04	$BDEN_{uninoc}$	Z007	Single trait, single family
9	134160053	137848869	9.05-9.06	$BDEN_{uninoc}$	Z009	Single trait, single family
9	146587518	147189867	9.06	FER, $BDEN_{uninoc}$	Z007, Z021	Multi-trait, multi-family
10	25976272	77678052	10.03*	Asymptomatic	Z021	Single trait, single family
10	141547773	143125860	10.06-10.07^	Asymptomatic	Combined, Z008	Single trait, multi-family

Families denoted as: Z007=CML333xB73; Z008=CML52xB73; Z009=CML69xB73; Z021=NC358xB73

*denotes "hot spot" FVI bins; ^ denotes bins unique to this study

Table 3.9. Correlations of all pairwise combinations of marker effects within and among families.

Trait 1	Trait 2	Family				
		Z007	Z008	Z009	Z021	Combined
$BDEN_{inoc}$	$BDEN_{uninoc}$	0.303***	0.569***	0.623***	0.392***	0.392***
FER	$BDEN_{uninoc}$	0.017	-0.487***	-0.421***	-0.126***	-0.116***
FER	$BDEN_{inoc}$	-0.738***	-0.731***	-0.528***	-0.574***	-0.585***
FUM	$BDEN_{uninoc}$	0.145***	0.042	-0.316***	0.151***	0.031***
FUM	$BDEN_{inoc}$	-0.439***	-0.44***	-0.338***	-0.246***	-0.329***
FUM:FER	$BDEN_{uninoc}$	0.103**	0.433***	0.012	0.17***	0.11***
FUM:FER	$BDEN_{inoc}$	0.195***	0.25***	0.06*	0.317***	0.13***
FER	FUM	0.303***	0.246***	0.417***	0.092**	0.279***
FER	FUM:FER	-0.529***	-0.612***	-0.365***	-0.708***	-0.467***
FUM	FUM:FER	0.642***	0.574***	0.685***	0.611***	0.696***
$BDEN_{uninoc}$	Asymptomatic	-0.178***	0.318***	0.079**	-0.065*	0.036***
$BDEN_{uninoc}$	Blush	0.162***	-0.02	0.355***	0.021	0.134***
$BDEN_{uninoc}$	Moldy	-0.121***	-0.369***	-0.32***	-0.204***	-0.097***
$BDEN_{uninoc}$	Purple	0.05	0.416***	-0.404***	-0.138***	-0.098***
$BDEN_{uninoc}$	Starburst	-0.224***	0.019	0.489***	-0.029	0.035***
$BDEN_{inoc}$	Asymptomatic	0.305***	0.524***	0.169***	0.108***	0.229***
$BDEN_{inoc}$	Blush	0.178***	0.147***	0.164***	-0.036	0.118***
$BDEN_{inoc}$	Moldy	-0.518***	-0.494***	-0.229***	-0.279***	-0.268***
$BDEN_{inoc}$	Purple	-0.307***	0.315***	-0.371***	0.211***	-0.131***
$BDEN_{inoc}$	Starburst	0.105***	-0.19***	0.242***	-0.505***	0.011
FER	Asymptomatic	-0.428***	-0.692***	-0.705***	-0.471***	-0.507***
FER	Blush	-0.056*	-0.03	-0.325***	0.361***	0.008
FER	Moldy	0.344***	0.417***	0.292***	0.466***	0.256***
FER	Purple	0.079**	-0.486***	-0.104**	-0.522***	-0.223***
FER	Starburst	0.046	0.424***	0.11***	0.742***	0.331***
FUM	Asymptomatic	-0.421***	-0.361***	-0.329***	0.095**	-0.201***
FUM	Blush	-0.032	0.035	-0.423***	0.31***	0.001
FUM	Moldy	0.147***	0.217***	0.341***	0.056*	0.137***
FUM	Purple	0.481***	-0.177***	0.18***	-0.023	0.033***
FUM	Starburst	-0.383***	0.213***	-0.2***	0.189***	-0.045***
FUM:FER	Asymptomatic	0.003	0.28***	0.231***	0.473***	0.233***
FUM:FER	Blush	0.001	-0.011	-0.157***	-0.005	-0.009
FUM:FER	Moldy	-0.156***	-0.247***	0.054*	-0.271***	-0.058***
FUM:FER	Purple	0.381***	0.284***	0.217***	0.408***	0.206***
FUM:FER	Starburst	-0.384***	-0.156***	-0.279***	-0.461***	-0.303***
Blush	Asymptomatic	-0.113***	0.107***	0.471***	0.049	0.109***
Moldy	Asymptomatic	-0.175***	-0.29***	-0.123***	0.064*	-0.027***
Moldy	Blush	-0.202***	0.23***	-0.177***	0.32***	-0.034***
Purple	Asymptomatic	-0.03	0.464***	0.139***	0.336***	0.15***
Purple	Blush	-0.331***	-0.108***	-0.231***	-0.229***	-0.233***
Purple	Moldy	0.185***	-0.359***	0.408***	-0.162***	0.047***
Starburst	Asymptomatic	0.064*	-0.502***	-0.131***	-0.36***	-0.241***
Starburst	Blush	-0.242***	0.112***	0.297***	0.315***	0.055***
Starburst	Moldy	-0.001	0.08**	-0.37***	0.386***	0.001
Starburst	Purple	-0.617***	-0.32***	-0.722***	-0.696***	-0.613***

Pairwise correlation significance is denoted as: **0.05>P≥0.0001; ***P<0.0001
Significant positive and negative correlations are blue and red, respectively

Table 3.10. Genes correlated with FER resistance in the 282 diversity panel and that were enriched in "hot spot" QTL for resistance to *F. verticillioides*.

Gene	Protein	Position	Bin
GRMZM2G049930	Germin-like protein	Chr10: 59,009,034-59,010,511	10.03
GRMZM2G019443 (ereb82)	AP2-EREBP-transcription factor 82	Chr7: 17,143,991-17,145,013	7.02
GRMZM2G178817	Putative uncharacterized protein	Chr10: 58,452,597-58,453,741	10.03
GRMZM2G404688	Trypsin/factor XIIA inhibitor	Chr7: 20,171,657-20,172,327	7.02
GRMZM2G071390	Germin-like protein	Chr10: 58,580,220-58,581,487	10.03
AF546188.1_FG001	α-zein protein	Chr7: 18,744,943-18,745,668	7.02
GRMZM2G319798	Xyloglucan:xyloglucosyl transferase	Chr7: 107,780,060-107,782,693	7.02
GRMZM2G364748	Xyloglucan:xyloglucosyl transferase	Chr10: 68,924,719-68,926,477	10.03

Figure 3.1. Photographic examples of kernels exhibiting the five symptom types.

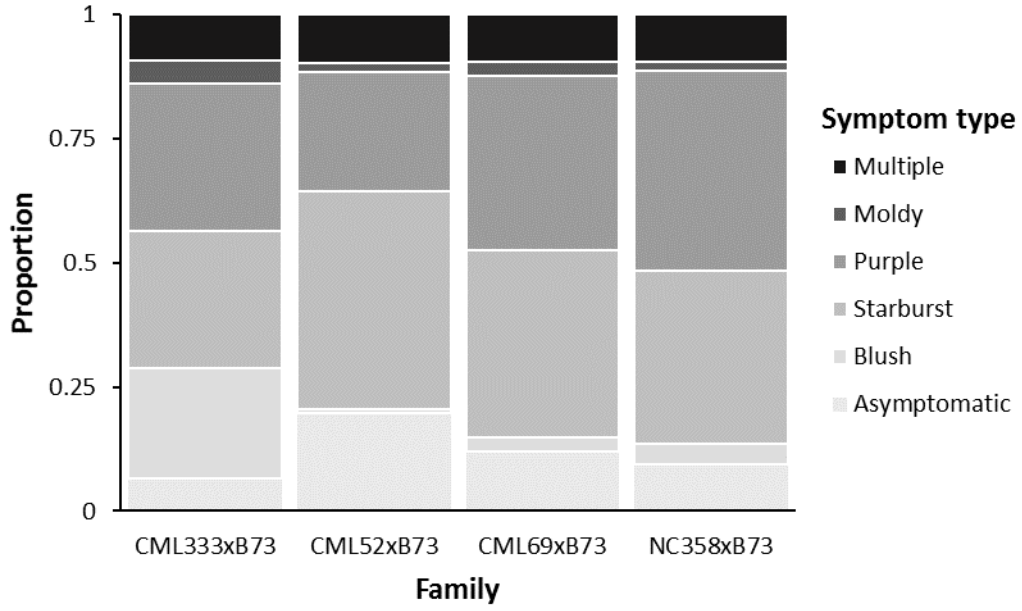

Figure 3.2. Proportions of symptom types present in the four families.

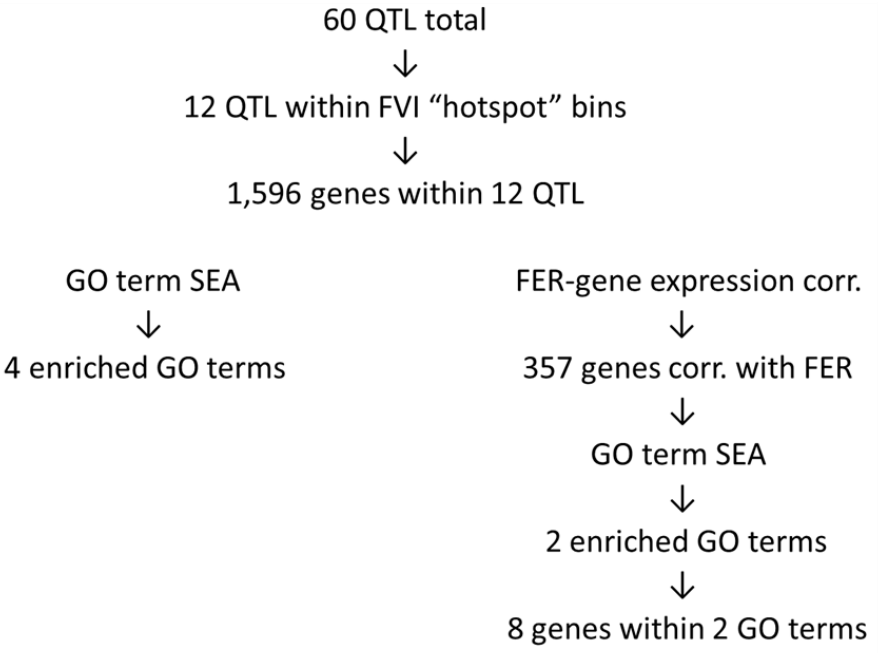

Figure 3.3. "Hot spot" candidate gene and GO term analysis pipeline.

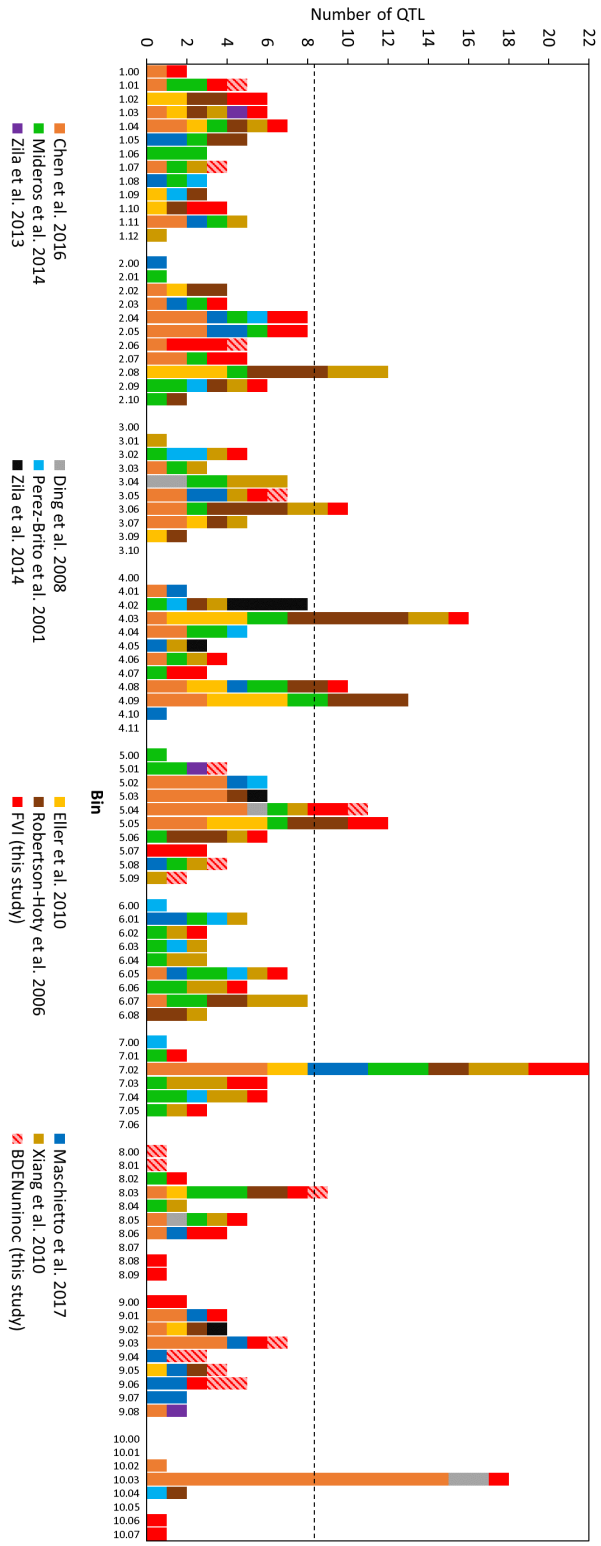

Figure 3.4. Loci mapped in this study and in previous publications along the 85 bins of the maize genome. The horizontal dashed line represents the average number of loci per bin + 1 standard deviation (8.09).

REFERENCES

1. Mueller DS, Wise KA, Sisson AJ, Allen TW, Bergstrom GC, Bosley DB, et al. Corn yield loss estimates due to diseases in the United States and Ontario, Canada from 2012 to 2015. Plant Heal Prog. 2016;17:211–22.
2. Wild CP, Gong YY. Mycotoxins and human disease: A largely ignored global health issue. Carcinogenesis. 2009;31:71–82.
3. Shelby RA, White DG, Bauske EM. Differential fumonisin production in maize hybrids. Plant Dis. 1994;78:582–4.
4. Parsons MW, Munkvold GP. Effects of planting date and environmental factors on Fusarium ear rot symptoms and fumonisin B1 accumulation in maize grown in six North American locations. Plant Pathol. 2012;61:1130–42.
5. Kimanya ME, De Meulenaer B, Roberfroid D, Lachat C. Fumonisin exposure through maize in complementary foods is inversely associated with linear growth of infants in Tanzania. Mol Nutr Food Res. 2010;54:1659–67.
6. Mutiga SK, Were V, Hoffmann V, Harvey JW, Milgroom MG, Nelson RJ. Extent and drivers of mycotoxin contamination: inferences from a survey of Kenyan maize mills. Phytopathology. 2014;104:1221–31.
7. Bankole S a, Mabekoje OO. Occurrence of aflatoxins and fumonisins in preharvest maize from southwestern Nigeria. Food Addit Contam. 2004;21:251–5.
8. Fandohan P, Gnonlonfin B, Hell K, Marasas WFO, Wingfield MJ. Natural occurrence of *Fusarium* and subsequent fumonisin contamination in preharvest and stored maize in Benin, West Africa. Int J Food Microbiol. 2005;99:173–83.
9. Missmer SA, Suarez L, Felkner M, Wang E, Alfred H, Rothman KJ, et al. Exposure to fumonisins and the occurrence of neural tube defects along the Texas-Mexico border. Environ Health Perspect. 2006;114:237–41.
10. Marasas WFO, Riley RT, Hendricks KA, Stevens VL, Sadler TW, Gelineau-van Waes J, et al. Fumonisins disrupt sphingolipid metabolism, folate transport, and neural tube development in embryo culture and in vivo: a potential risk factor for human neural tube defects among populations consuming fumonisin-contaminated maize. J Nutr. 2004;134:711–6.
11. Robertson LA, Kleinschmidt CE, White DG, Payne GA, Maragos CM, Holland JB. Heritabilities and correlations of Fusarium ear rot resistance and fumonisin contamination resistance in two maize populations. Crop Sci. 2006;46:353–61.
12. Robertson-Hoyt LA, Jines MP, Balint-Kurti PJ, Kleinschmidt CE, White DG, Payne GA, et al. QTL mapping for Fusarium ear rot and fumonisin contamination resistance in two maize populations. Crop Sci. 2006;46:1734–43.
13. Horne DW, Eller MS, Holland JB. Responses to recurrent index selection for reduced Fusarium ear rot and lodging and for increased yield in maize. Crop Sci. 2016;56:85–94.

14. Zila CT, Ogut F, Romay MC, Gardner CA, Buckler ES, Holland JB. Genome-wide association study of Fusarium ear rot disease in the U.S.A. maize inbred line collection. BMC Plant Biol. 2014;14:372.
15. Poland JA, Balint-Kurti PJ, Wisser RJ, Pratt RC, Nelson RJ. Shades of gray: the world of quantitative disease resistance. Trends Plant Sci. 2009;14:21–9.
16. Blandino M, Reyneri A. Effect of maize hybrid maturity and grain hardness on fumonisin and zearalenone contamination. Ital J Agron. 2008;2:107–17.
17. Sampietro DA, Vattuone MA, Presello DA, Fauguel CM. The pericarp and its surface wax layer in maize kernels as resistance factors to fumonisin accumulation by *Fusarium verticillioides*. Crop Prot. 2009;28:196–200.
18. Bluhm BH, Woloshuk CP. Amylopectin induces fumonisin B1 production by *Fusarium verticillioides* during colonization of maize kernels. MPMI. 2005;18:1333–9.
19. Sampietro DA, Fauguel CM, Vattuone MA, Presello DA, Catalán CAN. Phenylpropanoids from maize pericarp: Resistance factors to kernel infection and fumonisin accumulation by *Fusarium verticillioides*. Eur J Plant Pathol. 2013;135:105–13.
20. Mutiga SK, Morales L, Angwenyi S, Wainaina J, Harvey J, Das B, et al. Association between agronomic traits and aflatoxin accumulation in diverse maize lines grown under two soil nitrogen levels in Eastern Kenya. Field Crop Res. 2017;205:124–34.
21. Shetty PH, Bhat R V. A physical method for segregation of fumonisin-contaminated maize. Food Chem. 1999;66:371–4.
22. De Groote H, Kimenju SC. Comparing consumer preferences for color and nutritional quality in maize: Application of a semi-double-bound logistic model on urban consumers in Kenya. Food Policy. 2008;33:362–70.
23. Fox G, Manley M. Hardness methods for testing maize kernels. J Agric Food Chem. 2009;57:5647–57.
24. Czembor E, Ochodzki P. Resistance of flint and dent maize forms for colonization by *Fusarium* spp. and mycotoxins contamination. Maydica. 2009;54:263–7.
25. Chen J, Shrestha R, Ding J, Zheng H, Mu C, Wu J, et al. Genome-wide association study and QTL mapping reveal genomic loci associated with Fusarium ear rot resistance in tropical maize germplasm. G3. 2016;6:3803–3815.
26. Yu J, Holland JB, McMullen MD, Buckler ES. Genetic design and statistical power of nested association mapping in maize. Genetics. 2008;178:539–51.
27. Buckler ES, Holland JB, Bradbury PJ, Acharya CB, Brown PJ, Browne C, et al. The genetic architecture of maize flowering time. Science. 2009;325:714–8.
28. Zila CT, Samayoa LF, Santiago R, Butrón A, Holland JB. A genome-wide association study reveals genes associated with Fusarium ear rot resistance in a maize core diversity panel. G3. 2013;3:2095–104.
29. Owens B, Lipka A, Magallanes-Lundback M, Tiede T, Diepenbrock C, Kandianis CB, et al. A foundation for provitamin A biofortification of maize: genome-wide association and genomic prediction models of carotenoid levels. Genetics. 2014;198:1699–716.

30. Boutigny AL, Beukes I, Small I, Zuhlke S, Spiteller M, Van Rensburg BJ, et al. Quantitative detection of *Fusarium* pathogens and their mycotoxins in South African maize. Plant Pathol. 2012;61:522–31.
31. JMP®. Version Pro 12. SAS Institute Inc. 1989-2007.
32. Bates D, Maechler M, Bolker B, Walker S. Fitting linear mixed-effects models using lme4. J Stat Softw. 2015;67:1–48.
33. R Core Team. R: A Language and Environment for Statistical Computing. Version 3.3.1. R Foundation for Statistical Computing. 2017.
34. Piepho HP, Moehring J. Computing heritability and selection response from unbalanced plant breeding trials. Genetics. 2007;177:1881–8.
35. Zhao W. Panzea: a database and resource for molecular and functional diversity in the maize genome. Nucleic Acids Res. 2006;34:D752–7.
36. Elshire RJ, Glaubitz JC, Sun Q, Poland J a, Kawamoto K, Buckler ES, et al. A robust, simple genotyping-by-sequencing (GBS) approach for high diversity species. PLoS One. 2011;6:e19379.
37. Olukolu BA, Wang GF, Vontimitta V, Venkata BP, Marla S, Ji J, et al. A genome-wide association study of the maize hypersensitive defense response identifies genes that cluster in related pathways. PLoS Genet. 2014;10:e1004562.
38. Bradbury PJ, Zhang Z, Kroon DE, Casstevens TM, Ramdoss Y, Buckler ES. TASSEL: Software for association mapping of complex traits in diverse samples. Bioinformatics. 2007;23:2633–5.
39. Peiffer JA, Romay MC, Gore MA, Flint-Garcia SA, Zhang Z, Millard MJ, et al. The genetic architecture of maize height. Genetics. 2014;196:1337–56.
40. Ding J-Q, Wang X-M, Chander S, Yan J-B, Li J-S. QTL mapping of resistance to Fusarium ear rot using a RIL population in maize. Mol Breed. 2008;22:395–403.
41. Eller MS, Payne GA, Holland JB. Selection for reduced Fusarium ear rot and fumonisin content in advanced backcross maize lines and their topcross hybrids. Crop Sci. 2010;50:2249–60.
42. Maschietto V, Colombi C, Pirona R, Pea G, Strozzi F, Marocco A, et al. QTL mapping and candidate genes for resistance to Fusarium ear rot and fumonisin contamination in maize. BMC Plant Biol. 2017;17:20.
43. Mideros SX, Warburton ML, Jamann TM, Windham GL, Williams WP, Nelson RJ. Quantitative trait loci influencing mycotoxin contamination of maize: analysis by linkage mapping, characterization of near-isogenic lines, and meta-analysis. Crop Sci. 2014;54:127.
44. Perez-Brito D, Jeffers D, Gonzalez-de-Leon D, Khairallah M, Cortes-Cruz M, Velazquez-Cardelas G, et al. QTL mapping of *Fusarium moniliforme* ear rot resistance in high land maize, Mexico. Agrociencia. 2001;35:181–96.
45. Xiang K, Zhang ZM, Reid LM, Zhu XY, Yuan GS, Pan GT. A meta-analysis of QTL associated with ear rot resistance in maize. Maydica. 2010;55:281–90.
46. Andorf CM, Cannon EK, Portwood JL, Gardiner JM, Harper LC, Schaeffer ML, et al. MaizeGDB update: New tools, data and interface for the maize model organism database. Nucleic Acids Res. 2016;44:D1195–201.

47. Sekhon RS, Lin H, Childs KL, Hansey CN, Robin Buell C, De Leon N, et al. Genome-wide atlas of transcription during maize development. Plant J. 2011;66:553–63.
48. Tian T, Liu Y, Yan H, You Q, Yi X, Du Z, et al. agriGO v2.0: a GO analysis toolkit for the agricultural community, 2017 update. Nucleic Acids Res. 2017;1–8.
49. Binns D, Dimmer E, Huntley R, Barrell D, O'Donovan C, Apweiler R. QuickGO: a web-based tool for Gene Ontology searching. Bioinformatics. 2009;25:3045–6.
50. Flint-Garcia SA, Thuillet AC, Yu J, Pressoir G, Romero SM, Mitchell SE, et al. Maize association population: A high-resolution platform for quantitative trait locus dissection. Plant J. 2005;44:1054–64.
51. Monaco MK, Sen TZ, Dharmawardhana PD, Ren L, Schaeffer M, Naithani S, et al. Maize metabolic network construction and transcriptome analysis. Plant Genome. 2013;6.
52. Presello DA, Botta G, Iglesias J, Eyhérabide GH. Effect of disease severity on yield and grain fumonisin concentration of maize hybrids inoculated with *Fusarium verticillioides*. Crop Prot. 2008;27:572–6.
53. Clements MJ, Kleinschmidt CE, Maragos CM, Pataky JK, White DG. Evaluation of inoculation techniques for Fusarium ear rot and fumonisin contamination of corn. Plant Dis. 2003;87:147–53.
54. Robertson-Hoyt LA, Betrán J, Payne GA, White DG, Isakeit T, Maragos CM, et al. Relationships among resistances to Fusarium and Aspergillus ear rots and ccontamination by fumonisin and aflatoxin in maize. Phytopathology. 2007;97:311–7.
55. Kandianis CB, Michenfelder AS, Simmons SJ, Grusak MA, Stapleton AE. Abiotic stress growth conditions induce different responses in kernel iron concentration across genotypically distinct maize inbred varieties. Front Plant Sci. 2013;4:1–10.
56. Jansen C, Zhang Y, Liu H, Gonzalez-Portilla PJ, Lauter N, Kumar B, et al. Genetic and agronomic assessment of cob traits in corn under low and normal nitrogen management conditions. Theor Appl Genet. 2015;128:1231–42.
57. Blandino M, Reyneri A, Vanara F. Influence of nitrogen fertilization on mycotoxin contamination of maize kernels. Crop Prot. 2008;27:222–30.
58. Bacon CW, Glenn AE, Yates IE. *Fusarium verticillioides*: Managing the endophytic association with maize for reduced fumonisins accumulation. Toxin Rev. 2008;27:411–46.
59. Waldron KW, Faulds CB. Cell Wall Polysaccharides. In: Kamerling JP, editor. Comprehensive Glycoscience. Elsevier; 2007.
60. Perrot-Rechenmann C. Cellular responses to auxin: division versus expansion. Cold Spring Harb Perspect Biol. 2010;2:1–15.
61. Pratt RC, Paulis JW, Miller K, Nelsen T, Bietz JA. Association of zein classes with maize kernel hardness. Vol. 72, Cereal Chemistry. 1995. p. 162–7.
62. Lanubile A, Ferrarini A, Maschietto V, Delledonne M, Marocco A, Bellin D. Functional genomic analysis of constitutive and inducible defense responses to

Fusarium verticillioides infection in maize genotypes with contrasting ear rot resistance. BMC Genomics. 2014;15:710.
63. Song X, Li Y, Hou X. Genome-wide analysis of the AP2/ERF transcription factor superfamily in Chinese cabbage (*Brassica rapa* ssp. *pekinensis*). BMC Genomics. 2013;14:573.
64. Li B, Li Q, Mao X, Li A, Wang J, Chang X, et al. Two novel AP2/EREBP transcription factor genes TaPARG have pleiotropic functions on plant architecture and yield-related traits in common wheat. Front Plant Sci. 2016;7:1–13.
65. Miller JD, Schaafsma AW, Bhatnagar D, Bondy G, Carbone I, Harris LJ, et al. Mycotoxins that affect the North American agri-food sector: State of the art and directions for the future. World Mycotoxin J. 2014;7:63–82.

CHAPTER 4

GENOMIC EXPLORATION OF THE INTERSECTION BETWEEN DISEASE RESISTANCE AND MORPHOPHYSIOLOGY IN THE MAIZE CORE DIVERSITY PANEL

Introduction

Maize, a crop of global economic and dietary importance, is attacked in the field and in storage by diverse pathogens and pests. In the US corn-producing states and in Ontario, Canada, diseases have accounted for 8-16% of total annual yield losses in the past five years, with greater yields being associated with greater disease losses (1). Foliar diseases such as northern leaf blight (NLB) and gray leaf spot (GLS) were the major contributors to yield loss due to disease in the northern states and Ontario, while mycotoxin contamination and diseases caused by mycotoxigenic fungi, such as Fusarium ear rot (FER), led to the greatest losses in the southern states (1). In addition to reducing crop value, mycotoxins are harmful to human and animal health (2).

The inheritance of many economically important diseases in maize is quantitative, and linkage mapping and genome wide association studies (GWAS) have been employed to dissect their genetic architectures (3–10). Linkage mapping has the benefit of requiring low marker density and accurately estimating allele effects of quantitative trait loci (QTL), but is also limited by poor resolution, inefficient allelic diversity, and time-consuming biparental family development (11). Nested association mapping (NAM) populations relax many of these constraints by combining several biparental families derived from diverse lines crossed to one recurrent parent (11–13). Although NAM designs allow for accurate estimation of allelic series, mapping resolution is still relatively low. GWAS uses natural populations of diverse germplasm to maximize allelic diversity and mapping resolution (11). However, the power to

detect trait-associated loci in diverse germplasm via GWAS is limited by confounding population structure effects. A commonly noted pattern is the association between disease resistance and flowering time (3–6,8,10,14), a major driver of population structure (15). Incorporating GWAS results has been shown to enhance the accuracy of genomic prediction models (16,17), which employ genetic covariance matrices made from markers spanning the genome. (18).

The role of morphophysiology – the intersection between form and function – on disease resistance in maize has not been deeply explored, but some evidence for these phenomena exists. For example, various aspects of kernel composition and morphology have been shown to influence ear rots and mycotoxin accumulation at the phenotypic level (19–24), and pleiotropy for leaf interveinal distance and resistance to GLS has been reported in the NAM (4). Here we sought to further explore the relationships among disease resistance and morphophysiological traits.

Extensive genetic and phenotypic resources are publicly available in maize. The maize core diversity panel (25) is a powerful tool that has been used to dissect dozens of quantitatively-controlled morphophysiological and disease traits with high resolution GWAS (5,6,26–31). Here we attempt to disentangle the genetic mechanisms underlying morphophysiologically-mediated resistance using 26 morphophysiological and three disease resistance traits and more than 456,000 genotyping-by-sequencing (GBS) markers in the maize core diversity panel. We explore inter-trait relationships with correlation analyses and use GWAS to characterize disease-specific loci and loci shared among disease resistance and morphophysiological traits. We also attempt to predict disease resistance using GWAS loci for disease-associated morphophysiological traits.

Materials and methods

Morphophysiological and foliar disease phenotypes

We analyzed 33 morphophysiological and disease resistance traits (Tables 4.1-2) that had been phenotyped on the maize core diversity panel (25) in 21 environments (Tables 4.2-3). Twenty-nine of these traits were publicly accessed from Panzea (32) or from their respective publications (Table 4.1) (5,6,26–31,33). Cob density, cob volume, total kernel weight, and total kernel bulk density (hereafter referred to as bulk density) were calculated using raw cob diameter, cob length, cob weight, ear weight, and total kernel volume data (Table 4.1). Cob shape was assumed to be cylindrical.

Entry-means estimation

Entry-means for 23 traits were readily available (Table 4.1). The southern leaf blight (SLB) best linear unbiased predictor (BLUP) data was on a 1-9 scale, with one being the most susceptible and nine being the most resistant. All SLB BLUPs were subtracted from 9 so that the magnitude of the score was proportional to the severity of the symptoms (0=most resistant, 9=most susceptible).

The lme4 package (34) in R version 3.3.1 (35) was used to estimate entry-means for the remaining six traits (Table 4.1) as described here. Random linear models with cob density, cob volume, bulk density, tillering, germination count, and stand count as separate responses were fit as $y_{ijk} = \mu + L_i + Y[L]_{j[i]} + G_k + GL_{ik} + e_{ijk}$, where y is the response; μ is the grand mean; location (L), year[location] ($Y[L]$), entry (G), entry*location (GL), and error (e) are modelled as random effects. Entry best linear unbiased predictors (BLUPs) were extracted from the six models.

Genotypes, population structure analyses, and heritability estimation

Genotyping-by-sequencing (GBS) (36) single nucleotide polymorphisms (SNPs) had been called using the GBS version 2.7 Discovery Build (37) for the

diversity panel. The GBS SNP physical positions were in AGPv3 coordinates. A distance matrix of the diversity panel was built from the raw SNP set (N=955,960) and used for multidimensional scaling (MDS) in TASSEL (38). The first five coordinates for the diversity panel lines were extracted from the MDS analysis for use as covariates in GWAS.

The raw SNPs had been imputed with FILLIN (39) and were used to build a centered identity-by-descent (IBD) kinship matrix (40). For each of the 29 traits, a mixed linear model (MLM) was fit with the kinship matrix in TASSEL and the additive genetic (σ^2_a) and residual (σ^2_e) variance components from the MLM were used to estimate narrow-sense heritability (h^2) as $\sigma^2_a/(\sigma^2_a + \sigma^2_e)$ (40). The entry residuals from each of the 29 MLMs were extracted from TASSEL for population structure-controlled inter-trait analyses.

Trait correlation analyses

Sub-population classifications (non-stiff stalk, popcorn, stiff-stalk, sweet corn, tropical) were accessed from Flint-Garcia et al. (25) and Romay et al. (41). Using JMP® software (42), analysis of variance (ANOVA) models were fit to assess differences in the 29 traits among the sub-populations, and pairwise t-tests were conducted to assess specific differences in the three disease resistances among all pairs of sub-populations.

Pairwise Pearson correlations among all trait BLUPs were estimated using the Hmisc package (43) and p-values of the 812 pairwise correlations were then used to estimate the false discovery rate (FDR) using the qvalue package (44) in R. To visualize significant inter-trait correlations in each population, correlations with FDR-adjusted p-values less than 0.05 were used to create an unweighted correlation network using the “spring” layout with the qgraph package (45) in R. To visualize

inter-trait correlations under population structure control, the same process was conducted with the kinship-adjusted trait residuals for the combined diversity panel.

To investigate whether phenotypic covariance shows separation of the sub-populations of the diversity panel, we conducted two principal component analyses (PCA) using JMP® software: one including the 29 trait BLUPs and the other including the 29 kinship-adjusted trait residuals as covariates. From each PCA, the first two principal components (PC) for each line and for each trait covariate eigenvector were extracted. To compare inter-trait correlations before and after controlling for population structure, we regressed absolute BLUP correlations against absolute kinship-adjusted correlations.

Cross-validated GWAS and predictions

The FILLIN-imputed SNP set was filtered for minimum 2% minor allele frequency (MAF), maximum 10% heterozygosity, and minimum site coverage of 10 individuals, resulting in 456,381 SNPs. A five-fold cross-validated (with 10 replications) scheme was used for GWAS and predictions (Fig. 4.1). Fifty subsets of the diversity panel lines were generated via five-fold cross validation with 10 replications. From each subset, the lines not in the current fold (training set, 80% of diversity panel lines) were used for GWAS of each of the 29 traits. GWAS was conducted in TASSEL, including the kinship matrix and the first five MDS coordinates described previously to control for population structure. MLMs were fit for each trait individually as $y = X\beta + Zu + e$, where y is the vector of BLUPs from the training set, X is the design matrix of fixed covariates including SNP marker effects and five MDS coordinates, Z is the design matrix for random variables, which include the random background additive genetic effects with covariance defined by a kinship matrix and the error term (46). From each of the 1,450 trait/training set GWAS

models (29 traits x 50 subsets), the 0.1% most significant SNPs (N=456) were extracted. Kinship matrices for all the diversity panel lines were built from each set of top GWAS SNPs.

For each top GWAS kinship matrix and for each trait, a training GBLUP model was built with the emmreml package (47) in R, including the phenotypes of the training set and the top GWAS kinship matrix. The training model was then used to predict the phenotypes of the lines not used for GWAS (test set, 20% of diversity panel lines). This schema resulted in 42,050 prediction models (1,450 top GWAS kinships x 29 predicted traits). Predictive ability was defined as the correlation between the actual and predicted phenotypes of the test set (15). For each of the three disease resistances, we compared the predictive abilities of the top GWAS kinships of other 28 traits ("GWAS trait") on the disease with ANOVA and pairwise t-tests.

We also tested whether predictive abilities using top GWAS kinships were significantly different from predictive abilities using kinships matrices built from a random subset of SNPs. We randomly selected 30 subsets of 456 SNPs and built kinship matrices from them. Each of the 30 random kinship matrices was used to predict each of the 29 traits using the emmreml package in R with five-fold CV replicated 10 times. The predictive abilities of each combination of predicted trait and GWAS trait were compared to the predictive abilities of the random kinships on the predicted trait using two-tailed t-tests.

GWAS colocalization and candidate genes

From each fold, we identified top GWAS SNPs that were shared between each pairwise combination of traits. For each of the disease resistances, we compared the number of overlapping top GWAS SNPs it had with the other 28 traits using ANOVA and pairwise t-tests. Based on these tests, FER had significantly more colocalized top

GWAS SNPs with NLB and ear height; NLB had significantly more colocalizations with ear height, tassel branch number, and leaf length, and SLB had significantly more colocalizations with cob diameter, cob volume, and leaf length. We then subset top GWAS SNPs in four ways based on the colocalization results: (1) because both FER and NLB were colocalized with ear height, we identified the top GWAS SNPs that were shared among all three traits; (2) similarly, because NLB and SLB colocalized with leaf length, we searched for top SNPs that were associated with all three traits; we also identified the top GWAS SNPs shared (3) between NLB and tassel branch number and (4) between SLB and cob diameter and cob volume.

Given that (1) linkage disequilibrium rapidly decays after 1-10 kbp (41) and that (2) GWAS has been reported to be mostly likely to tag SNPs that are 1-5kbp away from genes (48), we searched from genes within 5 kbp (on either side) of our top GWAS SNPs with the MaizeGDB (49) AGP v3 gene atlas (50). We then identified the genes unique to and shared among the four colocalization sets described previously using a Venn diagram tool (51). We used MaizeCyc (52) to search for proteins encoded by these genes. We also conducted singular enrichment analysis to identify gene ontology (GO) terms that were significantly enriched in the four colocalization gene sets with agriGO (53).

Results

Disease resistance is associated with population structure

The five sub-populations of the diversity panel were significantly different with respect to days to silking (DTS), FER, NLB, and SLB, as revealed by ANOVA and pairwise t-tests (Table 4.4). The tropical sub-population had the longest DTS and the lowest disease severity for all three diseases (Fig. 4.2, Table 4.4). Of the five sub-populations, the stiff-stalks had the highest NLB, and the sweet corn lines were the

most susceptible to FER and SLB (Table 4.4). Population structure effects on disease resistance are further demonstrated in PCA and correlation analyses. Both the qgraph and biplot of PCA trait eigenvectors exhibit that FER, NLB, and SLB were significantly positively correlated with each other and negatively correlated with flowering time and other traits indicative of population structure (Figs. 4.2-4).

To disentangle the effects of population structure on morphophysiology and disease resistance, we ran MLMs using only a kinship matrix for the 29 traits and extracted the residuals. Controlling for population structure via kinship broke many of the inter-trait correlations, as evidenced by the fewer significant correlations among the trait residuals (N=234) than among trait BLUPs (N=447) and by the expansion of the qgraph of the trait residuals (Fig. 4.5). Within the trait residual qgraph, the three disease resistances clustered with cob and kernel traits (Fig. 4.5). However, disease resistance was still associated with population structure-related traits. For example, FER and NLB residuals were correlated with flowering time and plant height (Figs. 4.5-6). In addition, absolute correlations between disease resistance and other trait BLUPs (naïve) and between disease resistance and other trait residuals (kinship-adjusted) were positively associated (FER: R^2=0.23, P<0.0001; NLB: R^2=0.54, P<0.0001; SLB: R^2=0.14, P<0.0001). In other words, traits that were more highly correlated with disease resistance before controlling for population structure were also more highly correlated with disease resistance after population structure control.

Morphophysiology recapitulates phylogeny

Given the effects of population structure on morphophysiology and disease resistance, we sought to address the extent to which traits separate the diversity panel. Like MDS of genetic markers, PCA of the 29 traits demonstrated separation of the maize core diversity panel (Fig. 4.7). The first and second PCs of the trait PCA

explained 24% and 10% of the variance, respectively, and showed the temperate-tropical divide in the diversity panel (Fig. 4.7). The first and second coordinates of the MDS using genetic markers explained 39% and 23% of the variance in the diversity panel, respectively (Fig. 4.7). The first MDS coordinate separated temperate from tropical lines, and the second divided the two temperate heterotic groups (SS=stiff stalk; NSS=non-stiff stalk) (Fig. 4.7).

Loci associated with disease resistance colocalize with height, ear, and leaf traits

Given the inter-trait correlation phenomena, we sought to identify morphophysiological traits that shared top GWAS SNPs with disease resistance. FER had significantly more colocalized top GWAS SNPs with NLB and ear height than with the other 26 traits (Table 4.5). SLB had significantly more colocalized top GWAS SNPs with cob diameter, cob volume, and leaf length, and NLB had more top GWAS SNP colocalizations with ear height, tassel branch number, and leaf length (Table 4.5).

Candidate genes underlying colocalized regions for disease resistance and morphophysiological traits are largely composed of transcription factors

We then sought to identify candidate genes underlying regions colocalized for disease resistance and morphophysiological traits. Because both FER and NLB had significantly more colocalized top GWAS SNPs with ear height than other traits, we searched for genes located in top GWAS regions shared by FER, NLB, and ear height. There were 80 genes within these regions, 16 of which have been characterized (Table 4.6). The majority of these characterized genes (8/16) were involved in transcription, but others encoded proteins involved in diverse functions, such as a glutathionine transferase (*gst15*) and an S-receptor kinase (*srk1*) (Table 4.6). Transcription factor

activity was enriched in regions colocalized for FER, NLB, and ear height (Table 4.7). Similarly, both NLB and SLB had significantly more colocalized top GWAS SNPs with leaf length, so we identified genes underlying regions shared by NLB, SLB, and leaf length. Of the 39 genes underlying these shared regions, 10 have been characterized (Table 4.6). Half of the characterized genes underlying these regions encoded transcription factors (Table 4.6), but transcription factor activity was not enriched in these regions colocalized for NLB, SLB, and leaf length (Table 4.7). SLB and NLB were unique in that they shared top GWAS SNPs with cob diameter and volume and with tassel branch number, respectively. The majority (>50%) of genes underlying these colocalized regions also encoded transcription factors (Table 4.6), and transcription factor activity and transcription-related molecular functions were enriched in these regions (Table 4.7).

Although the majority of genes underlying these colocalized regions encoded transcription factors, few genes were shared among the four types of colocalized regions (FER/NLB/ear height, NLB/SLB/leaf length, NLB/tassel branch number, and SLB/cob diameter/cob volume) (Table 4.8). *Trpp7*, which encodes a trehalose-6-phosphate phosphatase, was the only gene shared among all four types (Table 4.8). Colocalized regions for NLB/SLB/leaf length and SLB/cob diameter/cob volume shared 21 genes, including three transcription factor genes (*bhlh5, btf3, wrky88*) and others involved in various processes, such as lipid metabolism (GRMZM2G044947, GRMZM2G055667) and metal ion binding (*lac10*, GRMZM2G028779) (Table 4.8). NLB/tassel branch number colocalized regions shared (a) 77 genes, including six transcription factors, *gst15*, and *srk1* with FER/NLB/ear height regions, (b) eight genes with NLB/SLB/leaf length colocalized regions, such as *tasselless1*, and (c) 11 genes with SLB/cob diameter/cob length colocalized regions, including an MYB transcription factor (Table 4.8).

Top GWAS SNPs are not predictive of diseases resistance

We first tested whether top GWAS kinships had better predictive ability than kinships made from an equal number of randomly selected SNPs (N=456). For all combinations of predicted trait and GWAS trait, predictive ability of the random kinships was significantly higher than that of the top GWAS kinships (Table 4.9). We also found that predictive ability on each of the three diseases did not differ among GWAS traits (Tables 4.10-11). Overall, top GWAS kinship matrices were not predictive of any trait, including when the GWAS trait and predicted trait were the same (Tables 4.9-11).

Traits that are correlated with disease resistance share loci with disease resistance

We sought to test whether traits that are correlated with disease resistance (before and after population structure correction) shared loci with or were predictive of disease resistance. For all disease traits, absolute correlations among trait BLUPs (naïve) were significantly positively correlated with absolute correlations among kinship-adjusted trait residuals (Table 4.12). For FER, we found that the greater the proportion of top GWAS SNPs that it shared with a given trait, the greater its absolute naïve and kinship-adjusted correlations were with the trait (Table 4.12). Similarly, the proportion of shared top GWAS SNPs was positively correlated with the absolute naïve correlation for SLB (Table 4.12). Interestingly, the proportion of shared top GWAS SNPs was negatively correlated with predictive ability for FER (Table 4.12).

Discussion

Here we demonstrate that morphophysiological traits that are correlated with disease resistance also share GWAS loci with disease resistance. These traits included

ear height, leaf length, tassel branch number, and cob diameter, which have been shown the be controlled by pleiotropic loci (26). The majority of genes underlying colocalized regions for disease resistance and said traits were transcription factors and transcription factor activity was enriched in colocalized regions, suggesting that similar mechanisms regulate plant architecture and disease resistance. For example, MYB and NAC transcription factors have been implicated in lignin biosynthesis (54), and we found that these types of transcription factors were located in regions colocalized for ear height, FER, NLB, SLB, and cob diameter/volume. The positive association between cob size traits and disease severity and negative association between height/leaf length and disease severity could be explained by lignification. The tissues most conducive to *F. verticillioides* in the cob are also the most lignified (55–57), and cob size and density have been shown to be negatively correlated (56). Thus, larger, less dense cobs may be more susceptible to *F. verticillioides* infection. Similarly, lignin content has been positively correlated with plant height (58) and lignification has been associated with defense against foliar pathogens (59).

Although these kinds of biological phenomena may link morphophysiology and disease resistance, the relationships among morphophysiological and disease traits have been structured by breeding. The reduced germination, increased plant height, and longer flowering time in the tropical sub-population are classic examples of the maladaptive syndrome that manifests when tropical germplasm is grown in sub-tropical and temperate environments (60). Thus, flowering time has proven to be barrier for introducing favorable tropical alleles into temperate-adapted germplasm (15). The temperate-tropical split is not the only contributor to population structure-driven differences in morphophysiology within the diversity panel. The temperate lines are representative of the two historical heterotic groups, and modern heterotic

breeding has polarized the two groups with respect to phenology and morphology (60).

We attempted to circumvent some of these population structure issues by combining GWAS and genomic prediction. We found that kinships made from top GWAS SNPs were significantly less predictive than kinships made from randomly selected SNPs, which sample the genomic relationships between individuals. This demonstrates that our GWAS models had indeed strong control of population structure, and that relationships among the diversity panel lines at the resulting top GWAS SNPs themselves did not explain any of the phenotypic variance. This is unsurprising, as it is unlikely that any of these SNPs are causal polymorphisms based on the marker density used, but highlights that persistent colocalization of top GWAS SNPs is unlikely to result from residual population structure. These results help explain the basis for increased prediction accuracies in enhanced genomic prediction models with GWAS SNPs as fixed effects (16,17).

The relationships between disease resistance and yield-associated traits, such as cob size (56), have implications for contemporary maize breeding. Maize yields and yield losses due to disease have been simultaneously increasing over time (1), further demonstrating the need for breeding programs to take into account the trade-offs between yield capacity and disease resistance. These associations could potentially be disentangled in populations with less population structure; the high disease resistance (5,6,33) and rapid LD decay (41) within tropical germplasm suggests that this material would be suited for this endeavor. We also show that inter-trait associations vary among maize sub-populations, indicating that the mechanisms connecting morphophysiology and disease resistance are diverse. However, disease resistance and morphophysiology are correlated even within tropical association panels (8),

supporting the hypothesis that these relationships are not entirely driven by population structure.

Tables and figures

Table 4.1. Morphophysiological and disease traits used in the analyses here.

Type	Trait	Calculation	Reference
Cob	Cob density[a]	*CobWeight/CobVol*	This study
Cob	Cob diameter		Brown et al. 2011
Cob	Cob length		Brown et al. 2011
Cob	Cob volume[a]	$\pi CobLen(CobDiam/2)^2$	This study
Cob	Cob weight[b]		Panzea
Cob	Ear row number (ERN)		Brown et al. 2011
Cob	Ear weight[b]		Panzea
Disease	Fusarium ear rot (FER)		Zila et al. 2013
Disease	Northern leaf blight (NLB)		Wisser et al. 2011
Disease	Southern leaf blight (SLB)		Kump et al. 2011
Maturity	Anthesis-silking interval (ASI)		Buckler et al. 2009
Maturity	Days to anthesis (DTA)		Buckler et al. 2009
Maturity	Days to silking (DTS)		Buckler et al. 2009
Height	Ear height (EHT)		Peiffer et al. 2014
Height	Plant height (PHT)		Peiffer et al. 2014
Kernel	Kernel type		Panzea
Kernel	Oil		Cook et al. 2012
Kernel	Protein		Cook et al. 2012
Kernel	Starch		Cook et al. 2012
Kernel	Total kernel bulk density[a]	*TKW/TKV*	This study
Kernel	Total kernel volume (TKV)[b]		Panzea
Kernel	Total kernel weight (TKW)[b]	*EarWeight−CobWeight*	This study
Leaf	Leaf length		Tian et al. 2011
Leaf	Leaf width		Tian et al. 2011
Leaf	Middle leaf angle (MLA)		Tian et al. 2011
Leaf	Upper leaf angle (ULA)		Tian et al. 2011
Stalk	Stalk strength (RPR)		Peiffer et al. 2013
Stalk	Tillering[a]		Panzea
Tassel	Branch number		Brown et al. 2011
Tassel	Spike length		Brown et al. 2011
Tassel	Tassel length		Brown et al. 2011
Vigor	Germination count[a]		Panzea
Vigor	Stand count[a]		Panzea

[a]Entry-means calculated from publicly available raw trait data
[b]Raw trait data used to calculate other traits but trait not used in further analyses

Table 4.2. Environments wherein the traits analyzed here were phenotyped.

Type	Trait	06A	06CL1	06FL1	06K	06PR	26M3	65	07A	07CL1	07FL1	07K	07U	27M3	08A	08P	10A	10ES	10M3	11ES	11NC	12NC
Cob	CobDiameter	✓	✓	✓	✓	✓	✓	✓	✓	✓					✓							
Cob	CobLength	✓	✓	✓	✓	✓	✓	✓	✓	✓					✓							
Cob	CobWeight	✓	✓	✓	✓	✓	✓	✓	✓	✓					✓							
Cob	ERN	✓	✓	✓	✓	✓	✓	✓	✓	✓					✓							
Cob	EarWeight	✓	✓	✓	✓	✓	✓	✓	✓	✓					✓							
Disease	FER																	✓				
Disease	GLS																		✓			
Disease	NLB				✓															✓		
Disease	SLB	✓	✓							✓											✓	
Maturity	DTA	✓	✓			✓	✓	✓	✓			✓	✓	✓								
Maturity	DTS	✓	✓			✓	✓	✓	✓			✓	✓	✓								
Height	EHT	✓	✓	✓		✓	✓	✓	✓	✓	✓	✓	✓	✓								
Height	PHT	✓	✓	✓	✓	✓	✓	✓	✓	✓		✓	✓									
Kernel	KernelType	✓	✓	✓	✓	✓		✓														
Kernel	Oil	✓	✓	✓	✓	✓			✓													
Kernel	Protein	✓	✓	✓	✓	✓	✓		✓													
Kernel	Starch	✓	✓	✓	✓	✓	✓		✓					✓								
Kernel	TKV	✓	✓	✓	✓	✓	✓	✓														
Leaf	LeafLength	✓	✓	✓	✓	✓	✓	✓	✓	✓		✓										
Leaf	LeafWidth	✓	✓	✓	✓	✓	✓	✓	✓	✓		✓										
Leaf	MLA	✓	✓	✓	✓	✓	✓	✓	✓	✓												
Leaf	ULA	✓	✓	✓	✓	✓	✓	✓	✓	✓		✓	✓	✓								
Stalk	RPR																✓					
Stalk	Tillering	✓	✓						✓	✓					✓	✓						
Tassel	BranchNumber	✓	✓	✓	✓	✓	✓	✓	✓									✓				
Tassel	SpikeLength	✓	✓	✓	✓	✓	✓	✓	✓				✓									
Tassel	TasselLength	✓	✓	✓	✓	✓	✓	✓	✓				✓									
Vigor	GermCount	✓	✓	✓		✓	✓	✓							✓							
Vigor	StandCount	✓	✓	✓	✓	✓	✓	✓	✓	✓			✓	✓	✓							

Table 4.3. Environment codes and their corresponding years and locations.

Environment	Year	Location
06A	2006	Aurora, NY
06CL1	2006	Clayton, NC
06FL1	2006	Homestead, FL
06K	2006	Aurora, NY
06PR	2006	Ponce, PR
26M3	2006	Columbia, MO
65	2006	Urbana, IL
07A	2007	Aurora, NY
07CL1	2007	Clayton, NC
07FL1	2007	Homestead, FL
07K	2007	Aurora, NY
07U	2007	Urbana, IL
27M3	2007	Columbia, MO
08A	2008	Aurora, NY
08P	2008	Ponce, PR
10A	2010	Aurora, NY
10ES	2010	Galicia, ES
10M3	2010	Columbia, MO
11ES	2011	Galicia, ES
11NC	2011	Clayton, NC
12NC	2012	Clayton, NC

Table 4.4. ANOVA and pairwise t-tests comparing 29 morphophysiological and disease traits among the diversity panel sub-populations.

Trait	Sub-population (mean ± SE)					ANOVA	
	Non-stiff stalk	Popcorn	Stiff stalk	Sweet corn	Tropical	F-ratio	p-value
FER	3.11±0.05 B	2.91±0.18 BC	3.09±0.06 B	3.69±0.31 A	2.65±0.07 C	11.24	<0.0001**
SLB	2.47±0.09 B	2.57±0.25 AB	2.75±0.16 AB	3.28±0.41 A	1.69±0.05 C	16.09	<0.0001**
NLB	-0.00384±0.0285 B	0.14±0.0297 AB	0.19±0.0246 A	0.165±0.0583 AB	-0.152±0.023 C	15.68	<0.0001**
TasselLen	320.89±3.4 B	324.13±11.98 AB	286.74±4.33 C	304.02±26.27 BC	343.44±3.82 A	18.32	<0.0001**
SpikeLen	233.95±3.14 A	220.54±7.79 AB	212.79±3.12 B	209.81±20.7 AB	232.27±4.24 A	4.01	0.0036*
BranchNum	21.72±0.39 B	25.71±0.9 A	20.1±0.47 C	24.09±0.62 AB	25.11±0.37 A	17.78	<0.0001**
CobLen	127.03±1.61 A	123.51±5.01 AB	128.06±1.72 A	109.16±3.36 B	124.12±1.49 A	2.74	0.0296
CobDiam	25.01±0.23 AB	21.18±0.59 C	25.71±0.27 A	23.46±0.75 BC	25.42±0.27 A	9.16	<0.0001**
CobDen	0.0727±0.000112 A	0.0726±0.0000152 AB	0.0727±0.0000129 AB	0.0726±0.000161 B	0.0726±0.00000738 B	3.93	0.0042*
CobVol	212000±4130 A	167000±8780 B	222000±4930 A	174000±10700 B	218000±5330 A	4.91	0.0008*
ERN	14.87±0.15 B	14.93±0.55 ABC	15.84±0.23 A	14.37±0.36 BC	14.37±0.16 C	6.76	<0.0001**
DTA	74.35±0.6 B	75.29±1.21 B	73.52±0.64 B	69.91±1.52 B	88.15±0.94 A	61.43	<0.0001**
DTS	75.56±0.65 B	76.89±1.34 B	74.94±0.68 B	72.01±1.87 B	90.59±1.17 A	52.62	<0.0001**
ASI	1.62±0.1 B	2.01±0.18 AB	1.83±0.13 B	2.37±0.43 AB	2.44±0.26 A	3.54	0.008*
KernelType	0.573±0.0237 B	0.913±0.0148 A	0.551±0.0374 B	0.776±0.0792 A	0.803±0.0163 A	19.48	<0.0001**
BulkDen	0.736±0.000889 C	0.737±0.000181 A	0.736±0.000121 C	0.735±0.000752 D	0.737±0.000786 B	9.90	<0.0001**
Starch	66.77±0.17 A	65.5±0.7 B	67.23±0.29 A	62.98±1.17 C	66.19±0.23 B	8.01	<0.0001**
Protein	14±0.11 B	13.75±0.26 B	13.89±0.11 B	15.65±0.69 A	13.76±0.11 B	4.49	0.0016*
Oil	4.35±0.05 C	4.14±0.06 BCD	3.95±0.07 D	6.06±0.59 A	4.53±0.07 B	19.02	<0.0001**
Tillering	0.637±0.00519 C	0.684±0.0269 B	0.633±0.00889 C	0.776±0.0896 A	0.669±0.00807 B	8.59	<0.0001**
RPR	6.18±0.15 B	5.25±0.53 BC	6.29±0.19 B	4.2±0.12 C	7.02±0.21 A	6.55	<0.0001**
PHT	146.22±1.94 B	141.39±5.6 BC	149.7±2.29 B	123.55±11.31 C	160.71±2.53 A	8.60	<0.0001**
EHT	63.75±1.85 C	78.76±4.56 B	68.07±2.12 BC	42.93±7.25 D	93.24±2.49 A	31.00	<0.0001**
LeafLen	694.87±7.91 BC	722.5±20.81 B	706.46±8.77 B	632.89±26.67 C	827.24±9.23 A	38.75	<0.0001**
LeafWid	86.02±1.13 B	77.94±3.21 C	80.09±1.49 C	66.33±5.18 D	90.39±1.16 A	12.44	<0.0001**
MLA	32.32±0.5 B	28.51±1.04 CD	31.46±0.69 BC	26.23±2.54 D	34.83±0.48 A	9.04	<0.0001**
ULA	26.72±0.85 B	21.59±2.5 BC	26.5±2.02 B	14.92±2.98 C	35.85±0.62 A	19.52	<0.0001**
StandCount	8.28±0.06 A	8.33±0.16 AB	8.46±0.1 A	7.67±0.39 B	8.36±0.08 A	2.05	0.0876
GermCount	6.74±0.1 AB	6.58±0.39 ABC	7.03±0.18 A	5.98±0.6 BC	6.15±0.11 C	5.86	0.0002*

Levels not connected by the same letter are significantly different (P<0.05)
*0.01>P≥0.0001; **P<0.0001

Table 4.5. ANOVA and pairwise t-tests comparing the number of colocalized top GWAS SNPs between each of the three diseases and the other 28 traits.

Disease	Pairwise comparisons				ANOVA					
	Trait	Mean	SE	Sig. group	Source	DF	SS	MS	F-ratio	p-value
FER	ASI	0.2	0.0904	E	Trait	27	7790.68	288.544	3.3431	<.0001
	BranchNum	5.2	2.439	BCD	Error	1372	118419.3	86.311		
	BulkDen	0.16	0.0597	E	Total	1399	126210			
	CobDen	0.36	0.106	E						
	CobDiam	3.16	1.6955	CDE						
	CobLen	0.94	0.4105	E						
	CobVol	0.36	0.1333	E						
	DTA	2.86	1.86	CDE						
	DTS	1.14	0.3332	E						
	EHT	7.4	2.8332	AB						
	ERN	0.86	0.3091	E						
	GermCount	0.3	0.1	E						
	KernelType	0.28	0.1179	E						
	LeafLen	2.06	0.7281	CDE						
	LeafWid	2.1	1.5754	CDE						
	MLA	0.04	0.028	E						
	NIROil	0.54	0.1316	E						
	NIRProtein	1.66	0.3924	DE						
	NIRStarch	2.48	0.4023	CDE						
	NLB	9.96	4.3532	A						
	PHT	1.98	0.919	CDE						
	RPR	0.58	0.1181	E						
	SLB	0.54	0.1622	E						
	SpikeLen	0.78	0.2745	E						
	StandCount	0.32	0.1008	E						
	TasselLen	3.32	0.7858	CDE						
	Tillering	0.92	0.1997	E						
	ULA	5.5	1.9135	BC						
NLB	ASI	0.4	0.216	E	Trait	27	498363.3	18457.9	18.4566	<.0001
	BranchNum	67.28	14.006	A	Error	1372	1372098	1000.1		
	BulkDen	3.14	0.79	DE	Total	1399	1870462			
	CobDen	0.72	0.176	E						
	CobDiam	11.5	5.499	CDE						
	CobLen	0.1	0.043	E						
	CobVol	4.96	2.498	CDE						
	DTA	9.2	5.399	CDE						
	DTS	5.82	3.511	CDE						
	EHT	79.04	12.063	A						
	ERN	0.84	0.147	E						
	FER	9.96	4.353	CDE						
	GermCount	0.34	0.133	E						
	KernelType	4.94	1.661	CDE						
	LeafLen	33.6	6.716	B						
	LeafWid	2.48	0.509	DE						
	MLA	3.04	2.15	DE						
	NIROil	1.2	0.439	E						
	NIRProtein	2.12	0.493	E						
	NIRStarch	0.64	0.148	E						
	PHT	16.48	6.099	C						
	RPR	0.36	0.208	E						
	SLB	7.96	2.726	CDE						
	SpikeLen	2.42	1.329	DE						
	StandCount	0.62	0.286	E						
	TasselLen	2.1	0.988	E						
	Tillering	0.48	0.108	E						
	ULA	14.76	4.476	CD						

Table 4.5. (continued)

Disease	Pairwise comparisons				ANOVA					
	Trait	Mean	SE	Sig. group	Source	DF	SS	MS	F-ratio	p-value
SLB	ASI	0.14	0.103	E	Trait	27	1505385	55755	32.8567	<.0001
	BranchNum	1.6	0.37	E	Error	1372	2328168	1696.9		
	BulkDen	0.26	0.094	E	Total	1399	3833553			
	CobDen	0.14	0.057	E						
	CobDiam	161.26	19.871	A						
	CobLen	1.66	0.459	E						
	CobVol	77.3	18.42	B						
	DTA	7.68	3.31	DE						
	DTS	1.12	0.454	E						
	EHT	6.02	1.776	E						
	ERN	5.1	2.745	E						
	FER	0.54	0.162	E						
	GermCount	0.06	0.034	E						
	KernelType	1.88	0.918	E						
	LeafLen	43.22	10.058	C						
	LeafWid	22.26	8.626	D						
	MLA	0.16	0.066	E						
	NIROil	0.2	0.081	E						
	NIRProtein	0.22	0.066	E						
	NIRStarch	1.76	0.674	E						
	NLB	7.96	2.726	DE						
	PHT	0.62	0.313	E						
	RPR	0.32	0.135	E						
	SpikeLen	4.78	1.667	E						
	StandCount	0.4	0.114	E						
	TasselLen	7.24	2.504	DE						
	Tillering	0.14	0.05	E						
	ULA	1.4	0.625	E						

Table 4.6. Genes underlying top GWAS regions colocalized for disease resistance and other traits.

FER, NLB, EHT		NLB, SLB, LeafLen	
ago2b	GRMZM2G051045	GRMZM2G158013	bhlh5	GRMZM2G102968
emp4	GRMZM2G055124	GRMZM2G158141	btf3	GRMZM2G108637
ereb209	GRMZM2G055643	GRMZM2G160463	fgp2	GRMZM2G116881
gata35	GRMZM2G061798	GRMZM2G164854	hsp1	GRMZM2G146219
gras75	GRMZM2G063156	GRMZM2G165005	lac10	GRMZM2G385635
gst15	GRMZM2G066101	GRMZM2G165099	tls1	GRMZM2G399433
hb83	GRMZM2G067734	GRMZM2G166665	trpp7	GRMZM2G480607
kch5	GRMZM2G069503	GRMZM2G166694	wrky42	GRMZM5G855304
mrpa7	GRMZM2G071846	GRMZM2G174310	wrky51	zma-MIR399a
mybr17	GRMZM2G072028	GRMZM2G175177	wrky88	zma-MIR399g
pin12	GRMZM2G075372	GRMZM2G179146	AC205122.4_FG005	
srk1	GRMZM2G075712	GRMZM2G400444	AC205122.4_FG006	
trpp7	GRMZM2G090010	GRMZM2G422576	GRMZM2G011136	
wrky116	GRMZM2G090528	GRMZM2G427603	GRMZM2G017013	
wrky99	GRMZM2G095397	GRMZM2G435294	GRMZM2G024607	
AC187243.3_FG005	GRMZM2G099003	GRMZM2G440259	GRMZM2G028779	
AC214227.4_FG013	GRMZM2G101741	GRMZM2G446394	GRMZM2G044448	
AC225222.2_FG004	GRMZM2G108040	GRMZM2G468702	GRMZM2G044947	
GRMZM2G006716	GRMZM2G109140	GRMZM5G815165	GRMZM2G048800	
GRMZM2G008819	GRMZM2G118579	GRMZM5G828661	GRMZM2G054387	
GRMZM2G015654	GRMZM2G120922	GRMZM5G833625	GRMZM2G054410	
GRMZM2G015739	GRMZM2G121868	GRMZM5G874562	GRMZM2G055667	
GRMZM2G015804	GRMZM2G123212		GRMZM2G064111	
GRMZM2G018416	GRMZM2G131012		GRMZM2G068398	
GRMZM2G024865	GRMZM2G131340		GRMZM2G070172	
GRMZM2G033805	GRMZM2G142802		GRMZM2G076313	
GRMZM2G034855	GRMZM2G145753		GRMZM2G079263	
GRMZM2G050072	GRMZM2G157749		GRMZM2G089241	
GRMZM2G050270	GRMZM2G157760		GRMZM2G093441	

Table 4.6. (continued)

SLB, CobDiam, CobVol									
agp2	hsftf21	AC202867.3_FG008	GRMZM2G018030	GRMZM2G057618	GRMZM2G078667	GRMZM2G114816	GRMZM2G145382	GRMZM2G173967	GRMZM2G411653	GRMZM5G831102
asc1	iaa7	AC203294.3_FG008	GRMZM2G018353	GRMZM2G058394	GRMZM2G078781	GRMZM2G114841	GRMZM2G146108	GRMZM2G174730	GRMZM2G411668	GRMZM5G844623
bhlh134	jmj18	AC204581.3_FG003	GRMZM2G018441	GRMZM2G058410	GRMZM2G083749	GRMZM2G116185	GRMZM2G146143	GRMZM2G178797	GRMZM2G413030	GRMZM5G852338
bhlh5	lac10	AC205122.4_FG005	GRMZM2G018798	GRMZM2G059526	GRMZM2G084397	GRMZM2G116823	GRMZM2G146219	GRMZM2G179279	GRMZM2G413822	GRMZM5G852968
bhlh7	mate3	AC205122.4_FG006	GRMZM2G022041	GRMZM2G059753	GRMZM2G084407	GRMZM2G116881	GRMZM2G146240	GRMZM2G180021	GRMZM2G414915	GRMZM5G861082
bhlh81	mbd111	AC209206.3_FG014	GRMZM2G022275	GRMZM2G059795	GRMZM2G085411	GRMZM2G117217	GRMZM2G147327	GRMZM2G300125	GRMZM2G415157	GRMZM5G863784
bnl9.11b(lts)	mez3	AC209768.3_FG005	GRMZM2G022777	GRMZM2G061354	GRMZM2G086269	GRMZM2G117240	GRMZM2G147422	GRMZM2G308689	GRMZM2G415172	GRMZM5G866627
btf3	myb119	AC209810.3_FG002	GRMZM2G024607	GRMZM2G061396	GRMZM2G086757	GRMZM2G117491	GRMZM2G149809	GRMZM2G321053	GRMZM2G416625	GRMZM5G866734
bzip22	myb126	AC211996.4_FG001	GRMZM2G024993	GRMZM2G062632	GRMZM2G089241	GRMZM2G120262	GRMZM2G151516	GRMZM2G322001	GRMZM2G428179	GRMZM5G866758
bzip52	myb74	AC211996.4_FG002	GRMZM2G025404	GRMZM2G062738	GRMZM2G090029	GRMZM2G121452	GRMZM2G151977	GRMZM2G322279	GRMZM2G429873	GRMZM5G878732
ca2p3	myb81	AC214648.3_FG001	GRMZM2G028779	GRMZM2G064111	GRMZM2G091919	GRMZM2G125072	GRMZM2G154029	GRMZM2G322952	GRMZM2G429982	GRMZM5G879570
cko4	nactf9	AC217977.3_FG001	GRMZM2G030305	GRMZM2G064473	GRMZM2G093441	GRMZM2G126077	GRMZM2G155762	GRMZM2G326933	GRMZM2G440785	GRMZM5G888860
crti2	natl1	AC233851.1_FG008	GRMZM2G032865	GRMZM2G064640	GRMZM2G094500	GRMZM2G126083	GRMZM2G156206	GRMZM2G331638	GRMZM2G447151	GRMZM5G891282
dof10	pip1f	AC233851.1_FG009	GRMZM2G034283	GRMZM2G064938	GRMZM2G098279	GRMZM2G127050	GRMZM2G157164	GRMZM2G336962	GRMZM2G472171	GRMZM6G792203
dof7	rpl17c	AC234156.1_FG004	GRMZM2G039725	GRMZM2G064941	GRMZM2G099767	GRMZM2G127386	GRMZM2G158300	GRMZM2G344848	GRMZM2G472266	pza02554
ereb161	rs2	AC234156.1_FG005	GRMZM2G043445	GRMZM2G068904	GRMZM2G100391	GRMZM2G129375	GRMZM2G159732	GRMZM2G345081	GRMZM2G473016	pzb01111
ereb193	serk1	GRMZM2G003530	GRMZM2G043943	GRMZM2G069176	GRMZM2G102502	GRMZM2G129783	GRMZM2G164265	GRMZM2G351832	GRMZM2G474658	si606065d12
ereb50	so1	GRMZM2G003814	GRMZM2G044055	GRMZM2G069455	GRMZM2G102968	GRMZM2G130333	GRMZM2G165679	GRMZM2G358693	GRMZM2G476593	umc109
expb8	srs6	GRMZM2G004715	GRMZM2G044947	GRMZM2G069511	GRMZM2G105025	GRMZM2G130943	GRMZM2G166445	GRMZM2G361256	GRMZM2G480607	umc1243
fae2	sun4	GRMZM2G005818	GRMZM2G045433	GRMZM2G070111	GRMZM2G105184	GRMZM2G132486	GRMZM2G167283	GRMZM2G363971	GRMZM2G480705	umc2621
fgp2	sut1	GRMZM2G008622	GRMZM2G046326	GRMZM2G070255	GRMZM2G107945	GRMZM2G133836	GRMZM2G167824	GRMZM2G364208	GRMZM2G481179	
ga20ox2	thl1	GRMZM2G008714	GRMZM2G046458	GRMZM2G070279	GRMZM2G108149	GRMZM2G134183	GRMZM2G168096	GRMZM2G375116	GRMZM2G535019	
gata26	tip2a	GRMZM2G011136	GRMZM2G047262	GRMZM2G070837	GRMZM2G111066	GRMZM2G134846	GRMZM2G168807	GRMZM2G376809	GRMZM2G701201	
glb3	trpp7	GRMZM2G011151	GRMZM2G048854	GRMZM2G070913	GRMZM2G111780	GRMZM2G135960	GRMZM2G169200	GRMZM2G385635	GRMZM2G701204	
glk1	wrky88	GRMZM2G011858	GRMZM2G054405	GRMZM2G071705	GRMZM2G111984	GRMZM2G137174	GRMZM2G171248	GRMZM2G389094	GRMZM2G702070	
glk27	AC187843.3_FG006	GRMZM2G014071	GRMZM2G055667	GRMZM2G074236	GRMZM2G112205	GRMZM2G139460	GRMZM2G171961	GRMZM2G398848	GRMZM5G804575	
gln1	AC196974.3_FG008	GRMZM2G016511	GRMZM2G056786	GRMZM2G074248	GRMZM2G112222	GRMZM2G140047	GRMZM2G172652	GRMZM2G400602	GRMZM5G817559	
hb128	AC197047.3_FG001	GRMZM2G017013	GRMZM2G056804	GRMZM2G077307	GRMZM2G113229	GRMZM2G141607	GRMZM2G173579	GRMZM2G408768	GRMZM5G818431	
hscf1	AC200725.4_FG003	GRMZM2G017789	GRMZM2G056815	GRMZM2G078500	GRMZM2G114552	GRMZM2G141634	GRMZM2G173615	GRMZM2G409343	GRMZM5G821267	

Table 4.7. Molecular functions that were significantly enriched in colocalized regions (P<0.05), as determined by singular enrichment analysis (SEA).

Colocalized regions	GO term	Term	Number in input list	Total number in input list	Input enrichment	Number in reference	Total number in reference	Reference enrichment	SEA p-value
NLB, BranchNum	GO:0030528	transcription regulator activity	19	239	0.079	974	25864	0.038	0.002
	GO:0003774	motor activity	5	239	0.021	118	25864	0.005	0.006
	GO:0043565	sequence-specific DNA binding	12	239	0.05	571	25864	0.022	0.008
	GO:0003700	transcription factor activity	16	239	0.067	891	25864	0.034	0.01
	GO:0046983	protein dimerization activity	14	239	0.059	759	25864	0.029	0.012
	GO:0046982	protein heterodimerization activity	5	239	0.021	167	25864	0.006	0.021
	GO:0060089	molecular transducer activity	5	239	0.021	181	25864	0.007	0.029
	GO:0004871	signal transducer activity	5	239	0.021	181	25864	0.007	0.029
	GO:0005515	protein binding	60	239	0.251	5187	25864	0.201	0.034
FER, NLB, EHT	GO:0003700	transcription factor activity	5	56	0.089	891	25864	0.034	0.044
NLB, SLB, LeafLen	None								
SLB, CobDiam, CobVol	GO:0003682	chromatin binding	8	204	0.039	434	25864	0.017	0.024
	GO:0042802	identical protein binding	5	204	0.025	204	25864	0.008	0.025
	GO:0003677	DNA binding	30	204	0.147	2665	25864	0.103	0.031

Table 4.8. Descriptions of genes underlying top GWAS regions colocalized for disease resistance and other traits.

Top GWAS colocalization	Gene	Protein	Function
FER, NLB, SLB, CobDiam, CobVol, EHT	trpp7	trehalose-6-phosphate phosphatase	trehalose biosynthesis
NLB, SLB, CobDiam, CobVol, LeafLen	bhlh5	bHLH-transcription factor	transcription factor
	btf3	TUB-transcription factor	transcription factor
	fgp2	folylpolyglutamate synthetase	folic acid-containing compound biosynthesis
	lac10	laccase	copper ion binding
	trpp7	trehalose-6-phosphate phosphatase	trehalose biosynthesis
	wrky88	WRKY-transcription factor	transcription factor
	AC205122.4_FG005	uncharacterized protein	unknown
	AC205122.4_FG006	uncharacterized protein	unknown
	GRMZM2G011136	uncharacterized protein	dicarboxylic acid transport
	GRMZM2G017013	protein binding protein	structural constituent of ribosome
	GRMZM2G024607	vipp1 -PspA like -1	thylakoid membrane biogenesis
	GRMZM2G028779	uncharacterized protein	zinc ion binding
	GRMZM2G044947	triacylglycerol lipase	lipid metabolism
	GRMZM2G055667	uncharacterized protein	fatty acid biosynthesis
	GRMZM2G064111	uncharacterized protein	structural constituent of cell wall
	GRMZM2G089241	cis-zeatin O-beta-D-glucosyltransferase	metabolism
	GRMZM2G093441	uncharacterized protein	proteolysis
	GRMZM2G102968	uncharacterized protein	unknown
	GRMZM2G116881	uncharacterized protein	unknown
	GRMZM2G146219	uncharacterized protein	unknown
	GRMZM2G385635	RuBisCO large chain Precursor	carbon fixation
	GRMZM2G480607	uncharacterized protein	protein kinase activity
NLB, SLB, BranchNum, LeafLen	trpp7	trehalose-6-phosphate phosphatase	trehalose biosynthesis
	tls1	aquaporin NIP	transport
	hsp1	heat shock protein	carbohydrate metabolism
	GRMZM2G028779	uncharacterized protein	zinc ion binding
	GRMZM2G054387	thiol-disulphide oxidoreductase DCC	cell part
	GRMZM2G054410	Polygalacturonase	carbohydrate metabolism
	GRMZM2G076313	uncharacterized protein	transport
	GRMZM2G480607	uncharacterized protein	protein kinase activity
NLB, SLB, BranchNum, CobDiam, CobVol	myb74	MYB transcription factor	transcription factor
	trpp7	trehalose-6-phosphate phosphatase	trehalose biosynthesis
	AC203294.3_FG008	hydroxymethylglutaryl-CoA reductase	coenzyme A metabolism
	GRMZM2G003814	uncharacterized protein	zinc ion binding
	GRMZM2G025404	uncharacterized protein	unknown
	GRMZM2G028779	uncharacterized protein	zinc ion binding
	GRMZM2G107945	uncharacterized protein	signal transduction
	GRMZM2G154029	uncharacterized protein	regulation of transcription
	GRMZM2G408768	uncharacterized protein	protein domain specific binding
	GRMZM2G480607	uncharacterized protein	protein kinase activity
	GRMZM5G891282	ribose-5-phosphate isomerase	pentose-phosphate shunt

Table 4.8. (continued)

Top GWAS colocalization	Gene	Protein	Function
NLB, FER, BranchNum, EHT	ago2b	argonaute2b	RNA interference
	emp4	pentatricopeptide repeat protein-like mRNA	mRNA modification
	ereb209	AP2-EREBP-transcription factor	transcription factor
	gata35	C2C2-GATA-transcription factor	transcription factor
	gras75	GRAS-transcription factor	transcription factor
	gst15	glutathione transferase	glutathione transferase activity
	hb83	homeobox-transcription factor	transcription factor
	kch5	potassium channel	ion transport
	mrpa7	acyl-protein thioesterase	hydrolase activity
	pin12	PIN-formed protein	transmembrane transport
	srk1	S-receptor kinase	protein kinase activity
	trpp7	trehalose-6-phosphate phosphatase	trehalose biosynthesis
	wrky116	WRKY-transcription factor	transcription factor
	wrky99	WRKY-transcription factor	transcription factor
	AC187243.3_FG005	uncharacterized protein	response to freezing
	AC214227.4_FG013	uncharacterized protein	zinc ion binding
	AC225222.2_FG004	uncharacterized protein	response to wounding
	GRMZM2G006716	uncharacterized protein	hydrolase activity
	GRMZM2G008819	uncharacterized protein	copper ion binding
	GRMZM2G015654	galactoside 2-alpha-L-fucosyltransferase	cell wall biogenesis
	GRMZM2G015739	uncharacterized protein	unknown
	GRMZM2G015804	uncharacterized protein	carbohydrate metabolism
	GRMZM2G018416	glycerophosphodiester phosphodiesterase	lipid metabolism
	GRMZM2G024865	serine-type peptidase	proteolysis
	GRMZM2G033805	uncharacterized protein	unknown
	GRMZM2G034855	BRASSINOSTEROID INSENSITIVE 1-associated receptor kinase	protein kinase activity
	GRMZM2G050072	10-deacetylbaccatin III 10-O-acetyltransferase	acyl group transferase activity
	GRMZM2G050270	3-N-debenzoyl-2-deoxytaxol N-benzoyltransferase	acyl group transferase activity
	GRMZM2G051045	uncharacterized protein	unknown
	GRMZM2G055124	cis-zeatin O-beta-D-glucosyltransferase	cis-zeatin O-beta-D-glucosyltransferase activity
	GRMZM2G055643	uncharacterized protein	zinc ion binding
	GRMZM2G061798	uncharacterized protein	unknown
	GRMZM2G063156	uncharacterized protein	response to freezing
	GRMZM2G066101	nucleoside-triphosphatase	DNA replication
	GRMZM2G067734	protein kinase	protein kinase activity
	GRMZM2G069503	triacylglycerol lipase	lipid metabolism
	GRMZM2G071846	adenine phosphoribosyltransferase	adenine salvage
	GRMZM2G075372	uncharacterized protein	unknown
	GRMZM2G075712	uncharacterized protein	unknown
	GRMZM2G090010	methionine aminopeptidase	proteolysis
	GRMZM2G090528	uncharacterized protein	transmembrane transport
	GRMZM2G095397	uncharacterized protein	protein domain specific binding
	GRMZM2G101741	TMV response-related protein	tobacco mosaic virus response
	GRMZM2G108040	uncharacterized protein	G-protein coupled receptor signaling pathway
	GRMZM2G109140	heterotrimeric G-protein GTPase	G-protein signaling
	GRMZM2G118579	xyloglucan:xyloglucosyl transferase	cellular glucan metabolism
	GRMZM2G120922	uncharacterized protein	transmembrane transport
	GRMZM2G121868	uncharacterized protein	G-protein coupled receptor signaling pathway
	GRMZM2G123212	ubiquitin-protein ligase	transcription regulation
	GRMZM2G131012	uncharacterized protein	unknown
	GRMZM2G131340	uncharacterized protein	transcription regulation
	GRMZM2G142802	stem-specific protein	unknown
	GRMZM2G145753	uncharacterized protein	protein kinase activity
	GRMZM2G157749	uncharacterized protein	membrane component
	GRMZM2G157760	phosphoinositide phospholipase C	lipid metabolism
	GRMZM2G158013	uncharacterized protein	transmembrane transport
	GRMZM2G158141	uncharacterized protein	response to freezing
	GRMZM2G160463	uncharacterized protein	unknown
	GRMZM2G164854	uncharacterized protein	unknown
	GRMZM2G165005	uncharacterized protein	unknown
	GRMZM2G165099	NPK1-related protein kinase-like protein	protein kinase activity
	GRMZM2G166665	uncharacterized protein	unknown
	GRMZM2G166694	uncharacterized protein	ubiquitin protein ligase activity
	GRMZM2G174310	uncharacterized protein	response to freezing
	GRMZM2G175177	uncharacterized protein	nucleic acid binding
	GRMZM2G179146	uncharacterized protein	unknown
	GRMZM2G400444	uncharacterized protein	zinc ion binding
	GRMZM2G422576	uncharacterized protein	protein kinase activity
	GRMZM2G427603	uncharacterized protein	unknown
	GRMZM2G435294	nucleoside-triphosphatase	nucleotide binding
	GRMZM2G440259	uncharacterized protein	zinc ion binding
	GRMZM2G466394	uncharacterized protein	unknown
	GRMZM2G468702	uncharacterized protein	photosynthesis
	GRMZM5G815165	uncharacterized protein	proteolysis
	GRMZM5G828661	uncharacterized protein	unknown
	GRMZM5G833625	uncharacterized protein	unknown
	GRMZM5G874562	uncharacterized protein	G-protein coupled receptor signaling pathway

Table 4.9. P-values of two-tailed t-tests comparing predictive abilities of top GWAS kinships and random kinships on each of the predicted traits

Predicted trait	Top GWAS kinship trait													
	ASI	Branch Num	Bulk Den	Cob Den	Cob Diam	Cob Len	Cob Vol	DTA	DTS	EHT	ERN	FER	Germ Count	Kernel Type
ASI	2.E-21	4.E-21	7.E-17	6.E-15	3.E-17	7.E-16	1.E-17	1.E-19	1.E-17	9.E-17	2.E-16	5.E-16	1.E-12	3.E-18
BranchNum	1.E-32	2.E-34	2.E-32	9.E-34	2.E-27	3.E-30	1.E-30	4.E-30	6.E-29	1.E-33	1.E-27	2.E-32	4.E-29	2.E-31
BulkDen	6.E-16	7.E-15	7.E-13	3.E-15	7.E-14	3.E-16	1.E-14	2.E-13	5.E-14	1.E-17	1.E-14	4.E-18	2.E-14	2.E-14
CobDen	5.E-19	7.E-21	2.E-18	7.E-20	1.E-18	2.E-16	3.E-19	2.E-19	6.E-20	2.E-16	1.E-18	6.E-19	2.E-20	2.E-19
CobDiam	5.E-25	7.E-25	2.E-28	1.E-25	1.E-26	2.E-28	1.E-27	3.E-26	8.E-29	5.E-27	6.E-27	7.E-29	4.E-27	8.E-31
CobLen	7.E-23	5.E-21	1.E-20	4.E-19	7.E-20	2.E-19	4.E-22	7.E-20	8.E-18	7.E-19	4.E-18	3.E-20	3.E-21	4.E-20
CobVol	1.E-19	8.E-20	7.E-23	9.E-20	1.E-21	1.E-24	1.E-21	2.E-19	3.E-22	2.E-20	3.E-21	3.E-22	2.E-23	1.E-22
DTA	6.E-39	1.E-39	1.E-39	8.E-36	5.E-39	9.E-38	7.E-38	4.E-38	7.E-36	2.E-38	9.E-38	4.E-39	3.E-39	1.E-37
DTS	5.E-39	1.E-39	2.E-38	6.E-36	1.E-38	1.E-36	2.E-37	2.E-38	8.E-36	3.E-37	2.E-38	4.E-39	2.E-38	4.E-37
EHT	9.E-33	7.E-33	2.E-27	3.E-31	4.E-28	5.E-28	3.E-30	6.E-30	2.E-29	3.E-32	8.E-30	2.E-29	5.E-30	3.E-29
ERN	7.E-29	3.E-27	2.E-28	2.E-26	9.E-30	1.E-29	3.E-32	4.E-30	3.E-28	4.E-27	1.E-28	1.E-30	3.E-32	2.E-29
FER	5.E-27	1.E-26	8.E-28	5.E-23	2.E-25	1.E-21	5.E-25	4.E-24	6.E-24	8.E-26	2.E-23	5.E-24	2.E-28	4.E-25
GermCount	1.E-21	2.E-21	1.E-21	6.E-23	6.E-22	3.E-20	1.E-21	1.E-24	7.E-23	3.E-21	1.E-20	1.E-19	7.E-20	4.E-19
KernelType	9.E-28	7.E-26	2.E-27	5.E-27	9.E-33	2.E-29	1.E-26	3.E-25	6.E-27	4.E-26	4.E-27	4.E-24	6.E-26	1.E-27
LeafLen	3.E-32	5.E-36	1.E-34	2.E-35	1.E-33	8.E-33	5.E-35	1.E-34	1.E-34	1.E-37	2.E-31	1.E-34	3.E-35	7.E-36
LeafWid	9.E-31	3.E-31	6.E-30	4.E-29	7.E-31	1.E-30	1.E-30	7.E-29	3.E-29	1.E-31	2.E-31	2.E-34	5.E-31	3.E-32
MLA	2.E-24	2.E-28	1.E-29	2.E-26	2.E-23	8.E-29	3.E-28	5.E-24	1.E-24	1.E-27	1.E-24	2.E-31	4.E-27	2.E-28
Oil	1.E-23	1.E-26	4.E-25	4.E-28	9.E-29	6.E-26	2.E-25	8.E-28	4.E-25	6.E-26	1.E-25	3.E-30	2.E-29	1.E-29
Protein	4.E-19	8.E-20	2.E-21	3.E-18	3.E-17	2.E-17	7.E-17	5.E-18	2.E-22	3.E-19	8.E-19	2.E-21	1.E-17	7.E-20
Starch	2.E-20	1.E-18	9.E-21	1.E-18	2.E-20	1.E-18	4.E-20	3.E-18	6.E-19	5.E-17	6.E-19	3.E-23	9.E-19	3.E-16
NLB	8.E-33	7.E-35	2.E-33	5.E-31	2.E-29	2.E-30	1.E-29	4.E-30	3.E-30	1.E-34	8.E-32	1.E-32	6.E-31	3.E-29
PHT	2.E-20	4.E-22	2.E-20	4.E-21	2.E-21	2.E-18	2.E-19	3.E-21	4.E-20	8.E-26	3.E-20	7.E-20	2.E-24	2.E-19
RPR	4.E-23	6.E-19	3.E-23	1.E-19	1.E-19	4.E-18	8.E-19	2.E-20	1.E-20	1.E-17	2.E-19	2.E-20	3.E-20	4.E-21
SLB	1.E-28	5.E-33	3.E-30	3.E-31	5.E-30	2.E-32	3.E-31	3.E-30	4.E-30	1.E-33	2.E-30	6.E-30	2.E-32	2.E-30
SpikeLen	2.E-19	7.E-19	4.E-21	6.E-17	5.E-17	1.E-18	2.E-20	1.E-17	6.E-17	4.E-20	8.E-19	8.E-18	5.E-17	1.E-20
StandCount	4.E-01	5.E-02	1.E-02	3.E-01	6.E-02	1.E-01	7.E-01	1.E-01	6.E-01	7.E-01	8.E-02	4.E-01	9.E-02	7.E-02
TasselLen	9.E-28	7.E-27	1.E-27	4.E-27	8.E-30	2.E-27	3.E-27	3.E-26	2.E-28	2.E-27	6.E-29	1.E-28	1.E-28	5.E-26
Tillering	3.E-08	2.E-09	3.E-10	6.E-11	5.E-08	2.E-07	4.E-10	4.E-06	8.E-07	8.E-09	6.E-07	6.E-11	3.E-07	2.E-10
ULA	4.E-33	6.E-33	1.E-34	2.E-30	1.E-33	7.E-35	1.E-33	1.E-32	1.E-32	4.E-35	2.E-30	5.E-35	1.E-34	3.E-33

Table 4.9. (continued)

Predicted trait	Top GWAS kinship trait													
	Leaf Len	Leaf Wid	MLA	Oil	Protein	Starch	NLB	PHT	RPR	SLB	Spike Len	Tassel Len	Tillering	ULA
ASI	5.E-18	2.E-19	2.E-17	5.E-19	5.E-18	1.E-16	4.E-20	6.E-17	1.E-14	1.E-15	9.E-15	3.E-17	3.E-17	5.E-17
BranchNum	3.E-30	1.E-29	2.E-33	1.E-32	2.E-32	4.E-28	4.E-36	5.E-28	1.E-31	5.E-31	6.E-31	4.E-32	1.E-32	4.E-30
BulkDen	2.E-13	2.E-19	2.E-16	2.E-15	1.E-15	1.E-12	2.E-16	1.E-15	7.E-16	1.E-15	5.E-18	3.E-14	8.E-16	3.E-14
CobDen	2.E-19	2.E-16	7.E-20	3.E-21	2.E-18	3.E-19	3.E-18	6.E-16	4.E-22	6.E-22	1.E-17	1.E-19	5.E-19	4.E-17
CobDiam	8.E-27	7.E-32	2.E-29	4.E-25	1.E-25	8.E-28	2.E-29	4.E-26	4.E-27	1.E-24	7.E-31	8.E-30	3.E-24	2.E-25
CobLen	5.E-25	9.E-22	2.E-22	3.E-16	3.E-18	4.E-20	4.E-20	7.E-22	6.E-18	2.E-22	9.E-19	8.E-17	2.E-17	3.E-17
CobVol	1.E-22	3.E-20	8.E-21	7.E-20	4.E-20	2.E-21	4.E-22	2.E-21	4.E-22	6.E-21	1.E-24	2.E-24	2.E-18	4.E-19
DTA	5.E-38	6.E-37	3.E-38	2.E-39	2.E-40	1.E-41	4.E-40	3.E-37	4.E-40	6.E-38	1.E-38	2.E-39	2.E-39	1.E-35
DTS	1.E-37	7.E-36	6.E-38	2.E-38	3.E-40	1.E-40	2.E-39	4.E-37	7.E-39	4.E-37	7.E-37	4.E-40	2.E-38	5.E-35
EHT	5.E-32	3.E-28	5.E-31	2.E-32	1.E-33	8.E-34	2.E-32	9.E-32	8.E-32	4.E-29	1.E-31	4.E-33	4.E-33	9.E-30
ERN	8.E-28	5.E-26	9.E-31	6.E-27	2.E-27	2.E-30	3.E-32	4.E-30	5.E-26	1.E-28	1.E-29	2.E-30	4.E-29	1.E-27
FER	2.E-26	1.E-23	6.E-26	1.E-22	6.E-24	3.E-25	4.E-24	2.E-28	3.E-25	9.E-23	1.E-23	2.E-25	3.E-21	2.E-25
GermCount	6.E-23	1.E-22	1.E-18	3.E-22	7.E-21	2.E-19	7.E-19	5.E-21	2.E-19	3.E-22	5.E-20	6.E-21	3.E-23	2.E-19
KernelType	6.E-30	2.E-28	3.E-27	1.E-25	7.E-26	1.E-30	2.E-26	2.E-27	6.E-26	2.E-29	4.E-28	3.E-26	3.E-27	1.E-24
LeafLen	8.E-35	3.E-34	2.E-38	2.E-35	3.E-36	5.E-36	2.E-35	2.E-35	4.E-34	5.E-35	2.E-37	5.E-36	2.E-33	3.E-33
LeafWid	5.E-33	3.E-27	7.E-32	8.E-33	1.E-31	4.E-29	3.E-33	2.E-29	1.E-34	4.E-33	1.E-31	2.E-31	2.E-34	5.E-28
MLA	2.E-25	6.E-29	6.E-29	4.E-26	1.E-28	9.E-26	4.E-27	3.E-29	9.E-27	2.E-25	6.E-26	4.E-26	3.E-25	1.E-27
Oil	3.E-22	5.E-25	6.E-26	8.E-32	5.E-26	2.E-24	3.E-25	4.E-27	2.E-22	9.E-25	9.E-25	2.E-24	3.E-31	2.E-24
Protein	1.E-19	6.E-20	2.E-19	4.E-17	4.E-18	4.E-17	6.E-20	3.E-19	4.E-19	3.E-18	3.E-18	1.E-18	5.E-16	1.E-21
Starch	3.E-22	1.E-17	4.E-18	3.E-20	5.E-17	9.E-19	9.E-20	1.E-15	2.E-20	8.E-21	5.E-20	4.E-19	6.E-19	2.E-21
NLB	2.E-31	3.E-34	8.E-31	6.E-31	8.E-32	1.E-34	2.E-35	3.E-30	3.E-33	1.E-28	3.E-30	7.E-32	2.E-30	6.E-31
PHT	3.E-21	1.E-19	4.E-22	3.E-23	1.E-27	4.E-24	3.E-22	6.E-24	1.E-20	9.E-19	5.E-21	1.E-23	4.E-24	8.E-22
RPR	2.E-22	2.E-21	3.E-18	1.E-18	4.E-21	1.E-18	3.E-20	3.E-22	5.E-17	1.E-18	5.E-19	4.E-20	7.E-18	2.E-20
SLB	5.E-32	3.E-31	2.E-30	9.E-33	3.E-30	2.E-31	1.E-30	9.E-29	2.E-34	3.E-30	3.E-29	5.E-32	1.E-30	2.E-32
SpikeLen	2.E-16	3.E-18	2.E-18	1.E-19	9.E-19	1.E-16	7.E-19	2.E-22	9.E-20	8.E-19	2.E-16	1.E-18	3.E-17	1.E-20
StandCount	3.E-01	6.E-02	8.E-03	3.E-02	1.E-01	1.E-01	3.E-01	2.E-01	4.E-02	5.E-02	1.E-01	3.E-02	6.E-02	4.E-01
TasselLen	3.E-29	6.E-29	2.E-29	4.E-28	4.E-27	8.E-26	4.E-27	3.E-28	5.E-28	3.E-29	3.E-30	8.E-31	4.E-29	5.E-29
Tillering	1.E-09	6.E-10	2.E-12	9.E-09	6.E-07	4.E-08	1.E-08	3.E-05	6.E-10	5.E-09	8.E-09	3.E-07	3.E-07	4.E-08
ULA	6.E-32	2.E-35	6.E-37	3.E-34	2.E-32	1.E-32	6.E-34	3.E-34	9.E-33	1.E-33	3.E-31	2.E-33	2.E-34	6.E-36

Table 4.10. Predictive abilities (means and standard errors) of all pairiwise combinations of GWAS trait and predicted trait.

Predicted trait	Top GWAS kinship trait									
	Random	ASI	BranchNum	BulkDen	CobDen	CobDiam	CobLen	CobVol	DTA	DTS
ASI	0.213 ± 0.004	-0.046 ± 0.026	-0.037 ± 0.018	-0.065 ± 0.072	-0.012 ± 0.031	-0.024 ± 0.022	0.002 ± 0.029	-0.026 ± 0.024	-0.004 ± 0.015	-0.01 ± 0.018
BranchNum	0.466 ± 0.002	0.019 ± 0.028	0.007 ± 0.017	-0.009 ± 0.064	0.019 ± 0.023	0.036 ± 0.024	0.025 ± 0.028	0.009 ± 0.024	0.007 ± 0.018	0.025 ± 0.019
BulkDen	0.234 ± 0.003	-0.032 ± 0.037	-0.005 ± 0.024	0.095 ± 0.084	0.038 ± 0.029	0.004 ± 0.027	-0.039 ± 0.034	-0.013 ± 0.03	0.022 ± 0.021	0.002 ± 0.023
CobDen	0.271 ± 0.004	0.065 ± 0.029	0.031 ± 0.018	0.017 ± 0.076	0.015 ± 0.028	0.03 ± 0.022	0.028 ± 0.033	0.027 ± 0.024	0.007 ± 0.019	-0.008 ± 0.019
CobDiam	0.383 ± 0.003	-0.022 ± 0.035	-0.003 ± 0.022	0.005 ± 0.064	0.007 ± 0.029	0.019 ± 0.021	-0.003 ± 0.026	0.001 ± 0.023	0.014 ± 0.018	-0.008 ± 0.017
CobLen	0.271 ± 0.003	0.011 ± 0.027	-0.011 ± 0.02	0.019 ± 0.067	0.01 ± 0.029	-0.006 ± 0.023	0 ± 0.029	-0.034 ± 0.024	0.014 ± 0.018	0.005 ± 0.021
CobVol	0.289 ± 0.004	-0.031 ± 0.036	-0.008 ± 0.022	0.091 ± 0.06	0.038 ± 0.028	0.006 ± 0.021	-0.007 ± 0.025	-0.002 ± 0.024	0.019 ± 0.019	0.011 ± 0.017
DTA	0.738 ± 0.001	0.015 ± 0.032	0.021 ± 0.02	0.066 ± 0.068	0.014 ± 0.033	0.016 ± 0.022	0.03 ± 0.03	0.005 ± 0.026	0.013 ± 0.019	0.027 ± 0.021
DTS	0.716 ± 0.002	0.007 ± 0.031	0.013 ± 0.019	0.032 ± 0.071	0.001 ± 0.032	0.009 ± 0.022	0.022 ± 0.031	-0.001 ± 0.026	0.01 ± 0.019	0.024 ± 0.021
EHT	0.541 ± 0.002	0.023 ± 0.032	0.02 ± 0.02	0.104 ± 0.089	0.006 ± 0.031	-0.004 ± 0.028	0.042 ± 0.035	0.011 ± 0.028	0.007 ± 0.021	0.018 ± 0.022
ERN	0.417 ± 0.002	0.002 ± 0.03	-0.017 ± 0.022	0.035 ± 0.067	0.016 ± 0.03	-0.011 ± 0.021	-0.025 ± 0.027	0.006 ± 0.02	0.006 ± 0.017	-0.015 ± 0.019
FER	0.377 ± 0.003	0.025 ± 0.029	-0.011 ± 0.021	0.102 ± 0.061	0.033 ± 0.031	0.017 ± 0.022	0.023 ± 0.035	-0.005 ± 0.026	0.021 ± 0.019	0.012 ± 0.02
GermCount	0.304 ± 0.002	0.03 ± 0.03	0.021 ± 0.02	0.054 ± 0.069	0.021 ± 0.026	0.018 ± 0.021	0.065 ± 0.027	0.042 ± 0.022	0.009 ± 0.016	0.024 ± 0.017
KernelType	0.444 ± 0.002	0.036 ± 0.032	0.026 ± 0.023	0.095 ± 0.073	0.027 ± 0.03	0.015 ± 0.018	0.028 ± 0.027	0.049 ± 0.025	-0.001 ± 0.023	0.028 ± 0.02
Leaflen	0.612 ± 0.002	0.02 ± 0.037	-0.021 ± 0.021	0.05 ± 0.073	-0.012 ± 0.029	-0.002 ± 0.025	0.013 ± 0.032	-0.03 ± 0.026	-0.002 ± 0.019	0.002 ± 0.02
LeafWid	0.46 ± 0.003	0.026 ± 0.03	0.022 ± 0.019	0.047 ± 0.069	0.034 ± 0.028	0.027 ± 0.02	0.011 ± 0.028	-0.002 ± 0.024	-0.007 ± 0.02	0.008 ± 0.019
MLA	0.37 ± 0.003	0.017 ± 0.033	-0.03 ± 0.019	-0.018 ± 0.06	-0.003 ± 0.028	0.008 ± 0.024	-0.038 ± 0.026	-0.029 ± 0.023	0.017 ± 0.019	0.002 ± 0.02
Oil	0.354 ± 0.003	-0.029 ± 0.035	0.001 ± 0.019	0.04 ± 0.068	0.002 ± 0.024	-0.01 ± 0.019	-0.018 ± 0.028	-0.021 ± 0.025	-0.035 ± 0.018	-0.026 ± 0.02
Protein	0.293 ± 0.003	0.033 ± 0.033	0.005 ± 0.022	0.06 ± 0.067	0.021 ± 0.032	0.058 ± 0.023	0.043 ± 0.032	0.05 ± 0.027	0.024 ± 0.02	0.024 ± 0.016
Starch	0.305 ± 0.003	0.065 ± 0.03	0.032 ± 0.022	0.123 ± 0.068	0.023 ± 0.032	0.019 ± 0.023	0.072 ± 0.029	0.053 ± 0.024	0.031 ± 0.021	0.036 ± 0.02
NLB	0.56 ± 0.002	-0.025 ± 0.034	-0.023 ± 0.02	-0.074 ± 0.074	0.029 ± 0.031	0.015 ± 0.027	0.01 ± 0.033	-0.004 ± 0.03	0.011 ± 0.022	0.026 ± 0.021
PHT	0.318 ± 0.003	0.009 ± 0.035	-0.01 ± 0.022	-0.081 ± 0.085	-0.049 ± 0.034	-0.012 ± 0.025	0.007 ± 0.036	0.001 ± 0.029	-0.007 ± 0.021	0.001 ± 0.022
RPR	0.288 ± 0.003	-0.002 ± 0.029	0.011 ± 0.022	-0.032 ± 0.065	-0.028 ± 0.032	-0.003 ± 0.024	0.026 ± 0.032	0.027 ± 0.026	-0.006 ± 0.019	-0.012 ± 0.02
SLB	0.519 ± 0.002	0.007 ± 0.038	-0.01 ± 0.02	-0.004 ± 0.078	0.019 ± 0.029	0.015 ± 0.024	-0.02 ± 0.029	0.005 ± 0.026	-0.008 ± 0.021	-0.001 ± 0.021
SpikeLen	0.262 ± 0.004	-0.026 ± 0.033	0.009 ± 0.02	-0.008 ± 0.065	0.025 ± 0.031	0 ± 0.025	-0.011 ± 0.031	0.019 ± 0.022	0.003 ± 0.02	0.018 ± 0.02
StandCount	0.049 ± 0.004	0.054 ± 0.033	0.011 ± 0.021	0.018 ± 0.066	0.044 ± 0.029	0.013 ± 0.024	0.035 ± 0.027	0.056 ± 0.025	0.02 ± 0.018	0.039 ± 0.019
TasselLen	0.425 ± 0.002	-0.018 ± 0.033	-0.016 ± 0.023	0.016 ± 0.073	-0.038 ± 0.032	-0.015 ± 0.021	-0.022 ± 0.031	-0.023 ± 0.027	0.003 ± 0.02	0 ± 0.019
Tillering	0.119 ± 0.003	-0.018 ± 0.034	-0.009 ± 0.019	-0.132 ± 0.075	-0.05 ± 0.028	-0.007 ± 0.023	0.016 ± 0.028	-0.007 ± 0.021	0.02 ± 0.019	-0.01 ± 0.023
ULA	0.574 ± 0.002	-0.014 ± 0.034	-0.015 ± 0.022	-0.025 ± 0.071	0.015 ± 0.034	-0.004 ± 0.023	-0.006 ± 0.028	0 ± 0.025	0.017 ± 0.02	0.004 ± 0.02

Table 4.10. (continued)

Predicted trait	Top GWAS kinship trait									
	EHT	ERN	FER	GermCount	KernelType	LeafLen	LeafWid	MLA	Oil	Protein
ASI	-0.039 ± 0.025	-0.021 ± 0.029	-0.001 ± 0.026	0.011 ± 0.055	-0.02 ± 0.026	-0.015 ± 0.02	-0.032 ± 0.02	-0.022 ± 0.024	-0.018 ± 0.026	-0.059 ± 0.036
BranchNum	0 ± 0.019	0.03 ± 0.03	-0.01 ± 0.024	0.039 ± 0.047	0.024 ± 0.026	0.008 ± 0.021	-0.001 ± 0.023	-0.009 ± 0.021	0.008 ± 0.026	0.02 ± 0.031
BulkDen	-0.013 ± 0.023	0.031 ± 0.03	-0.004 ± 0.026	0.031 ± 0.052	0.016 ± 0.032	0.02 ± 0.025	-0.035 ± 0.022	-0.015 ± 0.027	0.045 ± 0.029	0.009 ± 0.039
CobDen	0.046 ± 0.024	0.046 ± 0.027	0.043 ± 0.025	0.053 ± 0.042	0.022 ± 0.028	0.019 ± 0.021	0.038 ± 0.024	0.019 ± 0.023	-0.002 ± 0.028	0.051 ± 0.035
CobDiam	-0.006 ± 0.022	0.022 ± 0.026	-0.03 ± 0.025	-0.011 ± 0.045	-0.012 ± 0.023	-0.001 ± 0.021	-0.013 ± 0.018	-0.021 ± 0.022	0.022 ± 0.03	-0.003 ± 0.037
CobLen	0.011 ± 0.023	-0.011 ± 0.031	0.034 ± 0.024	-0.022 ± 0.044	0 ± 0.028	0.017 ± 0.015	0.011 ± 0.019	-0.001 ± 0.021	-0.007 ± 0.037	0.022 ± 0.037
CobVol	0.019 ± 0.022	0.018 ± 0.027	0 ± 0.025	0.017 ± 0.04	0.002 ± 0.026	0 ± 0.02	0.022 ± 0.022	0.014 ± 0.024	0.041 ± 0.029	0.01 ± 0.037
DTA	0.013 ± 0.023	0.02 ± 0.03	0.032 ± 0.026	0.033 ± 0.046	0.041 ± 0.03	0.014 ± 0.022	0.016 ± 0.024	0.012 ± 0.025	0.031 ± 0.029	0.059 ± 0.032
DTS	0.009 ± 0.024	0.008 ± 0.028	0.028 ± 0.026	0.018 ± 0.046	0.034 ± 0.03	0.011 ± 0.022	0.007 ± 0.025	0.011 ± 0.025	0.024 ± 0.03	0.04 ± 0.032
EHT	-0.001 ± 0.024	0.036 ± 0.031	0.011 ± 0.032	0.022 ± 0.053	0.03 ± 0.033	0.017 ± 0.022	0.012 ± 0.028	0.041 ± 0.025	0.016 ± 0.03	-0.003 ± 0.035
ERN	0.012 ± 0.023	-0.002 ± 0.027	-0.019 ± 0.024	-0.007 ± 0.038	-0.006 ± 0.026	-0.001 ± 0.021	0.002 ± 0.024	-0.021 ± 0.022	0.041 ± 0.029	-0.015 ± 0.037
FER	-0.002 ± 0.023	0.001 ± 0.032	0.013 ± 0.029	-0.048 ± 0.044	0.03 ± 0.028	0.004 ± 0.021	0.009 ± 0.025	0.023 ± 0.023	0.011 ± 0.035	0.018 ± 0.039
GermCount	0.019 ± 0.022	0.03 ± 0.028	0.061 ± 0.026	0.04 ± 0.049	0.059 ± 0.029	0.03 ± 0.018	0.018 ± 0.02	0.044 ± 0.026	0.039 ± 0.027	0.041 ± 0.035
KernelType	0.044 ± 0.024	0.027 ± 0.03	0.045 ± 0.032	0.051 ± 0.051	0.035 ± 0.029	0.029 ± 0.019	0.008 ± 0.023	0.029 ± 0.025	0.043 ± 0.033	0.078 ± 0.038
LeafLen	-0.012 ± 0.021	0.007 ± 0.034	0.006 ± 0.028	-0.002 ± 0.047	0.002 ± 0.028	-0.026 ± 0.023	-0.004 ± 0.024	-0.016 ± 0.022	0.028 ± 0.029	0.011 ± 0.034
LeafWid	-0.01 ± 0.021	0.005 ± 0.026	0.03 ± 0.021	-0.019 ± 0.045	0.036 ± 0.024	0.003 ± 0.018	-0.003 ± 0.025	0.009 ± 0.022	0.014 ± 0.026	0.052 ± 0.031
MLA	0.001 ± 0.021	-0.013 ± 0.03	-0.034 ± 0.022	-0.023 ± 0.044	-0.014 ± 0.026	0.009 ± 0.021	-0.024 ± 0.02	-0.004 ± 0.021	-0.023 ± 0.03	0.009 ± 0.031
Oil	-0.014 ± 0.022	-0.02 ± 0.028	-0.004 ± 0.021	-0.05 ± 0.039	-0.045 ± 0.024	0.003 ± 0.024	0.016 ± 0.021	0 ± 0.023	0.03 ± 0.021	-0.042 ± 0.035
Protein	0.028 ± 0.023	0.039 ± 0.029	0.004 ± 0.026	0.071 ± 0.051	0.028 ± 0.029	0.033 ± 0.021	0.005 ± 0.023	0.028 ± 0.025	0.011 ± 0.037	0.078 ± 0.036
Starch	0.049 ± 0.026	0.025 ± 0.031	0.022 ± 0.024	0.089 ± 0.049	0.104 ± 0.031	0.025 ± 0.02	0.052 ± 0.024	0.047 ± 0.027	0.039 ± 0.03	0.105 ± 0.038
NLB	-0.022 ± 0.023	-0.01 ± 0.031	-0.003 ± 0.028	-0.042 ± 0.054	0.049 ± 0.033	-0.012 ± 0.024	-0.005 ± 0.022	0.023 ± 0.027	-0.009 ± 0.034	0.049 ± 0.037
PHT	-0.02 ± 0.021	0 ± 0.032	0.001 ± 0.031	-0.037 ± 0.044	-0.007 ± 0.034	-0.001 ± 0.023	0.006 ± 0.026	-0.012 ± 0.026	-0.032 ± 0.031	-0.008 ± 0.028
RPR	0.011 ± 0.027	-0.011 ± 0.031	0.01 ± 0.027	-0.006 ± 0.048	-0.027 ± 0.03	-0.009 ± 0.02	-0.021 ± 0.023	0.007 ± 0.028	-0.032 ± 0.036	0.004 ± 0.035
SLB	-0.019 ± 0.022	0.022 ± 0.03	-0.004 ± 0.03	-0.019 ± 0.046	-0.01 ± 0.031	0.004 ± 0.021	0.013 ± 0.023	-0.012 ± 0.027	-0.005 ± 0.029	0.037 ± 0.038
SpikeLen	-0.024 ± 0.024	-0.019 ± 0.03	0.008 ± 0.028	-0.007 ± 0.053	-0.04 ± 0.029	0.007 ± 0.025	-0.012 ± 0.024	-0.02 ± 0.027	0.009 ± 0.029	-0.042 ± 0.04
StandCount	0.051 ± 0.023	0.021 ± 0.029	0.047 ± 0.029	0.042 ± 0.045	0.022 ± 0.029	0.031 ± 0.023	0.007 ± 0.027	-0.004 ± 0.024	0 ± 0.035	0.034 ± 0.039
TasselLen	-0.033 ± 0.025	-0.057 ± 0.029	-0.006 ± 0.027	-0.026 ± 0.046	-0.017 ± 0.033	-0.01 ± 0.021	-0.021 ± 0.022	-0.018 ± 0.024	-0.029 ± 0.031	-0.06 ± 0.04
Tillering	-0.013 ± 0.023	0.006 ± 0.03	-0.042 ± 0.026	-0.029 ± 0.055	-0.004 ± 0.024	-0.031 ± 0.022	-0.04 ± 0.024	-0.048 ± 0.022	-0.008 ± 0.029	0.012 ± 0.038
ULA	-0.017 ± 0.023	0.007 ± 0.034	-0.018 ± 0.027	0.067 ± 0.044	-0.006 ± 0.03	0.002 ± 0.024	0.006 ± 0.021	-0.003 ± 0.022	0.016 ± 0.029	0.03 ± 0.038

Table 4.10. (continued)

Predicted trait	Top GWAS kinship trait								
	Starch	NLB	PHT	RPR	SLB	SpikeLen	TasselLen	Tillering	ULA
ASI	-0.004 ± 0.038	-0.038 ± 0.019	-0.022 ± 0.032	0.001 ± 0.037	-0.027 ± 0.025	0.012 ± 0.022	-0.007 ± 0.027	-0.037 ± 0.054	-0.017 ± 0.02
BranchNum	0.037 ± 0.042	0.007 ± 0.015	0.026 ± 0.035	-0.015 ± 0.032	0.024 ± 0.021	0.028 ± 0.02	0.026 ± 0.025	0.004 ± 0.049	0.01 ± 0.02
BulkDen	0.035 ± 0.049	-0.005 ± 0.022	-0.006 ± 0.036	0.02 ± 0.035	0.003 ± 0.025	-0.014 ± 0.022	0.028 ± 0.031	0.043 ± 0.057	0.003 ± 0.024
CobDen	0.028 ± 0.039	0.036 ± 0.02	0.036 ± 0.038	-0.043 ± 0.033	0.016 ± 0.02	0.007 ± 0.024	0.007 ± 0.028	0.045 ± 0.056	0.017 ± 0.022
CobDiam	-0.016 ± 0.037	-0.008 ± 0.018	-0.051 ± 0.035	-0.069 ± 0.036	0.014 ± 0.024	0.005 ± 0.017	0.004 ± 0.024	-0.004 ± 0.062	0.008 ± 0.021
CobLen	0.002 ± 0.038	0.006 ± 0.02	-0.019 ± 0.03	-0.003 ± 0.038	-0.021 ± 0.021	0.003 ± 0.023	0.055 ± 0.029	0.026 ± 0.062	0.017 ± 0.022
CobVol	0.031 ± 0.037	0.011 ± 0.019	-0.019 ± 0.033	-0.009 ± 0.033	0.007 ± 0.023	0.024 ± 0.017	0.018 ± 0.023	0.035 ± 0.062	0.018 ± 0.021
DTA	-0.008 ± 0.036	0.002 ± 0.02	0.015 ± 0.035	0.046 ± 0.032	0.009 ± 0.024	0.03 ± 0.022	0.028 ± 0.028	0.019 ± 0.055	0.036 ± 0.023
DTS	-0.01 ± 0.036	-0.003 ± 0.02	0.014 ± 0.035	0.038 ± 0.033	0.004 ± 0.025	0.029 ± 0.023	0.019 ± 0.026	0.007 ± 0.057	0.028 ± 0.023
EHT	0.001 ± 0.038	0.004 ± 0.021	0.007 ± 0.034	0.051 ± 0.035	0.008 ± 0.027	0.034 ± 0.022	0.031 ± 0.027	0.03 ± 0.055	0.018 ± 0.023
ERN	-0.01 ± 0.035	-0.009 ± 0.017	-0.007 ± 0.029	0.002 ± 0.037	0.01 ± 0.021	-0.003 ± 0.02	-0.003 ± 0.025	0.03 ± 0.052	-0.016 ± 0.021
FER	-0.023 ± 0.042	-0.012 ± 0.023	-0.007 ± 0.03	-0.008 ± 0.036	0.01 ± 0.026	0.03 ± 0.023	0.037 ± 0.028	0.024 ± 0.07	0.01 ± 0.02
GermCount	0.097 ± 0.038	0.03 ± 0.022	0.035 ± 0.032	0.015 ± 0.038	0.012 ± 0.022	0.031 ± 0.022	0.051 ± 0.027	0.006 ± 0.052	0.017 ± 0.022
KernelType	0.059 ± 0.034	0.025 ± 0.022	0.041 ± 0.033	0.032 ± 0.038	0.058 ± 0.02	0.024 ± 0.022	0.055 ± 0.03	0.078 ± 0.058	0.045 ± 0.023
LeafLen	-0.029 ± 0.039	-0.016 ± 0.021	-0.017 ± 0.033	0.023 ± 0.036	0.004 ± 0.023	0.001 ± 0.02	-0.002 ± 0.028	-0.001 ± 0.062	0.003 ± 0.022
LeafWid	0.037 ± 0.039	0.004 ± 0.018	0.035 ± 0.032	0.058 ± 0.026	0.003 ± 0.02	0.021 ± 0.019	0.008 ± 0.026	0.028 ± 0.045	0.009 ± 0.022
MLA	-0.03 ± 0.041	-0.011 ± 0.02	-0.022 ± 0.028	0.009 ± 0.032	0.006 ± 0.023	0.005 ± 0.021	-0.007 ± 0.028	-0.008 ± 0.058	0.012 ± 0.018
Oil	-0.013 ± 0.041	-0.014 ± 0.021	-0.059 ± 0.032	0.016 ± 0.038	-0.032 ± 0.024	-0.006 ± 0.022	0.009 ± 0.028	0.052 ± 0.04	-0.008 ± 0.021
Protein	0.046 ± 0.046	0.028 ± 0.02	0.04 ± 0.033	0.033 ± 0.036	0.037 ± 0.024	0.018 ± 0.024	0.031 ± 0.03	0.085 ± 0.068	0.014 ± 0.019
Starch	0.08 ± 0.041	0.035 ± 0.021	0.101 ± 0.038	0.042 ± 0.035	0.032 ± 0.022	0.016 ± 0.023	0.015 ± 0.032	0.096 ± 0.059	0.014 ± 0.02
NLB	0.001 ± 0.038	-0.022 ± 0.02	0.023 ± 0.037	-0.044 ± 0.036	0.015 ± 0.029	0.007 ± 0.025	0.01 ± 0.031	0.002 ± 0.065	0.021 ± 0.022
PHT	-0.022 ± 0.038	-0.01 ± 0.022	-0.059 ± 0.034	0.054 ± 0.035	0.021 ± 0.027	0.005 ± 0.023	0.016 ± 0.026	-0.041 ± 0.055	-0.014 ± 0.022
RPR	0.039 ± 0.042	0.009 ± 0.021	-0.022 ± 0.032	0.031 ± 0.04	0.028 ± 0.024	-0.02 ± 0.025	0.01 ± 0.029	-0.109 ± 0.074	-0.011 ± 0.021
SLB	-0.025 ± 0.042	-0.003 ± 0.022	0.019 ± 0.038	-0.012 ± 0.031	0.002 ± 0.025	0.018 ± 0.024	0.031 ± 0.028	0.059 ± 0.058	0.019 ± 0.019
SpikeLen	0.002 ± 0.046	-0.007 ± 0.022	-0.037 ± 0.03	-0.044 ± 0.036	-0.035 ± 0.026	0.022 ± 0.024	-0.018 ± 0.031	0.008 ± 0.062	-0.03 ± 0.021
StandCount	0.032 ± 0.045	0.033 ± 0.02	0.04 ± 0.035	0.013 ± 0.037	0.013 ± 0.023	0.02 ± 0.022	0.012 ± 0.029	0.02 ± 0.065	0.039 ± 0.018
TasselLen	-0.058 ± 0.047	-0.021 ± 0.023	-0.035 ± 0.034	-0.026 ± 0.036	-0.041 ± 0.023	-0.002 ± 0.02	-0.001 ± 0.025	-0.094 ± 0.057	-0.036 ± 0.021
Tillering	0.004 ± 0.038	-0.012 ± 0.021	0.039 ± 0.036	-0.032 ± 0.033	-0.008 ± 0.022	-0.023 ± 0.023	0.018 ± 0.028	0.011 ± 0.059	0.005 ± 0.019
ULA	-0.029 ± 0.044	-0.021 ± 0.022	-0.044 ± 0.034	0.032 ± 0.036	0.005 ± 0.024	0.014 ± 0.025	-0.003 ± 0.03	0.036 ± 0.055	0.02 ± 0.018

Table 4.11. ANOVA summaries of predictive ability on each disease trait versus GWAS trait.

Predicted trait	Source	DF	SS	MS	F-ratio	p-value
FER	GWAS trai	28	0.20611	0.007361	0.3927	0.9982
	Error	1421	26.63674	0.018745		
	Total	1449	26.84285			
NLB	GWAS trai	28	0.339677	0.012131	0.5824	0.9602
	Error	1421	29.60056	0.020831		
	Total	1449	29.94024			
SLB	GWAS trai	28	0.164162	0.005863	0.307	0.9998
	Error	1421	27.1405	0.0191		
	Total	1449	27.30466			

Table 4.12. Correlations among absolute naïve trait correlations, absolute kinship-adjusted trait correlations, proportions of colocalized top GWAS SNPs, and predictive abilities between each of the three disease resistances and the other 28 traits.

FER	$AbsCorr_{naive}$	$AbsCorr_{kinship-adj.}$	PropColocGWAS	PredictiveAbility
$AbsCorr_{naive}$	---	0.23	0.13	-0.02
$AbsCorr_{kinship-adj.}$	<.0001	---	0.12	0.00
PropColocGWAS	<.0001	<.0001	---	-0.11
PredictiveAbility	0.43	0.98	<.0001	---

NLB	$AbsCorr_{naive}$	$AbsCorr_{kinship-adj.}$	PropColocGWAS	PredictiveAbility
$AbsCorr_{naive}$	---	0.54	0.04	0.03
$AbsCorr_{kinship-adj.}$	<.0001	---	0.02	0.02
PropColocGWAS	0.16	0.37	---	-0.04
PredictiveAbility	0.29	0.39	0.18	---

SLB	$AbsCorr_{naive}$	$AbsCorr_{kinship-adj.}$	PropColocGWAS	PredictiveAbility
$AbsCorr_{naive}$	---	0.14	0.33	-0.01
$AbsCorr_{kinship-adj.}$	<.0001	---	-0.05	-0.01
PropColocGWAS	<.0001	0.05	---	0.01
PredictiveAbility	0.66	0.68	0.73	---

Pearson correlations are in the upper diagonal and their respective p-values are in the lower diagonal

REFERENCES

1. Mueller DS, Wise KA, Sisson AJ, Allen TW, Bergstrom GC, Bosley DB, et al. Corn yield loss estimates due to diseases in the United States and Ontario, Canada from 2012 to 2015. Plant Heal Prog. 2016;17:211–22.
2. Wild CP, Gong YY. Mycotoxins and human disease: A largely ignored global health issue. Carcinogenesis. 2009;31:71–82.
3. Poland JA, Bradbury PJ, Buckler ES, Nelson RJ. Genome-wide nested association mapping of quantitative resistance to northern leaf blight in maize. PNAS. 2011;108:6893–8.
4. Benson JM, Poland JA, Benson BM, Stromberg EL, Nelson RJ. Resistance to gray leaf spot of maize: genetic architecture and mechanisms elucidated through nested association mapping and near-isogenic line analysis. PLoS Genet. 2015;11:1–23.
5. Kump KL, Bradbury PJ, Wisser RJ, Buckler ES, Belcher AR, Oropeza-Rosas MA, et al. Genome-wide association study of quantitative resistance to southern leaf blight in the maize nested association mapping population. Nat Genet. 2011;43:163–8.
6. Zila CT, Samayoa LF, Santiago R, Butrón A, Holland JB. A genome-wide association study reveals genes associated with fusarium ear rot resistance in a maize core diversity panel. G3. 2013;3:2095–104.
7. Chen G, Wang X, Hao J, Yan J, Ding J. Genome-wide association implicates candidate genes conferring resistance to maize rough dwarf disease in maize. PLoS One. 2015;10:e0142001.
8. Chen J, Shrestha R, Ding J, Zheng H, Mu C, Wu J, et al. Genome-wide association study and QTL mapping reveal genomic loci associated with Fusarium ear rot resistance in tropical maize germplasm. G3. 2016;6:3803–3815.
9. Gowda M, Das B, Makumbi D, Babu R, Semagn K, Prasanna BM. Genome-wide association and genomic prediction of resistance to maize lethal necrosis disease in tropical maize germplasm. Theor Appl Genet. 2015;128:1957–68.
10. Inghelandt D Van, Melchinger AE, Martinant J, Stich B. Genome-wide association mapping of flowering time and northern corn leaf blight (*Setosphaeria turcica*) resistance in a vast commercial maize germplasm set. BMC Plant Biol. 2012;12:56.
11. Yu J, Holland JB, McMullen MD, Buckler ES. Genetic design and statistical power of nested association mapping in maize. Genetics. 2008;178:539–51.
12. Li C, Li Y, Bradbury PJ, Wu X, Shi Y, Song Y, et al. Construction of high-quality recombination maps with low-coverage genomic sequencing for joint linkage analysis in maize. BMC Biol. 2015;13:78.
13. Giraud H, Lehermeier C, Bauer E, Falque M, Segura V, Bauland C, et al. Linkage disequilibrium with linkage analysis of for hybrid performance in the flint and dent. Genetics. 2014;198:1717–34.
14. Zila CT, Ogut F, Romay MC, Gardner CA, Buckler ES, Holland JB. Genome-wide association study of Fusarium ear rot disease in the U.S.A. maize inbred line collection. BMC Plant Biol. 2014;14:372.

15. Swarts KL, Bauer E, Glaubitz JC, Ho T, Johnson L, Li Y, et al. A large scale joint analysis of flowering time reveals independent temperate adaptations in maize. bioRxiv. 2016;https://doi.org/10.1101/086082.
16. Bian Y, Holland JB. Enhancing genomic prediction with genome-wide association studies in multiparental maize populations. Heredity. 2017;118:585–93.
17. Spindel J, Begum H, Akdemir D, Collard B, Redoña E, Jannink J-L, et al. Genome-wide prediction models that incorporate de novo GWAS are a powerful new tool for tropical rice improvement. Heredity. 2016;116:395–408.
18. Heslot N, Jannink J-L, Sorrells ME. Perspectives for genomic selection applications and research in plants. Crop Sci. 2015;55:1–12.
19. Sampietro DA, Vattuone MA, Presello DA, Fauguel CM. The pericarp and its surface wax layer in maize kernels as resistance factors to fumonisin accumulation by *Fusarium verticillioides*. Crop Prot. 2009;28:196–200.
20. Blandino M, Reyneri A, Colombari G, Pietri A. Comparison of integrated field programmes for the reduction of fumonisin contamination in maize kernels. Field Crop Res. 2009;111:284–9.
21. Bluhm BH, Woloshuk CP. Amylopectin induces fumonisin B1 production by *Fusarium verticillioides* during colonization of maize kernels. MPMI. 2005;18:1333–9.
22. Sampietro DA, Fauguel CM, Vattuone MA, Presello DA, Catalán CAN. Phenylpropanoids from maize pericarp: Resistance factors to kernel infection and fumonisin accumulation by *Fusarium verticillioides*. Eur J Plant Pathol. 2013;135:105–13.
23. Gao X, Kolomiets MV. Host-derived lipids and oxylipins are crucial signals in modulating mycotoxin production by fungi. Toxin Rev. 2009;28:79–88.
24. Mutiga SK, Morales L, Angwenyi S, Wainaina J, Harvey J, Das B, et al. Association between agronomic traits and aflatoxin accumulation in diverse maize lines grown under two soil nitrogen levels in Eastern Kenya. Field Crop Res. 2017;205:124–34.
25. Flint-Garcia SA, Thuillet AC, Yu J, Pressoir G, Romero SM, Mitchell SE, et al. Maize association population: A high-resolution platform for quantitative trait locus dissection. Plant J. 2005;44:1054–64.
26. Brown PJ, Upadyayula N, Mahone GS, Tian F, Bradbury PJ, Myles S, et al. Distinct genetic architectures for male and female inflorescence traits of maize. PLoS Genet. 2011;7:e1002383.
27. Buckler ES, Holland JB, Bradbury PJ, Acharya CB, Brown PJ, Browne C, et al. The genetic architecture of maize flowering time. Science. 2009;325:714–8.
28. Cook JP, McMullen MD, Holland JB, Tian F, Bradbury P, Ross-Ibarra J, et al. Genetic architecture of maize kernel composition in the nested association mapping and inbred association panels. Plant Physiol. 2012;158:824–34.
29. Peiffer JA, Flint-Garcia SA, De Leon N, McMullen MD, Kaeppler SM, Buckler ES. The genetic architecture of maize stalk strength. PLoS One. 2013;8:e67066.
30. Peiffer JA, Romay MC, Gore MA, Flint-Garcia SA, Zhang Z, Millard MJ, et al. The genetic architecture of maize height. Genetics. 2014;196:1337–56.

31. Tian F, Bradbury PJ, Brown PJ, Hung H, Sun Q, Flint-Garcia S, et al. Genome-wide association study of leaf architecture in the maize nested association mapping population. Nat Genet. 2011;43:159–62.
32. Zhao W. Panzea: a database and resource for molecular and functional diversity in the maize genome. Nucleic Acids Res. 2006;34:D752–7.
33. Wisser RJ, Kolkman JM, Patzoldt ME, Holland JB, Yu J, Krakowsky M. Multivariate analysis of maize disease resistances suggests a pleiotropic genetic basis and implicates a GST gene. PNAS. 2011;108:7339–44.
34. Bates D, Maechler M, Bolker B, Walker S. Fitting linear mixed-effects models using lme4. J Stat Softw. 2015;67:1–48.
35. R Core Team. R: A Language and Environment for Statistical Computing. Version 3.3.1. R Foundation for Statistical Computing. 2017.
36. Elshire RJ, Glaubitz JC, Sun Q, Poland J a, Kawamoto K, Buckler ES, et al. A robust, simple genotyping-by-sequencing (GBS) approach for high diversity species. PLoS One. 2011;6:e19379.
37. Glaubitz JC, Casstevens TM, Lu F, Harriman J, Elshire RJ, Sun Q, et al. TASSEL-GBS: A high capacity genotyping by sequencing analysis pipeline. PLoS One. 2014;9:e90346.
38. Bradbury PJ, Zhang Z, Kroon DE, Casstevens TM, Ramdoss Y, Buckler ES. TASSEL: Software for association mapping of complex traits in diverse samples. Bioinformatics. 2007;23:2633–5.
39. Swarts K, Li H, Romero Navarro JA, An D, Romay MC, Hearne S, et al. Novel methods to optimize genotypic imputation for low-coverage, next-generation sequence data in crop plants. Plant Genome. 2014;7.
40. Endelman JB, Jannink J-L. Shrinkage estimation of the realized relationship matrix. G3. 2012;2:1405–13.
41. Romay MC, Millard MJ, Glaubitz JC, Peiffer J a, Swarts KL, Casstevens TM, et al. Comprehensive genotyping of the USA national maize inbred seed bank. Genome Biol. 2013;14:R55.
42. JMP®. Version Pro 12. SAS Institute Inc. 1989-2007.
43. Harrell FE Jr. Hmisc: Harrell Miscellaneous. Version 4.0-2. 2016.
44. Storey JD. qvalue: Q-value estimation for false discovery rate control. 2015.
45. Epskamp S, Cramer A, Waldorp L, Schmittmann V, Borsboom D. qgraph: Network visualizations of relationships in psychometric data. J Stat Softw. 2012;48:1–18.
46. Yu J, Pressoir G, Briggs WH, Bi IV, Yamasaki M, Doebley JF, et al. A unified mixed-model method for association mapping that accounts for multiple levels of relatedness. Nat Genet. 2006;38:203–8.
47. Akdemir D, Okeke U. EMMREML: Fitting mixed models with known covariance structures. 2015.
48. Wallace JG, Bradbury PJ, Zhang N, Gibon Y, Stitt M, Buckler ES. Association mapping across numerous traits reveals patterns of functional variation in maize. PLoS Genet. 2014;10:e1004845.

49. Andorf CM, Cannon EK, Portwood JL, Gardiner JM, Harper LC, Schaeffer ML, et al. MaizeGDB update: New tools, data and interface for the maize model organism database. Nucleic Acids Res. 2016;44:D1195–201.
50. Sekhon RS, Lin H, Childs KL, Hansey CN, Robin Buell C, De Leon N, et al. Genome-wide atlas of transcription during maize development. Plant J. 2011;66:553–63.
51. Venn diagram tool (VIB/UGent Bioinformatics and Evolutionary Genomics). Available from: http://bioinformatics.psb.ugent.be/webtools/Venn/
52. Monaco MK, Sen TZ, Dharmawardhana PD, Ren L, Schaeffer M, Naithani S, et al. Maize metabolic network construction and transcriptome analysis. Plant Genome. 2013;6:0.
53. Tian T, Liu Y, Yan H, You Q, Yi X, Du Z, et al. agriGO v2.0: a GO analysis toolkit for the agricultural community, 2017 update. Nucleic Acids Res. 2017;1–8.
54. Yoon J, Choi H, An G. Roles of lignin biosynthesis and regulatory genes in plant development. J Integr Plant Biol. 2015;57:902–12.
55. Foley K, Hooven V. Properties and industrial uses of corncobs. In: Pomeranz Y, Munck L, editors. Cereals - A renewable resource - Theory and practice. St. Paul, MN: The American Association of Cereal Chemists; 1981.
56. Jansen C, Zhang Y, Liu H, Gonzalez-Portilla PJ, Lauter N, Kumar B, et al. Genetic and agronomic assessment of cob traits in corn under low and normal nitrogen management conditions. Theor Appl Genet. 2015;128:1231–42.
57. Zummo N, Scott GE. Cob and kernel infection by *Aspergillus flavus* and *Fusarium moniliforme* in inoculated, field-grown maize ears. Plant Dis. 1990;74:627–31.
58. Riedelsheimer C, Lisec J, Czedik-eysenberg A, Sulpice R, Flis A, Grieder C, et al. Genome-wide association mapping of leaf metabolic profiles for dissecting complex traits in maize. PNAS. 2012;109:8872–7.
59. Wiesner-Hanks T, Nelson R. Multiple disease resistance in plants. Annu Rev Phytopathol. 2016;54:229–52.
60. Teixeira JEC, Weldekidan T, Leon N De, Holland JB, Lauter N, Murray SC, et al. Hallauer's Tusón: a decade of selection for tropical-to-temperate phenological adaptation in maize. Hereditas. 2015;114:229–40.